AD NUMBER

ADB020118

LIMITATION CHANGES

TO:

Approved for public release; distribution is unlimited.

FROM:

Distribution authorized to U.S. Gov't. agencies only; Test and Evaluation; JUN 1977. Other requests shall be referred to Air Force Flight Dynamics Laboratory, FBED, Wright-Patterson AFB, OH 45433.

AUTHORITY

affdl notice, 16 dec 1977

AFFDL-TR-77-45

SONIC FATIGUE DESIGN DATA FOR BONDED ALUMINUM AIRCRAFT STRUCTURES

Northrop Corporation
Aircraft Division
3901 West Broadway
Hawthorne, California 90250

June 1977

TECHNICAL REPORT AFFDL-TR-77-45
Final Report for Period 17 December 1975 - 20 April 1977

AIR FORCE FLIGHT DYNAMICS LABORATORY
AIR FORCE WRIGHT AERONAUTICAL LABORATORIES
AIR FORCE SYSTEMS COMMAND
WRIGHT-PATTERSON AIR FORCE BASE, OHIO 45433

NOTICE

When Government drawings, specifications, or other data are used for any purpose other than in connection with a definitely related Government procurement operation, the United States Government thereby incurs no responsibility nor any obligation whatsoever; and the fact that the government may have formulated, furnished, or in any way supplied the said drawings, specifications, or other data, is not to be regarded by implication or otherwise as in any manner licensing the holder or any other person or corporation, or conveying any rights or permission to manufacture, use, or sell any patented invention that may in any way be related thereto.

This technical report has been reviewed and is approved for publication.

_____	_____
Signature	Signature
Name	Name
Project Engineer/Scientist	Supervisor

FOR THE COMMANDER

_____
Signature and Title

Copies of this report should not be returned unless return is required by security considerations, contractual obligations, or notice on a specific document.

Unclassified

SECURITY CLASSIFICATION OF THIS PAGE (When Data Entered)

REPORT DOCUMENTATION PAGE

READ INSTRUCTIONS BEFORE COMPLETING FORM

1. REPORT NUMBER: AFFDL-TR-77-45	2. GOVT ACCESSION NO.
3. RECIPIENT'S CATALOG NUMBER	
4. TITLE (and Subtitle): SONIC FATIGUE DESIGN DATA FOR BONDED ALUMINUM AIRCRAFT STRUCTURES.	5. TYPE OF REPORT & PERIOD COVERED: Final Technical Report. 17 December 1975 - 20 April 1977
	6. PERFORMING ORG. REPORT NUMBER: NOR-77-79
7. AUTHOR(s): Marcus J. Jacobson	8. CONTRACT OR GRANT NUMBER(s): F33615-75-C-3144
9. PERFORMING ORGANIZATION NAME AND ADDRESS: Northrop Corporation, 3901 West Broadway, Hawthorne, California 90250	10. PROGRAM ELEMENT, PROJECT, TASK AREA & WORK UNIT NUMBERS: Project No. 14710130
11. CONTROLLING OFFICE NAME AND ADDRESS: Air Force Flight Dynamics Laboratory, Air Force Systems Command, Wright-Patterson Air Force Base, Ohio 45433	12. REPORT DATE: June 1977
	13. NUMBER OF PAGES: 137
14. MONITORING AGENCY NAME & ADDRESS (if different from Controlling Office)	15. SECURITY CLASS. (of this report): Unclassified
	15a. DECLASSIFICATION/DOWNGRADING SCHEDULE

16. DISTRIBUTION STATEMENT (of this Report)

Distribution limited to U. S. government agencies only; test and evaluation; statement applied June 1977. Other requests for this document must be referred to Air Force Flight Dynamics Laboratory (FBED), Wright-Patterson Air Force Base, Ohio 45433

17. DISTRIBUTION STATEMENT (of the abstract entered in Block 20, if different from Report)

18. SUPPLEMENTARY NOTES

19. KEY WORDS (Continue on reverse side if necessary and identify by block number)

Sonic fatigue
Beam fatigue
Phosphoric acid anodizing
Bonded multi-bay panels

20. ABSTRACT (Continue on reverse side if necessary and identify by block number)

A combined analytic and experimental program was conducted to determine sonic fatigue design properties of bonded structural sections based on skin-stringer-frame design commonly applied in aircraft and to formulate data and criteria for the development of sonic fatigue resistant designs of such structure. The FM73/BR127 adhesive system was used in the bonding of beam and multibay panel test specimens with 7075-T6 aluminum alloy skins and substructure. The metal surfaces that were bonded were treated with a

DD FORM 1 JAN 73 1473 EDITION OF 1 NOV 65 IS OBSOLETE

Unclassified

SECURITY CLASSIFICATION OF THIS PAGE (When Data Entered)

phosphoric acid anodizing process that complied with the BAC-5555 specifications. Beam tests were conducted under narrow band shaker excitation and multibay panel tests were conducted under broadband acoustic excitation. The test results were evaluated and used in the development of a semi-empirical method for predicting sonic fatigue lives of multibay panels in acoustic environments. The range of applicability of the sonic fatigue design method is only partly determined. The sonic fatigue lives of the multibay acoustic test panels compared favorably with the lives of riveted panels of comparable size and skin thicknesses.

PREFACE

The activity that is documented in this report was performed under Contract F33615-75-C-3144, "Sonic Fatigue Design Data for Bonded Aluminum Aircraft Structures," Project No. 14710130, from 17 December 1975 through 20 April 1977 at the Northrop Corporation, Aircraft Division, Hawthorne, California. This research is part of a continuing effort to establish tolerance levels and design criteria for sonic fatigue prevention under the exploratory development program of the Air Force Systems Command.

The Air Force Flight Dynamics Laboratory (AFFDL) personnel who served as project engineers for this program were Mr. O. F. Maurer (AFFDL/FYA) and Mr. C. L. Rupert (AFFDL/FBED). Northrop acknowledges the assistance and good advice received from the two Air Force project engineers and Mr. H. F. Wolfe (AFFDL/FBED) throughout the contract.

Dr. M. J. Jacobson of the Structural Dynamics Research Department was the Principal Investigator. Mr. B. B. Bowen was the adviser on bonding. Major tasks were carried out under the leadership of Mr. D. C. Skilling, who directed the acoustic and shaker test programs; Mr. P. D. Adams who directed the manufacturing, other than bonding; and Mr. M. A. Bandic, who directed the bonding operations. The program was conducted under the technical supervision of Dr. C. Hwang, Manager of the Structural Dynamics Research Department.

TABLE OF CONTENTS

TABLE OF CONTENTS (CONTINUED)

TABLE OF CONTENTS (CONTINUED)

LIST OF ILLUSTRATIONS

LIST OF ILLUSTRATIONS (CONTINUED)

LIST OF ILLUSTRATIONS (CONTINUED)

LIST OF ILLUSTRATIONS (CONTINUED)

LIST OF TABLES

LIST OF TABLES (CONTINUED)

LIST OF TABLES (CONTINUED)

LIST OF SYMBOLS

SYMBOLS		UNITS
D	Bending rigidity	lb. in.
E	Young's modulus	psi
H	Torsional rigidity	lb. in.
K	Generalized plate stiffness in fundamental mode	lb./in
L_o	Length of beam or beam segment	in.
L	Sound pressure level (either in a 1/3 octave band or the overall level)	dB
L_{SL}	Spectrum level	dB
M'	Bending moment in a beam	lb. in.
M	Bending moment in a panel	lb. in./in.
N	Number of cycles	cycles
PSD	Power spectral density	$(-)^2$/Hz
SPL	Sound pressure level	dB
S_p	Acoustic pressure PSD at fundamental frequency f	psi^2/Hz
Q	Shear in a panel	lb./in.
V'	Shear in a beam	lb
a	Edge length of rectangular panel in x-direction	in.
b	Edge length of rectangular panel y-direction	in.
c	Viscous damping coefficient	lb sec/in.
c_c	Critical viscous damping coefficient	lb sec/in.
dB	Unless otherwise stated, dB refers to a SPL re $20\mu N/m^2$	decibels
e	Strain	in/in.
f	Frequency (in some cases, the fundamental frequency)	Hz
h	Panel thickness	in.

LIST OF SYMBOLS (CONTINUED)

SYMBOLS		UNITS
s	Stress	psi
t	Time	sec
x,y	Cartesian coordinates (parallel to the edges of a rectangular multi-bay panel or plate)	in.
Γ	Participation factor in plate response	in^2
α	Nondimensional beam function parameter	
β	Beam function parameters	$(in.)^{-1}$
γ	Beam function parameters	$(in.)^{-1}$
γ'	Weight density per unit volume	lb/in^3
Δf	Frequency band	Hz
ζ	Nondimensional viscous damping factor, $\zeta = c/c_c$	
θ	Nondimensional beam function parameter	
μ"/"	Micro-inch per inch	
ν	Poisson's ratio	
ρ	Mass density per unit length	$lb\ sec^2/in^2$
σ	Principal stress	ksi
$\bar{\sigma}_s$	Skin stress in riveted panels	ksi-rms
σ'	Effective stress in bonded panels	ksi-rms
σ_v	Skin stress in beam tests	ksi-rms
τ	Shear stress	ksi
ϕ	Nondimensional clamped-clamped beam function	
ψ	Nondimensional clamped-clamped beam function	
ω	Natural circular frequency	rad/sec

SUMMARY

A combined analytic and experimental program was conducted under Contract F33615-75-C-3144, "Sonic Fatigue Design Data for Bonded Aluminum Aircraft Structures," to determine sonic fatigue properties of bonded structural sections based on skin-stringer-frame design commonly applied in aircraft and to formulate data and criteria for the development of sonic fatigue resistant designs of such structure. In the test program, the FM73/BR127 adhesive system was used in the bonding of beam and multibay panel test specimens with 7075-T6 aluminum alloy skin and substructure whose surfaces had been treated in accordance with a phosphoric acid anodizing process that complied with the BAC 5555 specification. Beam tests were conducted under narrow band shaker excitation and multibay panel tests were conducted under broadband acoustic excitation. The test results were evaluated and used in the development of a semi-empirical method for predicting sonic fatigue lives of multibay panels in acoustic environments. The range of applicability of the sonic fatigue design method was only partly determined. The sonic fatigue lives of the multibay bonded acoustic test panels were, in general, significantly longer than the lives of riveted panels of comparable size and skin thicknesses.

SECTION I

INTRODUCTION

There is extensive information in the general literature (e.g., References 1 through 9) on sonic fatigue design data and approaches to guard against the sonic fatigue of riveted structures. However, the sonic fatigue data for riveted structures is not directly transferable to bonded structures, principally because of the different nature of the riveted joint assemblies versus bonded joint assemblies. For example, in the event of a sonic fatigue failure of a skin-frame-stringer assembly, the riveted joint assemblies often experience the failure in the skin along the line of rivets, whereas the bonded joint assemblies often experience the failure in the bond between the skin and the substructural elements.

Because of recent advances in the bonding technology, considerable attention is being directed at developing design and manufacturing techniques that will permit the use of bonded metallic structure in significant applications in aircraft. The use of the Boeing Process Specification BAC-5555 has been shown to be a superior method for preparing the surfaces of aircraft aluminum alloys for bonding. Under Contract F33615-75-C-3016, "Primary Adhesively Bonded Structure Technology (PABST)," the Government is sponsoring a significant R&D program to develop, design, fabricate, and ground test a full-scale cargo aircraft fuselage segment using adhesive bonding in the primary structure, in lieu of mechanical fasteners. PABST is part of a long-term effort that may result in the design and manufacture of portions of bonded primary structure that may experience high-intensity noise environments. Because of the expected use of bonded structure in sonic environments featuring the application of the BAC-5555 Process Specification or its equivalent, the need for sonic fatigue guidelines for the new generation bonded structures becomes evident.

The program objective of the analytical and experimental activity that was conducted under Contract F33615-75-C-3144 and is being reported in this document was the determination of sonic fatigue properties of bonded structural sections based on skin-stringer-frame design commonly applied in aircraft and the formulation of data and criteria for the development of sonic fatigue resistant designs for such structures.

The surfaces of the test specimens fabricated in this program for acoustic and shaker tests were treated with a phosphoric acid anodizing process that complied with the BAC-5555 process specifications. The FM73/BR127 adhesive system was used in the bonding of beam and multibay panel test specimens with 7075-T6 aluminum alloy skins and substructure.

Beam tests were conducted under narrow band random shaker excitation and multibay panel tests were conducted under broadband acoustic excitation. The test results were evaluated and used in the development of a semi-empirical method for predicting the sonic fatigue lives of multibay aircraft panels in acoustic environments. The sonic fatigue lives of the bonded multibay acoustic test panels were, in general, significantly longer than the lives of multibay riveted panels of comparable size and skin thicknesses.

Prior to developing in this program a semi-empirical method to predict sonic fatigue, finite element analyses based on conventional structural theory were conducted to predict natural frequencies and stresses in sonic fatigue sensitive locations

of the multibay bonded panels. However, because of complexities centering on: the finite element modeling techniques, the nonlinear acoustic pressures versus test strain relations, the effects of details of the substructure design of multibay panels on the stress state and sonic fatigue life at the failure locations in the bonded joints, and other factors, it was determined that the development of a strictly analytic approach for predicting the stress response and sonic fatigue lives of the bonded panels was impractical. Therefore, a sonic fatigue design nomograph based on a semi-empirical approach was developed for the bonded panels. However, the range of applicability of the design nomograph was only partly determined.

This report is organized into seven sections. The specimen design, manufacturing, instrumentation and general test procedures are discussed in Section II, the shaker test results in Section III, and the acoustic test results and modal data in Section IV. The sonic fatigue design nomograph that was developed is in Section V, a brief discussion of failure modes that were observed is in Section VI, and the conclusions are summarized in Section VII. Acoustic test data are presented in Appendix A and a discussion of finite element modeling techniques is in Appendix B.

SECTION II

SPECIMEN DESIGN, MANUFACTURING, INSTRUMENTATION AND TEST PROCEDURES

2.1 Approach and Objectives

The test plan, including the number and configuration of test specimens, was developed to gather an optimum amount of useful information in meeting the overall program objective. The configuration of the test specimens was chosen to be compatible with present and expected future flight vehicle requirements and with analytic and test data that were available.

The principal objective of the sonic fatigue test program was to obtain sonic fatigue data for utilization in the establishment of sonic fatigue design criteria. To achieve this objective, the acoustic test specimens were subjected to tests under loudspeaker excitation to obtain frequency, modal shape, and damping data that are needed in the development of sonic design criteria. Then tests were conducted under high-intensity acoustic excitation to obtain strain response versus SPL data, damping data, and sonic fatigue data and to provide information that would permit comparisons to be made between bonded and riveted structure on the basis of joint stiffness, structural damping, and sonic fatigue resistance. Sonic fatigue data on riveted structure are available from Government-sponsored programs (e.g., Reference 1 and 2) and from other sources.

The principal objectives of the shaker test program were to obtain random S-N data for use in the acoustic design of metal panels with the skin bonded to internal structure and to determine the effect of a change of particular variable (e.g., skin thickness or symmetrical versus nonsymmetrical internal structure configuration) on the fatigue life and mode of fatigue failure.

2.2 Design of Acoustic Test Panels

Ten cross-stiffened 9-bay specimens were designed and manufactured for acoustic tests in the 48- by 48-inch test section of Northrop's progressive wave acoustic test chamber (Figure 1). The configurations were chosen to simulate bonded skin-frame-stringer construction that is a candidate for applications on lightweight aircraft structure. For the 10 panels, there were five panel designs (Table 1 and Figure 2) and two identical panels per panel design to permit the scheduling of identical tests with identical panels (except for panels A-3-1 and A-3-2) to obtain a measure of test repeatability.

Panels A-3-1 and A-3-2 were the two panels with the A-3 design; panels A-1-1 and A-1-2 were the two panels with the A-1 design; etc. The material for the skins and simulated frames and longerons was 7075-T6 nonclad aluminum alloy. The scarfing of the flanges of the J-section and I-section stiffeners was performed to reduce stress concentration effects at the ends of the bonded joints and hence to increase the sonic fatigue lives of the joints.

The -71 and -73 angle on the panel specimens (Figure 2) were to simulate a flange on zee section components of frame members expected in frame section designs for production aircraft. The -71 angles were not installed on the

TABLE 1. DESCRIPTION OF ACOUSTIC TEST PANELS

PANEL DESIGN	NUMBER OF PANELS	OVERALL PANEL DIMENSIONS	CENTRAL BAY DIMENSIONS	SKIN THICK-NESS
		(inch)	(inch)	(inch)
A-1	2	29 x 20	18 x 9	.032
A-2	2	29 x 20	18 x 9	.040
A-3	2	29 x 20	18 x 9	.050
A-4	2	36 x 24	24 x 12	.050
A-5	2	36 x 24	24 x 12	.063

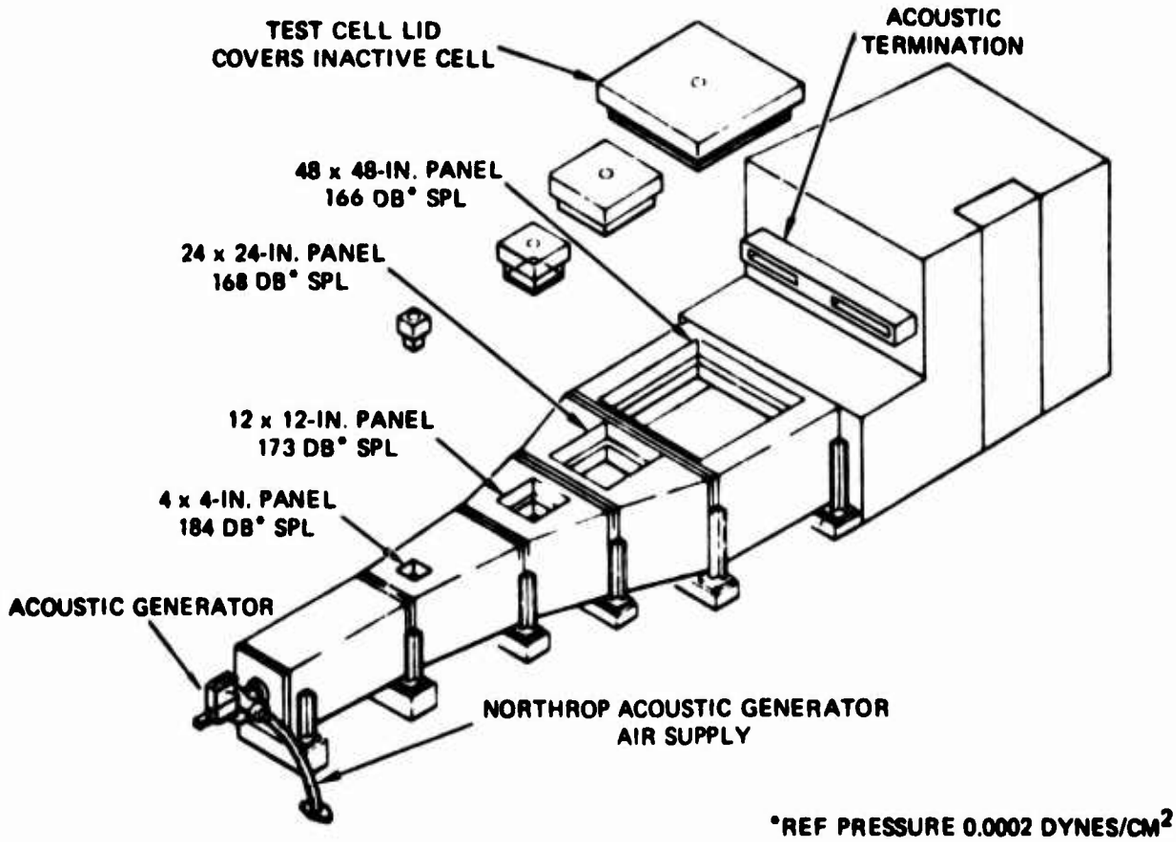

Figure 1. Progressive Wave Acoustic Test Chamber

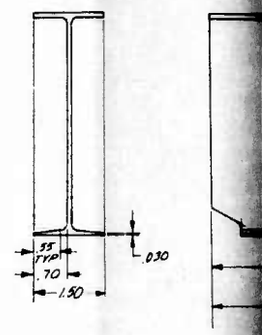

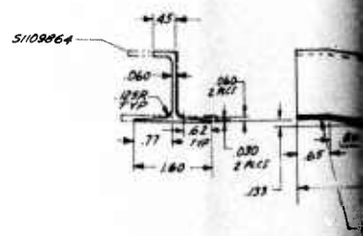

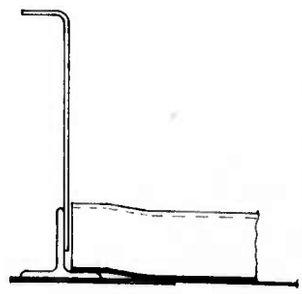

SECTION 1-1
TYP 4 PLACES

Figure 2. Acoustic Test Panel Designs (Drawing SR-008001)

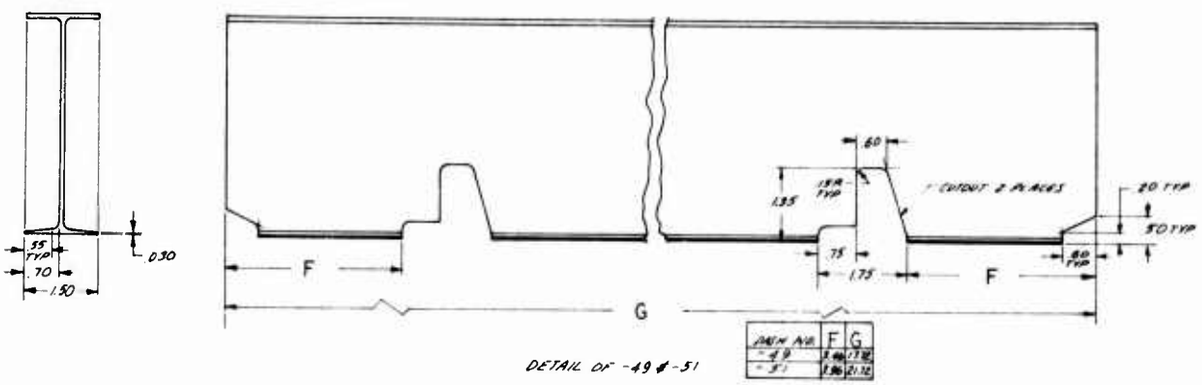

PART NO	F	G
-49	3.90	17.82
-51	1.96	21.16

DETAIL OF -49 & -51

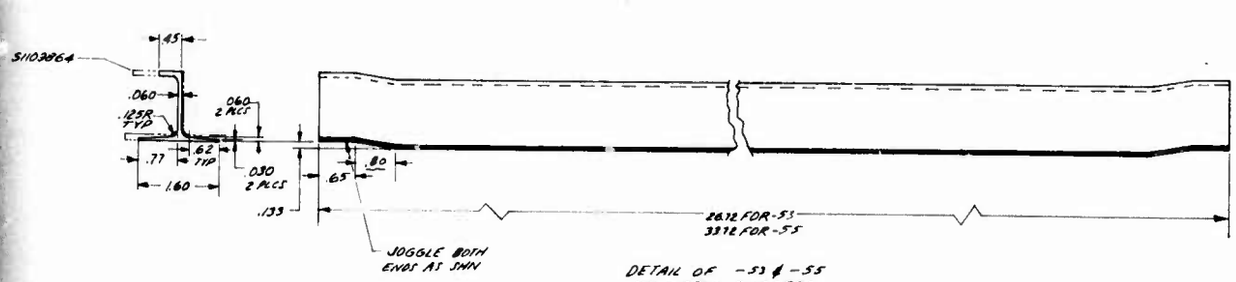

DETAIL OF -53 & -55
MAKE FROM S1103864

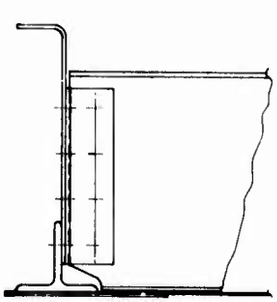

SECTION H-H
TYP 4 PLACES

DETAIL -65

SR008001 | REV A | SH

2

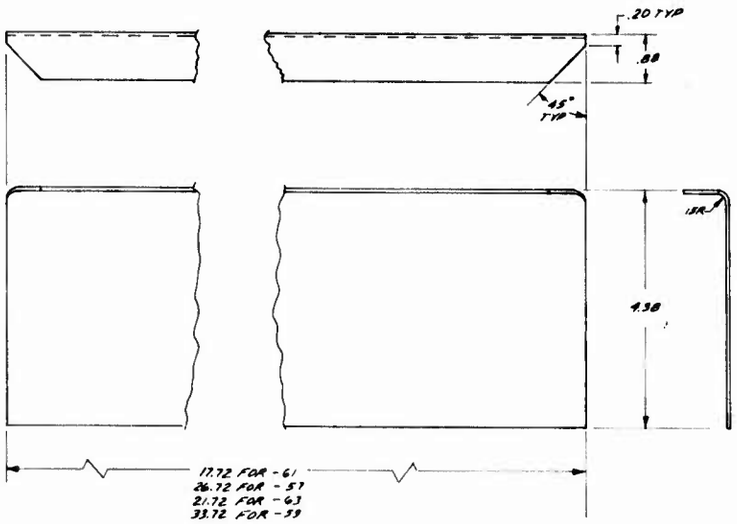

DETAIL OF -57, -59, -61 & -63

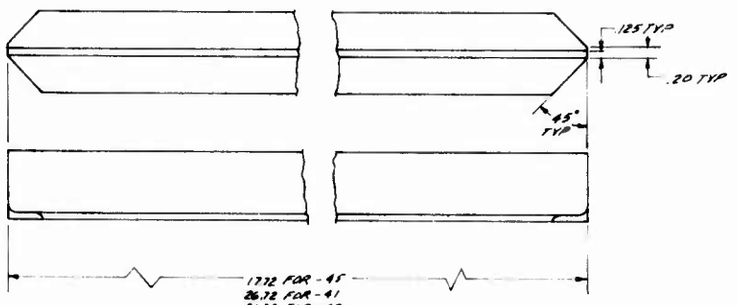

DETAIL OF -41, -43, -45 & -47

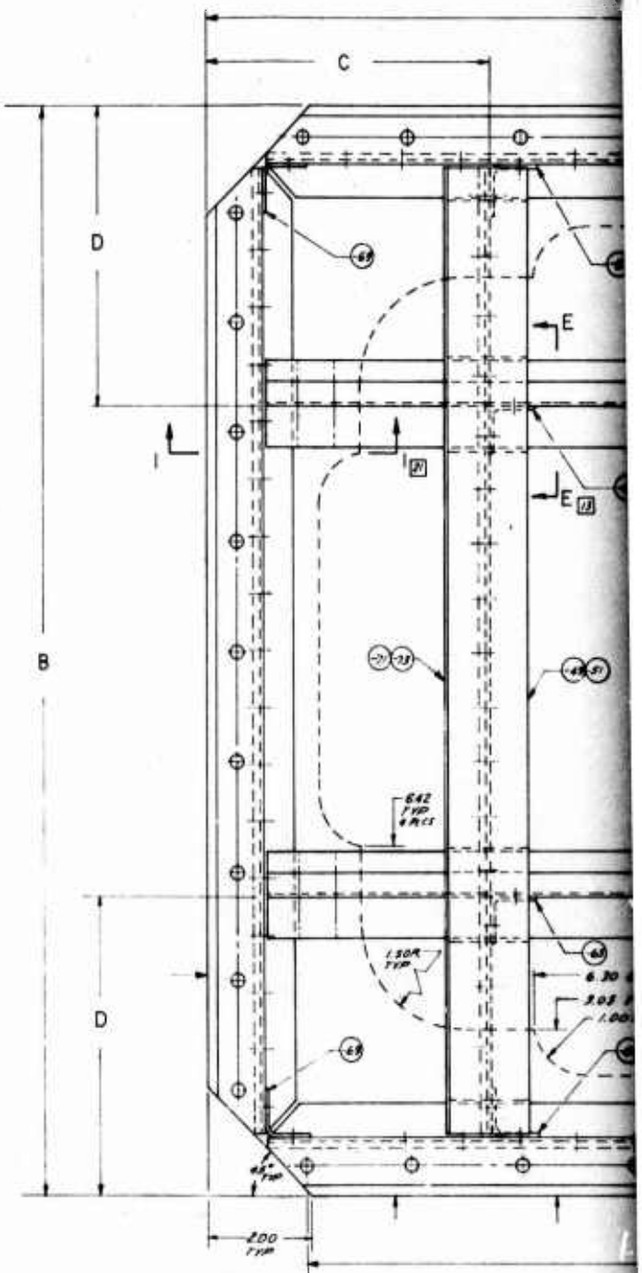

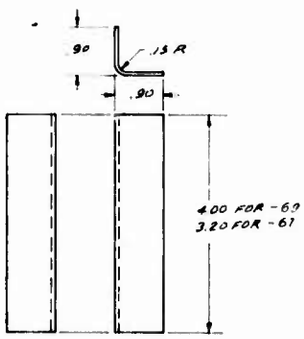

DETAIL -67 & -69

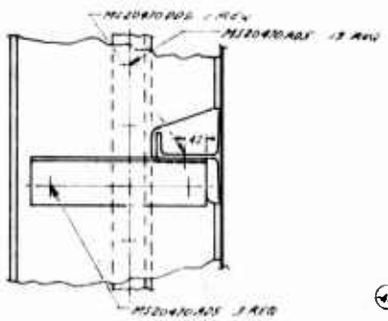

SECTION E-E
TYP 4 PLACES

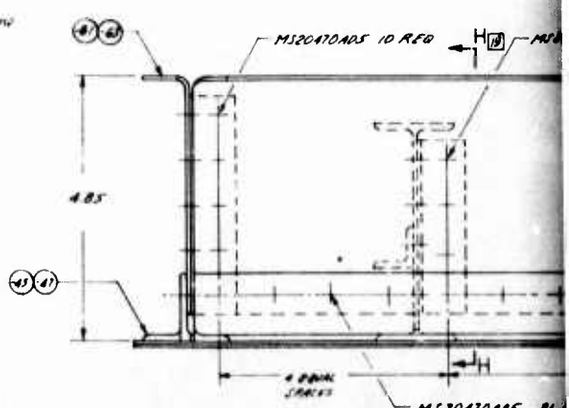

SR008001 REV A SH

REVISION NOTES
1 REFER TO APPLICATION (USAGE) LIST FOR EFF

REV NOTE	ZONE	LTR	REVI DESCRIPTI
		A	REVISED NOTE 1, ADD

RIVET DESIGN	DASH NO.	DIMENSION A	B	C	D
A-1	-1	29.00	20.00	5.50	5.50
A-2	-3	29.00	20.00	5.50	5.50
A-3	-5	29.00	20.00	5.50	5.50
A-4	-7	36.00	24.00	6.00	6.00
A-5	-9	36.00	24.00	6.00	6.00

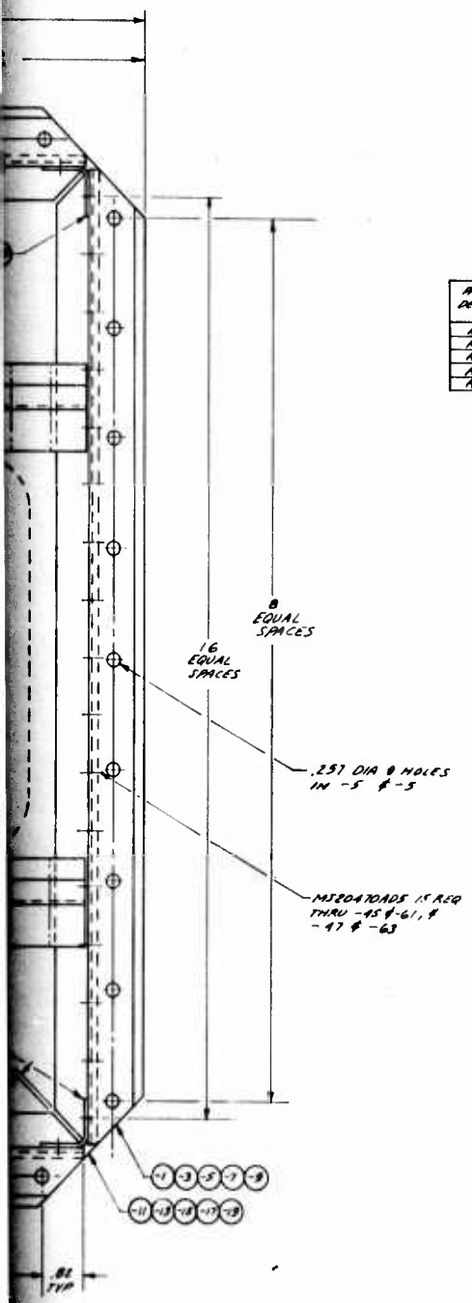

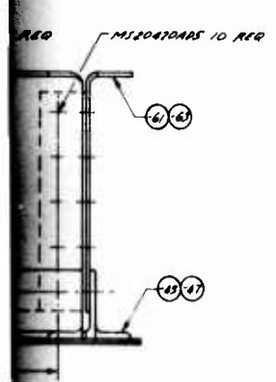

-19	-17	-15	-13	-11	-9	-7	-5	-3	-1	PART OR IDENTIFYING NO.	SEE NOTES	NOMENCLATURE OR DESCRIPTION	MATERIAL OR CODE IDENT NO.
QTY REQD													
					4	4	4	4	4	MS20470AD6		RIVET	
					168	168	168	168	168	MS20470AD5		RIVET	
					2	2				-33		STIFFENER	
							2	2	2	-71		STIFFENER	
					4	4	4	4	4	-69		CLIP	SHEET STEEL 4130
					4	4	4	4	4	-67		CLIP	SHEET STEEL 4130
					4	4	4	4	4	-65		CLIP	
1	1									-63		ANGLE	SHEET STEEL 4130
		1	1	1						-61			
1	1									-59			
		1	1	1						-57		ANGLE	SHEET STEEL 4130
1	1									-55		LONGERON	
		1	1	1						-53		LONGERON	
1	1									-51		FRAME	
		1	1	1						-49		FRAME	
1	1									-47		TEE	
		1	1	1						-45			
1	1									-43			
		1	1	1						-41		TEE	
1										-39		DOUBLER	AL ALLOY SHEET 7075-T6
	1									-37			
		1								-35			
			1							-33			
				1						-31		DOUBLER	
1										-29		WEB	
	1									-27			
		1								-25			
			1							-23			
				1						-21		WEB	AL ALLOY SHEET 7075-T6
					1					-19	1	BAND ASSY	
						1				-17	1		
							1			-15	1		
								1		-13	1		
									1	-11	1	BAND ASSY	

PARTS LIST

3. BAND PER NORTHROP ASSEMBLY DOCUMENT 3780-76-148.
4. -71 TO BE INSTALLED ONLY BY ORDER OF PROGRAM MANAGER.
3 RIVETS TO BE EQUALLY SPACED BETWEEN THOSE LOCATED.
2 EDGE DIST FOR .156 DIA RIVETS, .25; FOR .188 DIA, .63.
1 PROCESS -21 THRU -39 & -49 THRU -55 TO COMPLY WITH BRAZING PROCESS SPEC BAC 5555 & PRIME THEIR SURFACES THAT ARE TO BE BONDED, WITH BR-127 PRIMER PER NORTHROP ARDC SPEC. MA-108, PARAGRAPH 3.15.2.

NOTE

KEY TO BASIC CODES — BASIC CODE — INSTALL PER PROCESS SPEC — DASH NO. FOR LENGTH — PARTNER CODE

UNLESS OTHERWISE NOTED LINEAR TOLERANCES .XX ± .01, .XXX ± .005 — LINEAR DIM. ARE IN INCHES — ANGULAR TOL EXCEPT SHEET METAL FILL ± 2° 30' — MFG ACCEPTANCE TOL PER — FINISH PER — FOR USAGE DATA SEE APPLICATION LIST

CONTRACT NO.

DRAWN	
DESIGN	
CHECKED	
PROGRAM	
NORTHROP APPROVAL	
OTHER APPROVAL	

NORTHROP

SONIC TEST

SIZE J — CODE IDENT NO. 70025 — SCALE FULL

REVISION NOTES
1 REFER TO APPLICATION (USAGE) LIST FOR EFF

REV NOTE	ZONE	LTR	REVISIONS DESCRIPTION	DATE	APPROVED
	ADDL AREA	A	REVISED NOTE 1, ADDED NOTES	4/24/76	F&J

PANEL DESIGN	DASH NO.	DIMENSION A	B	C	D
A-1	-1	28.00	20.00	5.50	5.50
A-2	-3	28.00	20.00	5.50	5.50
A-3	-5	28.00	20.00	5.80	5.80
A-4	-7	36.00	24.00	6.00	6.00
A-5	-9	36.00	24.00	6.00	6.00

-19	-17	-15	-13	-11	-9	-7	-5	-3	-1	PART OR IDENTIFYING NO	SEE NOTES	NOMENCLATURE OR DESCRIPTION	MATERIAL OR CODE IDENT NO	SIZE	SPECIFICATION OR PROCUREMENT DATA	ZONE	ITEM
					4	4	4	4	4	MS20470DDG		RIVET					35
					168	168	168	168	168	MS20470AD5		RIVET					34
					2	2				-73		STIFFENER	AND10133-0603 ELTAU 7075 T6	21.8 LG	QQ-A-200/11	11	33
							2	2	2	-71		STIFFENER	AND10133-0603 ELTAU 7075 T6	18.8 LG	QQ-A-200/11	11	32
					4	4	4	4	4	-69		CLIP	SHEET STEEL 4130	.071 x 1.8 x 14.1 LG	MIL-S-18729 COND N	11	31
					4	4	4	4	4	-67		CLIP	SHEET STEEL 4130	.071 x 1.8 x 13.9 LG	MIL-S-18729 COND N	10	30
					4	4	4	4	4	-65		CLIP	AND10133-0701 ELTAU 7075T6	3.5 LG	QQ-A-200/11	10	29
1	1									-63		ANGLE	SHEET STEEL 4130	.071 x 5.3 x 21.8	MIL-S-18729 COND N	6	28
		1	1	1						-61				.071 x 5.3 x 18.8		6	27
1	1									-59				.071 x 5.3 x 33.8		9	26
		1	1	1						-57		ANGLE	SHEET STEEL 4130	.071 x 5.3 x 26.8	MIL-S-18729 COND N	9	25
1	1									-55		LONGERON	5110966 ELTAU 7075T6	33.8 LG	QQ-A-200/11	10	24
		1	1	1						-53		LONGERON	5110966 ELTAU 7075T6	26.8 LG		10	23
1	1									-51		FRAME	AND10100-4002 ELTAU 7075T6	21.8 LG		10	22
		1	1	1						-49		FRAME	AND10100-4002 ELTAU 7075T6	18.8 LG		10	21
1	1									-47		TEE	AND10136-1407 ELTAU 7075T6	21.8 LG		6	20
		1	1	1						-45				18.8 LG		6	19
1	1									-43				33.8 LG		8	18
		1	1	1						-41		TEE	AND10136-1407 ELTAU 7075T6	26.8 LG	QQ-A-200/11	8	17
1										-39		DOUBLER	AL ALLOY SHEET 7075T6	.063x24.1 x36.1	QQ-A-250/12	7	16
	1									-37				.050x24 x36.1		7	15
		1								-35				.050x20. x29.1		7	14
			1							-33				.040x20.1 x29.1		7	13
				1						-31		DOUBLER		.032x20.1 x29.1		7	12
1										-29		WEB		.063x24.1 x36.1		8	11
	1									-27				.050x24.1 x36.1		8	10
		1								-25				.050x20.1 x29.1		8	9
			1							-23				.040x20.1 x29.1		8	8
				1						-21		WEB	AL ALLOY SHEET 7075T6	.032x20.1 x29.1	QQ-A-250/12	8	7
					1					-19	1	BAND ASSY				6	6
						1				-17	1					6	5
							1			-15	1					6	4
								1		-13	1					6	3
									1	-11	1	BOND ASSY				6	2

QTY REQD

PARTS LIST

3. BOND PER NORTHROP ASSEMBLY DOCUMENT 3780-76-168.
4. -71 TO BE INSTALLED ONLY BY ORDER OF PROGRAM MANAGER.
3. RIVETS TO BE EQUALLY SPACED BETWEEN PNOTS LOCATED.
2. EDGE DIST FOR .156 DIA RIVETS, .35, FOR .188 DIA, .42.
1. PROCESS -21 THRU -39 & -49 THRU -55 TO COMPLY WITH BONDING PROCESS SPEC. BAC 5555 & PRIME THEIR SURFACES THAT ARE TO BE BONDED, WITH BR-127 PRIMER PER NORTHROP ARDC SPEC. MA-108, PARAGRAPH 3.5.2.

NOTE

KEY TO BASIC CODES — INSTALL PER PROCESS SPEC

UNLESS OTHERWISE NOTED: LINEAR TOLERANCES .XX ± .03, .XXX ± .010; LINEAR DIM ARE IN INCHES; ANGULAR TOL EXCEPT SHEET METAL ± 1/2°; MFG ACCEPTANCE TOL PER

FINISH PER

DOD DASH NO. SHOWN EVEN DASH NO. OPPOSITE

FOR USAGE DATA SEE APPLICATION LIST

CONTRACT NO

DRAWN — F. ARTERO 8/5/76

DESIGN

CHECKED

PROGRAM — M. HUBBEN 5/6/76

NORTHROP APPROVAL

OTHER APPROVAL

NORTHROP Northrop Corporation Aircraft Division 1801 West Broadway Hawthorne, California 90250

SONIC FATIGUE TEST PANEL

SIZE J | CODE IDENT NO 70823 | SR008001

SCALE FULL | SHEET 1 OF 2

SR008001

6

simulated frames of panel A-3-1 to assess the effect of their absence. It was the absence of the -71 angles on panel A-3-1 that was the difference in the panel designs between panels A-3-1 and A-3-2.

The boundary frame of the acoustic test panels shown in Figure 2 is essentially a part of the test fixture. This type of boundary frame design was used successfully in the 9-bay graphite-epoxy acoustic panel tests under Contract F33615-70-C-1463.

The edge doubler that was bonded to the skin of the acoustic test panels was to safeguard against sonic fatigue failures that may occur at the attachment of the skin to the boundary frame. Such failures may happen unless precautions are taken to prevent their occurrence. Inasmuch as structural failures at the boundary frame may influence the location and time of subsequent sonic fatigue failures and raise questions on the meaning of the test results, it is prudent to guard against their occurrence. The type of the edge doubler that was used in this acoustic test program was to simulate the edge doubler that was successfully used in the 9-bay graphite-epoxy acoustic panel tests under Contract F33615-70-C-1463.

2.3 Design of Shaker Test Specimens

The design of 27 beam specimens for the shaker test program is described in Table 2 and Figures 3 and 4. The length of the beams was 12 inches and the width was 2 inches. The material for the skin and simulated internal structural components was 7075-T6 nonclad aluminum alloy. All of the simulated internal structure, i.e., the stiffeners (see Table 2) were bonded to the skins of the specimens. The angle configuration for internal structure was to simulate one flange and the web of zee or channel construction. All shaker test specimens were tested as free-free beams that were attached to the shaker assembly by clamping the outstanding leg of the angle and tee sections.

TABLE 2. DESCRIPTION OF BEAM SPECIMENS

BEAM SPECIMEN DESIGN	NUMBER OF FABRICATED SPECIMENS(1)	SKIN THICKNESS	SCARFED FLANGE	STIFFENER CONFIGURATION
		(inch)		
V-1	4	.032	Yes	Tee
V-2	4	.040	Yes	Tee
V-3	7	.050	Yes	Tee
V-4	4	.063	Yes	Tee
V-5	4	.050	No	Tee
V-6	4	.050	No	Angle

(1) Only 21 of the 27 specimens were tested at Northrop in this program. The remaining 6 specimens consisting of one specimen per specimen design were forwarded to AFFDL for Air Force inspection and testing.

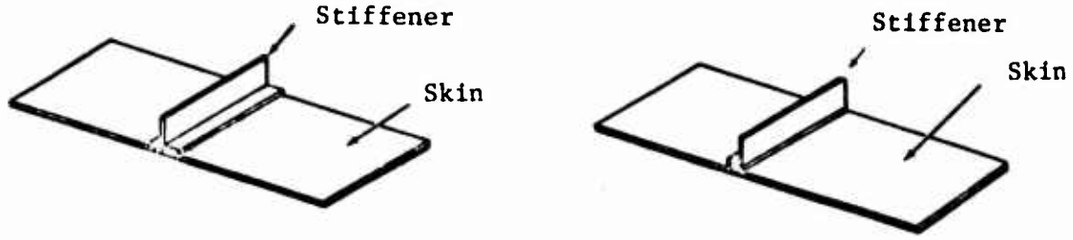

Beam with Tee Section Stiffener

Beam with Angle Section Stiffener

Figure 3. Perspective of Beam Specimens with Bonded Stiffeners

2.4 Material Properties of the 7075-T6 Skins

Tensile tests were performed at room temperature on coupons from the 7075-T6 (bare) sheets from which the skins of the acoustic test panels were obtained. The tensile tests were conducted in accordance with the Northrop Process Specification IT-65. There were fifteen tensile test coupons and the thicknesses were .063, .050, .040, and .032 inch. The test values of yield stress, ultimate strength, elongation, and Young's modulus that were obtained are listed in Table 3.

2.5 The Bonding System

The FM73/BR127 adhesive/primer system was used in this program to bond the skins of the acoustic test panels and the beam specimens to the stiffeners simulating internal structure. The FM73/BR127 system is representative of the new-technology adhesive systems for 250F service temperature capability under intensive development by the USAF and contractors of new aircraft programs. The weight density of the FM73 supported film adhesive used in the manufacture of the acoustic panels and the beams was 0.085 psf. The FM73 adhesive conforms to the Boeing Specification BMS-5-101.

The FM73 adhesive that was used in the shaker and acoustic test program was accepted on the basis of lap shear tests (Table 4) of eight specimens at room temperature that were performed in accordance with Northrop Process Specification IT-34. All the lap shear test failures were cohesive. Inasmuch as a minimum strength of 5,000 psi was a criterion for accepting the adhesive, the material passed the acceptance test.

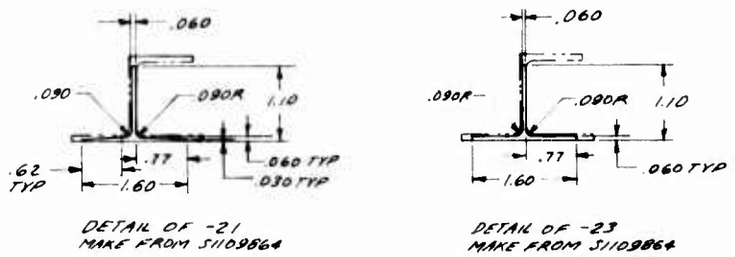

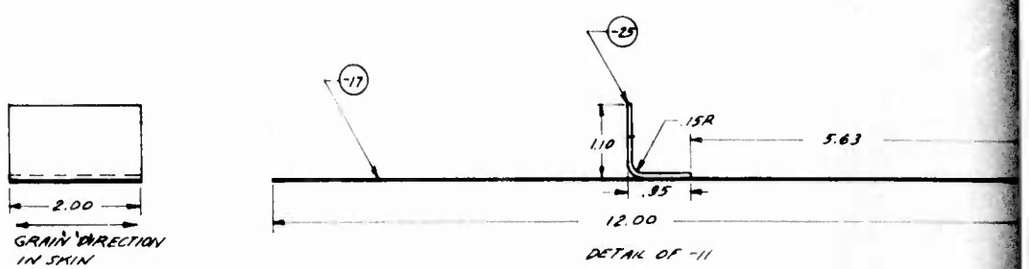

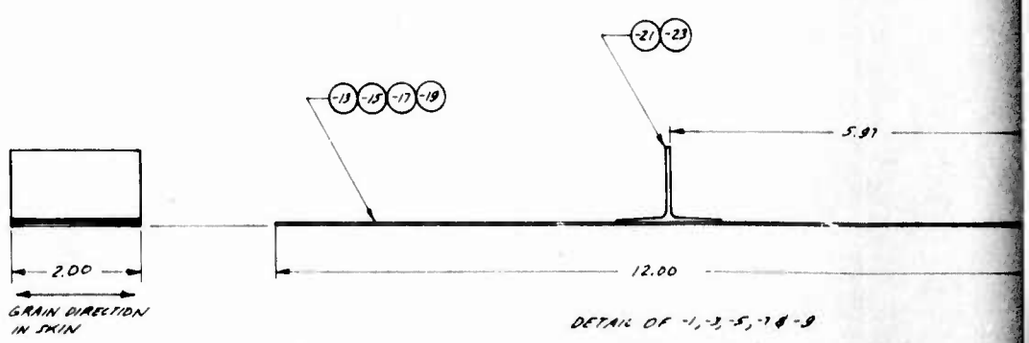

Figure 4. Beam Specimen Designs for Shaker Testing (Drawing SR-008002)

REVISION NOTES
1. REFER TO APPLICATION (USAGE) LIST FOR EFF

REV. NOTE	ZONE	LTR	REVISION DESCRIPTION
	EFF. ABOVE	A	REVISED NOTE 2, ADDED A

SHAKER SPECIMEN	DASH NO.
V1	-1
V2	-3
V3	-5
V4	-7
V5	-9
V6	-11

5.63

5.97

QTY REQD						PART OR IDENTIFYING NO	SEE NOTES	NOMENCLATURE OR DESCRIPTION	MATERIAL OR CODE IDENT NO
-11	-9	-7	-5	-3	-1				
					1	-25		STIFFENER	AL ALLOY SHEET 7075-0
					1	-23		STIFFENER	S1109864 EQUIV AL 7075T651
				1	1	-21		STIFFENER	S1109864 EQUIV AL 7075T651
			1			-19		SKIN	AL ALLOY SHEET 7075-T6
		1		1		-17		↕	↕
					1	-15		↕	↕
					1	-13		SKIN	AL ALLOY SHEET 7075-T6

PARTS LIST

3. BOND -1 THRU -11 PER NORTHROP ASSEMBLY DOCUMENT 3780-76-148.
2. PROCESS -13 THRU -25 DETAILS TO COMPLY WITH BOEING PROCESS SPEC. BAC 5555 & PRIME THEIR SURFACES THAT ARE TO BE BONDED WITH BR-127 PRIMER PER NORTHROP DOCUMENT MA-108, PARAGRAPH 3.1.5.2.
1. HEAT TREAT -25 TO T6 COND PER NORTHROP PROC SPEC. NT-1 NOTE

2

KEY TO BASIC CODES	INSTALL PER PROCESS SPEC.
BASIC CODE	DASH NO. FOR DIA
BASIC CODE IN BOX = INSTALL WET PER PS FH - - - -	D = 100° HEAD SHEAR SIDE F = 100° HEAD FAR SIDE R = RADIUSED DRIVEN HEAD
WITH PLUSH COND ONLY	DASH NO. FOR LENGTH
B = DIMPLE FHS = TOTAL NO. SHEETS TO BE DIMPLED C = COUNTERSINK	(NOT SHOWN FOR ALL TYPES OF FASTENERS)
FASTENER CODE	

UNLESS OTHERWISE NOTED
LINEAR X ± .1
TOLERANCES XX ± .06
XXX ± .010
LINEAR DIM. ARE IN INCHES
ANGULAR TOL EXCEPT SHEET METAL FLG ± 0° 30'
MFG ACCEPTANCE TOL PER
FINISH PER
ODD DASH NO. SHOWN
EVEN DASH NO. OPPOSITE
FOR USAGE DATA SEE APPLICATION LIST

CONTRACT NO

DRAWN	K. HEFFORD 6/2/76	
DESIGN		
CHECKED		
PROGRAM	M. JACOBSON 1/19/76	
NORTHROP APPROVAL		
OTHER APPROVAL		

NORTHROP

SHAKE
SPECI

SIZE H | CODE IDENT NO 76823 | SCALE FULL

(08002)

REVISION NOTES
1. REFER TO APPLICATION (USAGE) LIST FOR EFF

REVISIONS					
REV NOTE	ZONE	LTR	DESCRIPTION	DATE	APPROVED
	GEN. NOTE	A	REVISED NOTE 2, ADDED NOTE 3	3/22/76	FGJ

SHAKER SPECIMEN	DASH NO.
V1	-1
V2	-3
V3	-5
V4	-7
V5	-9
V6	-11

QTY REQD						PART OR IDENTIFYING NO	SEE NOTES	NOMENCLATURE OR DESCRIPTION	MATERIAL OR CODE IDENT NO	SIZE	SPECIFICATION OR PROCUREMENT DATA	ZONE	ITEM
1						-25		STIFFENER	AL ALLOY SHEET 7075-0	.063 x 2.1 x 2.1	QQ-A-250/12	6	8
	1					-23		STIFFENER	S1109864 EXTRU AL 7075T6511	2.1 LG	QQ-A-200/11	6	7
		1	1	1	1	-21		STIFFENER	S1109864 EXTRU AL 7075T6511	2.1 LG	QQ-A-200/11	6	6
		1				-19		SKIN	AL ALLOY SHEET 7075 T6	.063 x 12.1 x 2.1	QQ-A-250/12	7	5
1	1		1			-17		↓	↓	.090 x 12.1 x 2.1	↓	7	4
				1		-15		↓	↓	.090 x 12.1 x 2.1	↓	7	3
					1	-13		SKIN	AL ALLOY SHEET 7075 T6	.125 x 12.1 x 2.1	QQ-A-250/12	7	2
													1
-11	-9	-7	-5	-3	-1								

PARTS LIST

3. BOND -1 THRU -11 PER NORTHROP ASSEMBLY DOCUMENT 3780-76-148.
2. PROCESS -13 THRU -25 DETAILS TO COMPLY WITH BOEING PROCESS SPEC. BAC 5555 & PRIME THEIR SURFACES THAT ARE TO BE BONDED WITH BR-127 PRIMER PER NORTHROP DOCUMENT MA-108, PARAGRAPH 3.1.5.2.
1. HEAT TREAT -25 TO T6 COND PER NORTHROP PROC. SPEC NT-1 NOTE

REV TO BASIC CODES	INSTALL PER PROCESS SPEC
BASIC CODE BASIC CODE IN BOX = INSTALL WET PER PS FN ____	DASH NO FOR DIA 0 = .190 HEAD REAR SIDE F = .190 HEAD FAR SIDE R = RADIUSED DRIVER HEAD
WITH FLUSH COND ONLY S = SIMPLE FIG = TOTAL OF SHEETS TO BE SIMPLED C = COUNTERSINK	DASH NO FOR LENGTH (NOT SHOWN FOR ALL TYPES OF FASTENERS)
FASTENER CODE	

UNLESS OTHERWISE NOTED	
LINEAR TOLERANCES	X = ± .1 XX = ± .04 XXX = ± .010
LINEAR DIM. ARE IN INCHES	
ANGULAR TOL EXCEPT SHEET METAL FLG ± 0° 30'	
MFG ACCEPTANCE TOL PER	
FINISH PER	
ODD DASH NO SHOWN EVEN DASH NO. OPPOSITE	
FOR USAGE DATA SEE APPLICATION LIST	

CONTRACT NO

DRAWN	K. JEFFORS	6/2/76
DESIGN		
CHECKED		
PROGRAM	M. JACOBSEN	1/11/76
NORTHROP APPROVAL		
OTHER APPROVAL		

NORTHROP Northrop Corporation Aircraft Division 3901 West Broadway Hawthorne, California 90250

SHAKER FATIGUE SPECIMEN

SIZE	CODE IDENT NO	
H	76823	SR008002

SCALE FULL SHEET 1 OF 1

SR008002 A

3

TABLE 3. TENSILE TEST RESULTS OF 7075-T6 COUPONS

SPECIMEN IDENTIFICATION	THICKNESS	YIELD, 0.2% OFFSET	ULTIMATE STRENGTH	ELONGATION	YOUNG'S MODULUS
	(inch)	(ksi)	(ksi)	(%)	(psi)
A-1	.032	78.3	87.4	13.5	10.2×10^6
A-2	.032	77.0	85.7	14.0	9.8×10^6
A-3	.032	77.0	85.7	14.0	9.7×10^6
A-4	.032	77.8	85.0	14.5	10.4×10^6
A-5	.032	77.7	84.6	13.5	10.2×10^6
A-6	.032	78.4	85.6	13.0	10.1×10^6
B-1	.040	74.4	81.7	15.0	9.7×10^6
B-2	.040	74.4	81.9	13.5	9.6×10^6
B-3	.040	74.8	82.2	14.0	9.6×10^6
C-1	.050	78.1	85.3	14.0	9.7×10^6
C-2	.050	78.1	85.5	15.0	9.6×10^6
C-3	.050	78.3	85.3	15.0	9.4×10^6
D-1	.063	79.5	86.5	13.5	9.5×10^6
D-2	.063	80.6	87.7	13.5	9.8×10^6
D-3	.063	80.5	87.3	14.0	9.7×10^6

TABLE 4. LAP SHEAR TEST DATA IN ACCEPTING THE FM73 ADHESIVE

SPECIMEN DESIGNATION	MAXIMUM LOAD	ULTIMATE STRENGTH
	(lb)	(psi)
FM73-1	2,850	5,700
FM73-2	3,000	6,000
FM73-3	3,110	6,220
FM73-4	2,910	5,820
FM73-5	3,260	6,520
FM73-6	3,060	6,120
FM73-7	3,180	6,360
FM73-8	3,140	6,280

The metal surface preparation (for bonding) consisted of a phosphoric acid anodize treatment that conforms to the Boeing Process Specification BAC-5555. The priming with the BR127 primer conformed to the Northrop Process Specification MA-108. The phosphoric acid anodize treatment and

the priming were performed in the Long Beach facility of McDonnell Douglas Aircraft Corporation by Douglas Aircraft Company personnel. The details to be bonded for the acoustic and shaker test program were phosphoric acid anodized in accordance with Douglas Process Standard (DPS) 11.08 and the adhesive primer application was in accordance with DPS 1.950 (Process Engineering Order D-001C). Crack wedge tests and lap shear tests were successfully performed on test specimens to demonstrate that the surface preparation and BR127 primer application met minimum requirements. After the primer was applied to the acoustic and shaker test specimen parts, they were wrapped with clean chemically neutral paper and returned from McDonnell Douglas to Northrop. Following delivery of the primed details to Northrop, all of the parts were handled with clean white gloves to avoid contamination of the primed surfaces prior to bonding.

The storage time (i.e., from the primer application to the bonding at Northrop) was up to approximately eleven days. The bonding (at Northrop) of the (picture frame) edge doubler and the simulated frames and longerons to the skin of the acoustic test panels was performed in a one stage cure cycle. The acoustic test panels were individually processed through the autoclave (i.e., there was no simultaneous bonding of different acoustic test panels). On the other hand, all the beam specimens for shaker tests were bonded simultaneously.

The phosphoric acid anodize treatment and primer application were performed in three different runs at approximately two week intervals. In the first run, the parts for panels A-3-1 and A-3-2 and all the beam specimens were prepared for bonding. In the second run, the parts for panels A-4-1, A-4-2, A-5-1, and A-5-2 were prepared for bonding. In the third run, the parts for panels A-1-1, A-1-2, A-2-1, and A-2-2 were prepared for bonding.

Prior to the phosphoric acid anodize treatment, primer application, and bonding of the initial acoustic test panels, an impression prefit was performed by using the non-adherent impression film FM-643-2 in place of the adhesive film. The verifilming was discontinued after it was ascertained that the panel designs and the fabrication of the parts caused no bonding problems. The cure procedure consisted of the following steps:

(1) Apply full vacuum

(2) Apply 50 psi autoclave pressure

(3) Vent vacuum bag to atmosphere

(4) Raise temperature from ambient to 225F in a maximum of 120 minutes

(5) Maintain temperature at 225F to 250F for a minimum of 90 minutes

(6) Cool to 150F or lower under pressure

Following the bonding, nondestructive inspection (NDI) was conducted on the bonded acoustic panel structure utilizing the Erdman Nanoscope 412 with a B&C Scan Attachment Model 512. The data display was obtained on a Textronic Storage Display Unit Type 611. The C-scan records provided evidence of satisfactory bonding. After the NDI inspection was performed, the remainder of the assembly of the test panels was completed. Photographs of the unstiffened side of typical panels are in Figures 5 and 7. Photographs of the stiffened side of the same panels (after acoustic testing) are in Figures 6 and 8, respectively.

The beam specimens of a given type were bonded as a stiffened plate assembly. Following the bonding, the stiffened plate was sectioned into stiffened beams of 2 inch width and the edges were deburred. The adequacy of the bonds of all beam specimens was confirmed with a Model Mark II Shurtronics Harmonic Bond Tester. In addition, the bonding of Specimen V-3-3 was also verified with a C-scan inspection. Photographs of the three types of stiffeners on the shaker specimens (i.e., tapered tee sections, untapered tee sections, and angle sections) are in Figures 9 through 12.

2.6 Strain Gaging of Panels for Acoustic and Shaker Tests

Micro Measurements WD-DY-250BG-350 strain gages were installed on the acoustic test panels and the beam specimens. Strain gage locations on the acoustic test panels are shown in Figure 13 and described in Table 5. No acoustic test panel was instrumented with all of the gages that are located in Figure 13. However, all acoustic test panels were instrumented with strain gage Nos. 1, 2, 3, 4, and 11.

Strain gage locations on the shaker test specimens with tee section stiffeners are shown in Figure 14. Strain gage No. 1 is on the skin, centered over the midplane of the web of the stiffener. The other strain gages in Figure 14 were on the skin and centered over the edge of a tee section stiffener flange. All of the beam specimens with tee section stiffeners were instrumented with strain gage Nos. 3 and 5.

Strain gage locations on the shaker test specimens with angle section stiffeners are shown in Figure 15. Strain gage A is centered above the edge of the stiffener's flat section that was bonded to the beam. Strain gage B was centered above the vertical leg of the angle stiffener and was nearly centered over the edge of the adhesive flash in contact with the curved portion of the angle stiffener.

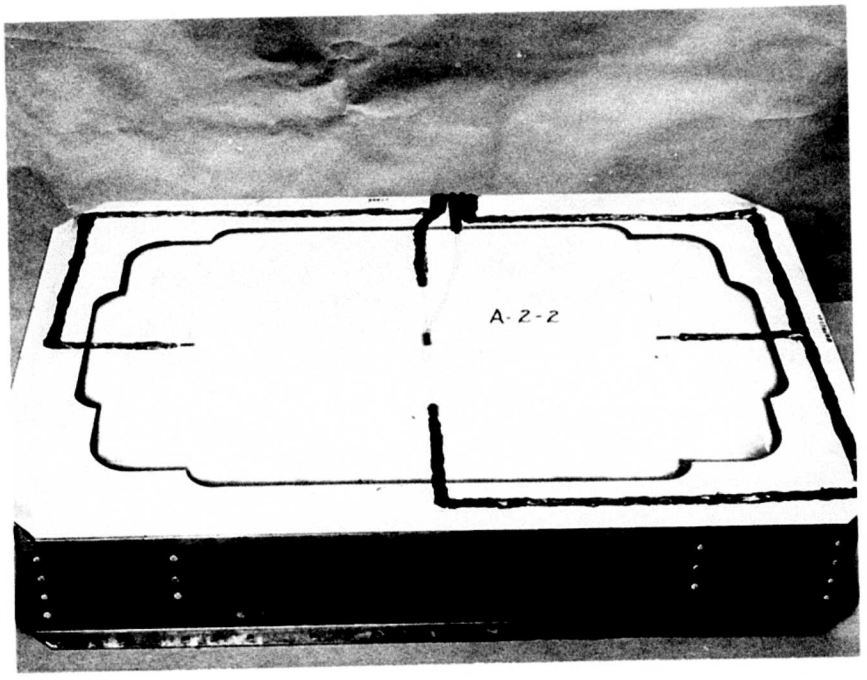

Figure 5. Unstiffened Side of Panel A-2-2

Figure 6. Stiffened Side of Panel A-2-2 (After Acoustic Test)

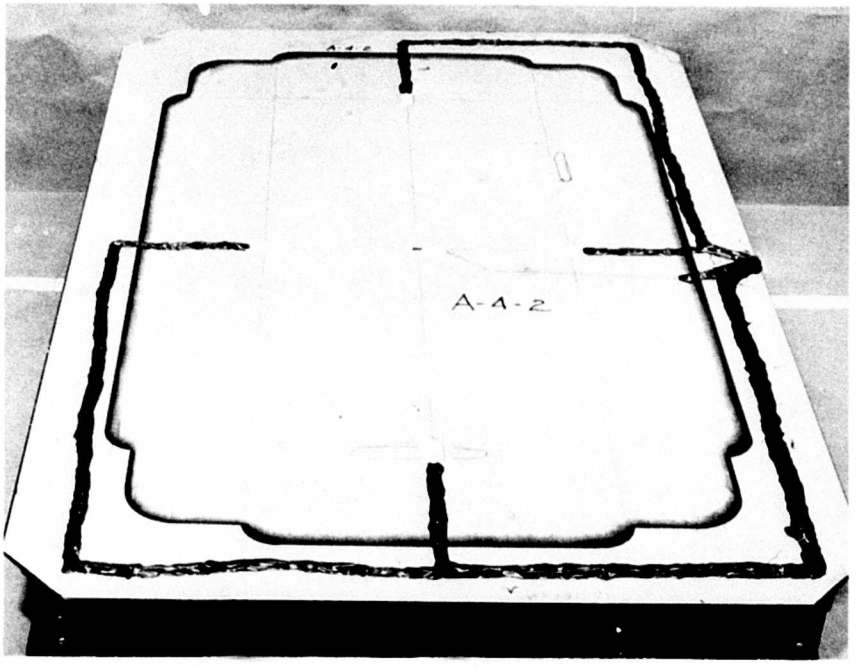

Figure 7. Unstiffened Side of Panel A-4-2

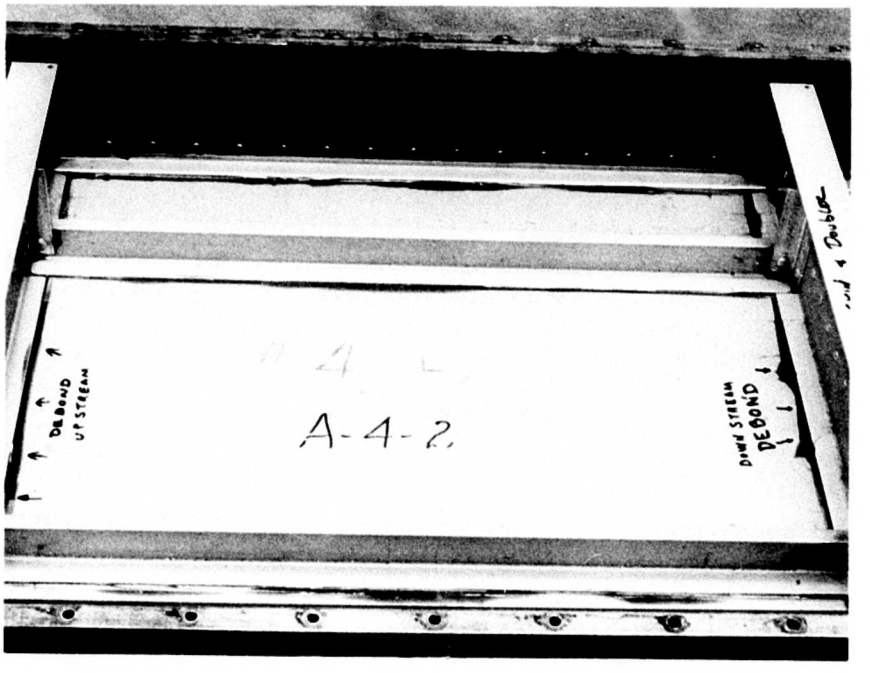

Figure 8. Stiffened Side of Panel A-4-2 (After Acoustic Test)

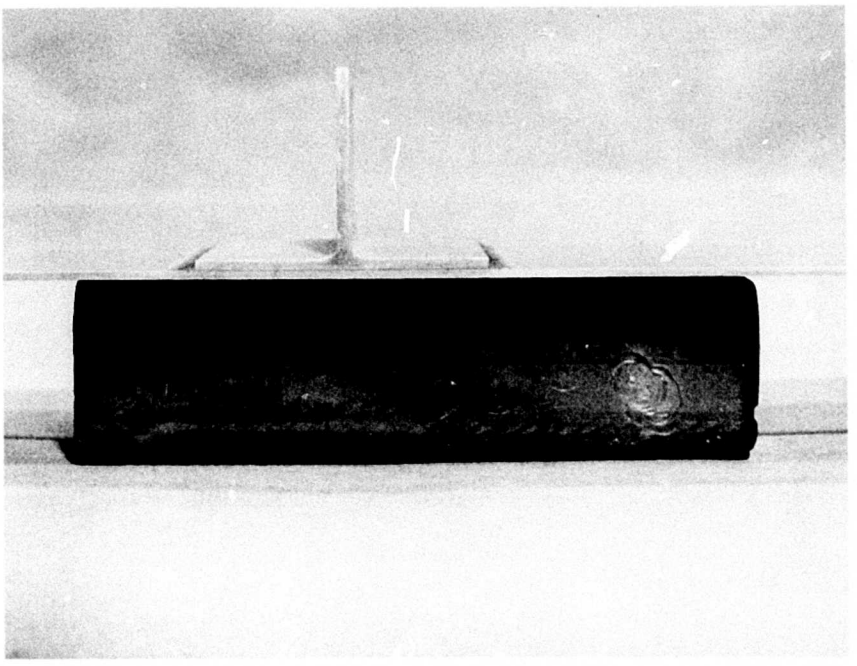

Figure 9. Beam Specimen with Untapered Tee Stiffener

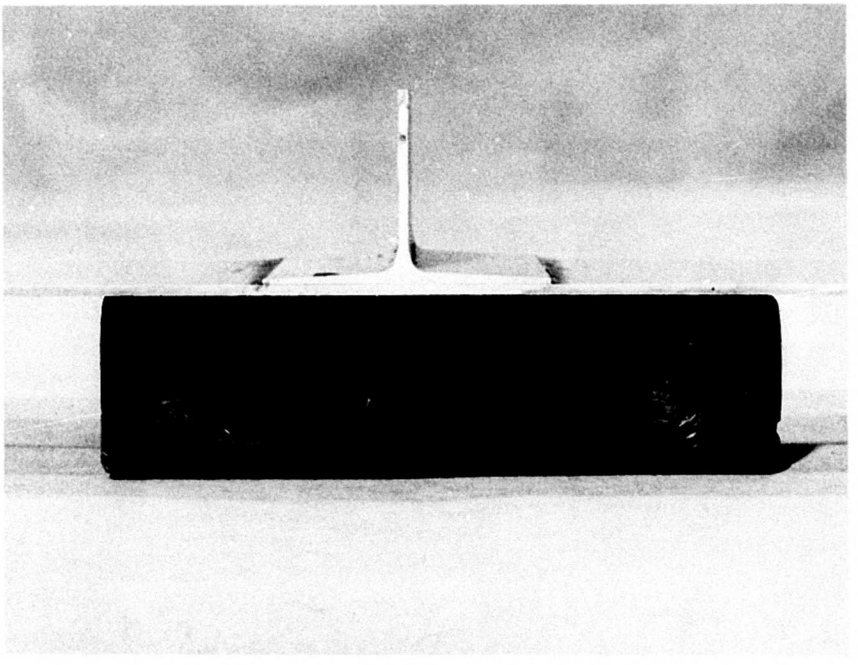

Figure 10. Beam Specimen with Tapered Tee Stiffener

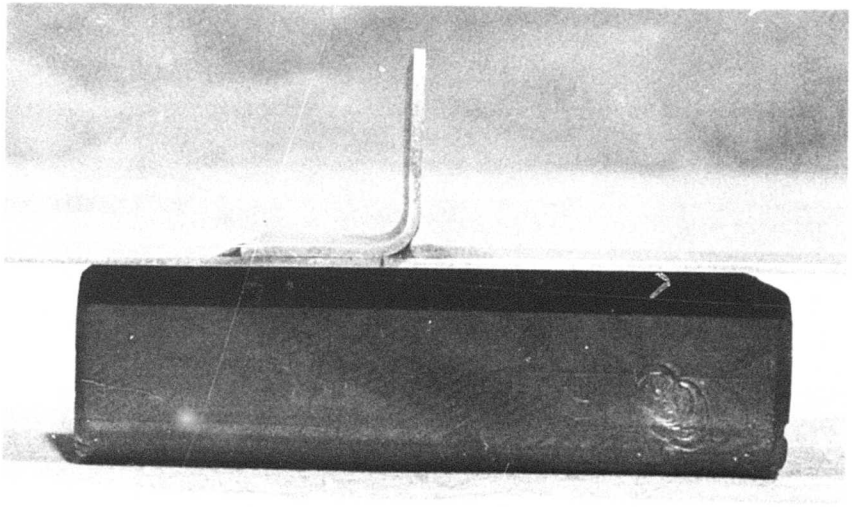

Figure 11. Beam Specimen with Angle Stiffener

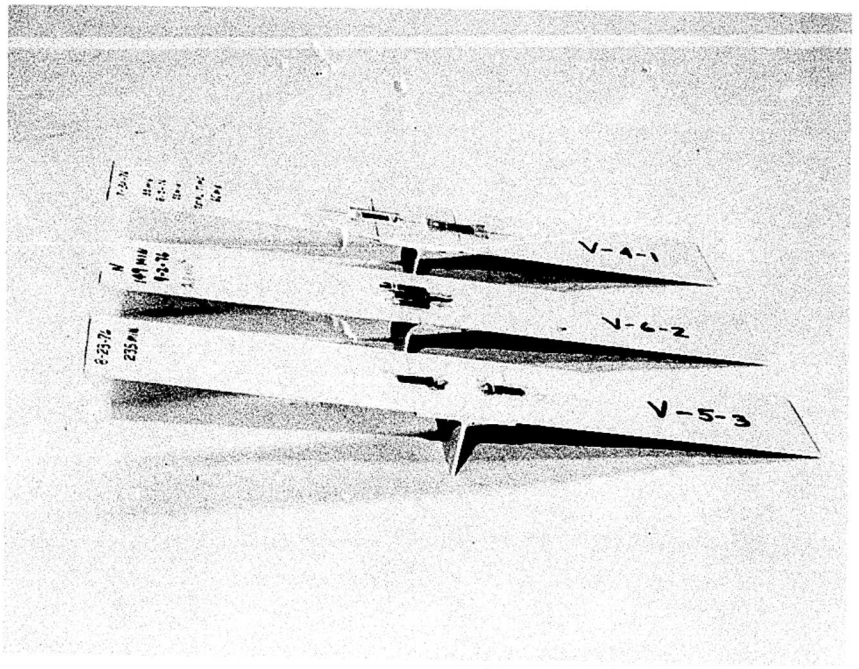

Figure 12. Three Types of Stiffened Beam Specimens

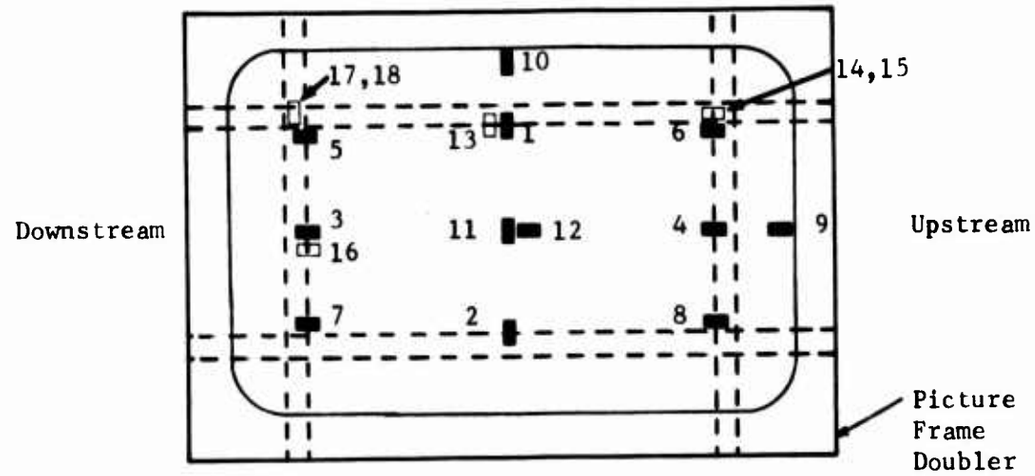

NOTE: Strain Gages No.1 through 12 on the exposed surface of the skins; No. 13, 14, and 15 on longerons; and No. 16, 17, and 18 on I-sections

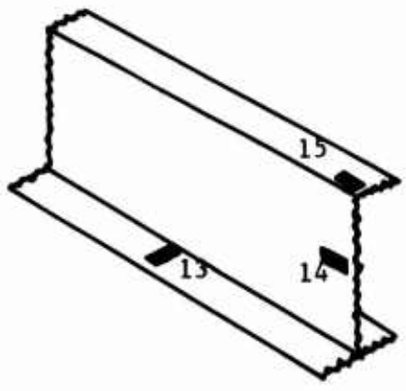

Longeron Section with Strain Gages

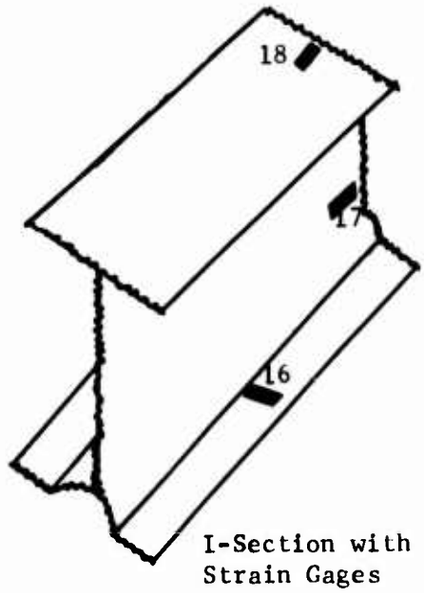

I-Section with Strain Gages

Figure 13. Strain Gage Locations for Acoustic Test Panels

TABLE 5. DESCRIPTION OF STRAIN GAGE LOCATIONS FOR ACOUSTIC TEST PANELS

STRAIN GAGE NO.	STRAIN GAGE LOCATION
1,2	Midway between I-sections and centered over the edge of the longeron that is in the center bay.
3,4	Midway between longerons and centered over the edge of the I-sections that is in the center bay.
5,6,7,8	At the I-section edge that is cut-away to permit passage of the longeron.
9	Midway between longerons and at the junction of the skin with the picture frame doubler.
10	Midway between I-sections and at the junction of the skin with the picture frame doubler.
11	Parallel to the I-sections and at the center of the acoustic test panel.
12	Parallel to the longerons and at the center of the acoustic test panel.
13	Midway between I-sections on the longeron flange that is in contact with the skin, and at the junction with the web of the longeron.
14	On the web of the longeron, midway between the flanges of the longeron, and at the connection of the longeron to the I-section.
15	On the free flange of the longeron and at the intersection of the longeron with the I-section.
16	Midway between longerons on the I-beam flange that is in contact with the skin, and at the junction with the web of the I-section.
17	On the web of the I-section, midway between the flanges of the I-section, and at the connection of the I-section to the longeron.
18	On the free flange of the I-section and at the intersection of the I-section with the longeron.

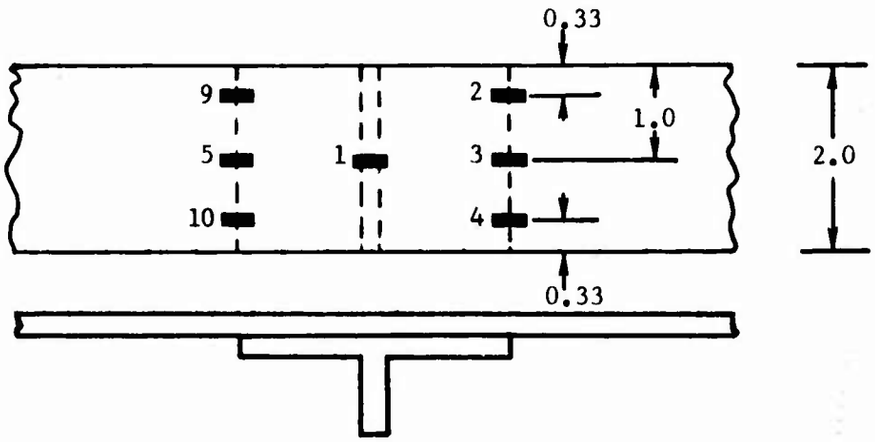

Figure 14. Strain Gage Locations for Shaker Test Specimens with Tee Section Stiffeners

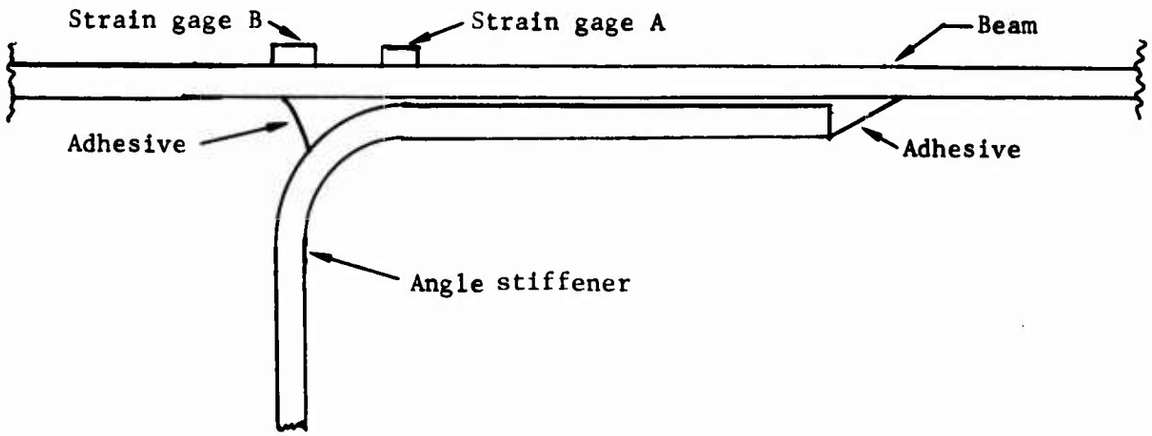

Figure 15. Strain Gage Locations and Schematic of Adhesive Flash for Shaker Test Specimens with Angle Stiffeners

2.7 Fixture Design and Boundary Conditions of Specimens in Acoustic and Shaker Tests

In previous sonic fatigue test programs conducted in the Northrop Progressive Wave Test Chamber, acoustic panels were attached to a test fixture (e.g., the jig plate in Figure 16) which fits into the upper wall of the 48- by 48-inch test cell (Figure 1). A motivation for using this type of fixture design was to obtain fatigue failures in the central bay region of the nine-bay cross-stiffened test panels rather than in edge members. For this program, the jig plate shown in Figure 16 was modified by replacing the 8 small holes with two larger holes that were each 11 inches square providing a minimum porting area of 240 square inches. In addition, a three-foot high termination box was fabricated and installed above the jig plate porting which leads to the stiffened side of the acoustic test panel. A schematic of an acoustic test panel, the jig plate, and the test cell termination box is shown in Figure 17. The termination box was constructed from one-inch plywood and was lined internally with open cell polyurethane foam of four-inch thickness.

The fixture design and boundary conditions for the beam tests with shaker excitation were the same as used under Contract F33615-70-C-1463. The webs of the stiffeners of the beam were clamped to the shaker assembly during the shaker tests (Figure 18).

Test Panel, Jig Plate, and Filler Blocks

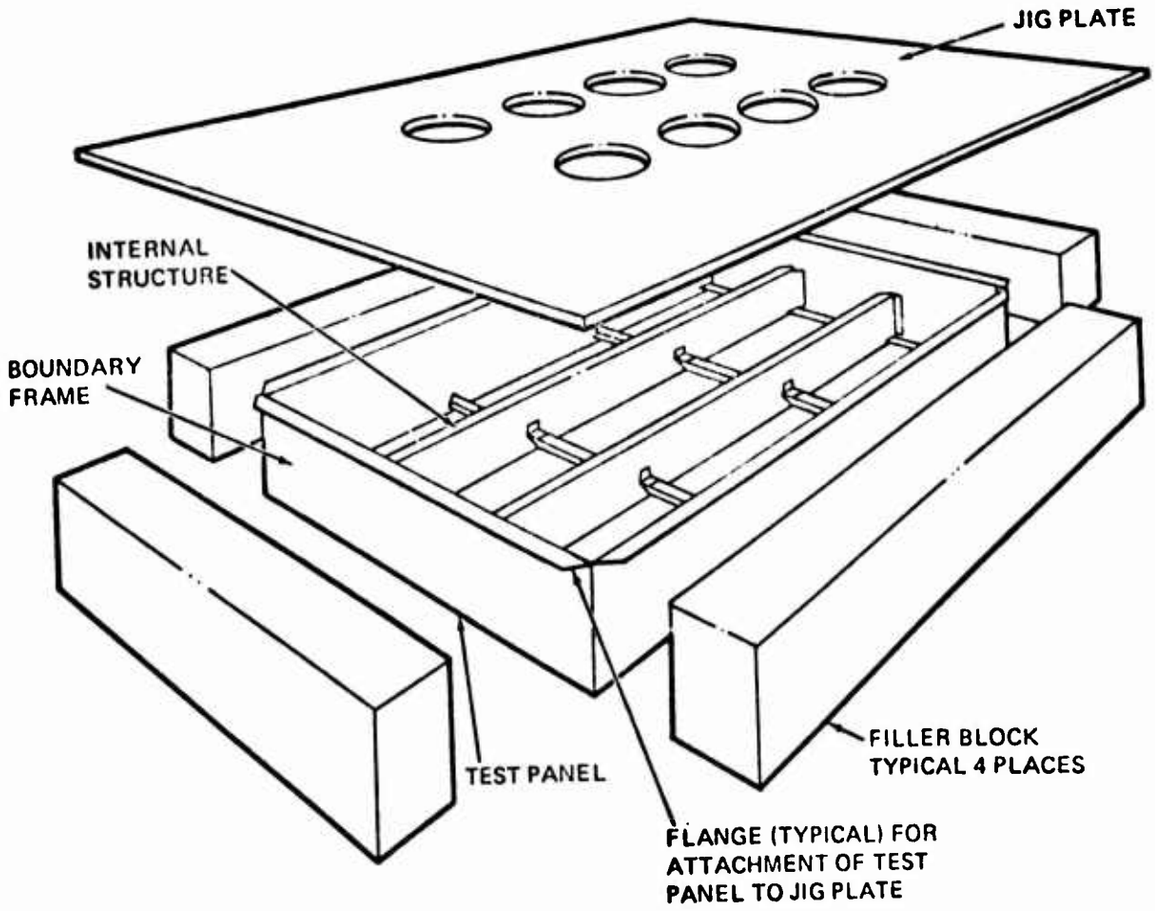

Progressive Wave Test Cell

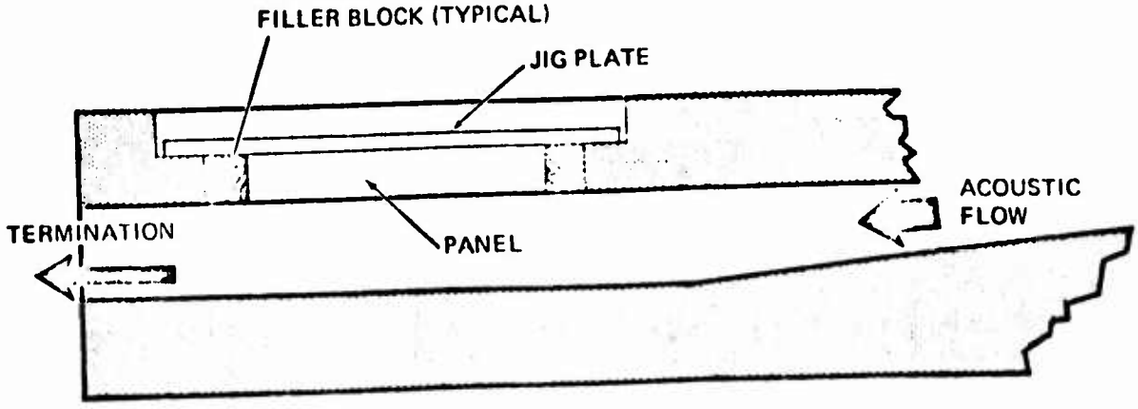

Figure 16. Nine-Bay Acoustic Panel and Its Location in the Progressive Wave Test Cell

NOTE: the termination box is the structure above the jig plate.

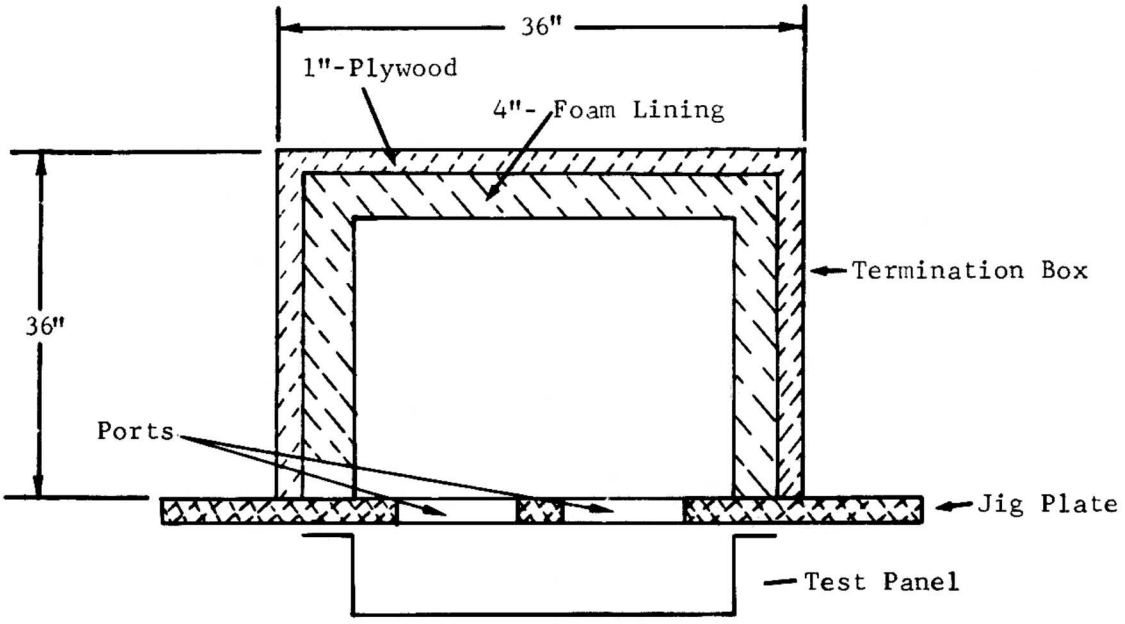

Figure 17. Schematic of Termination Box

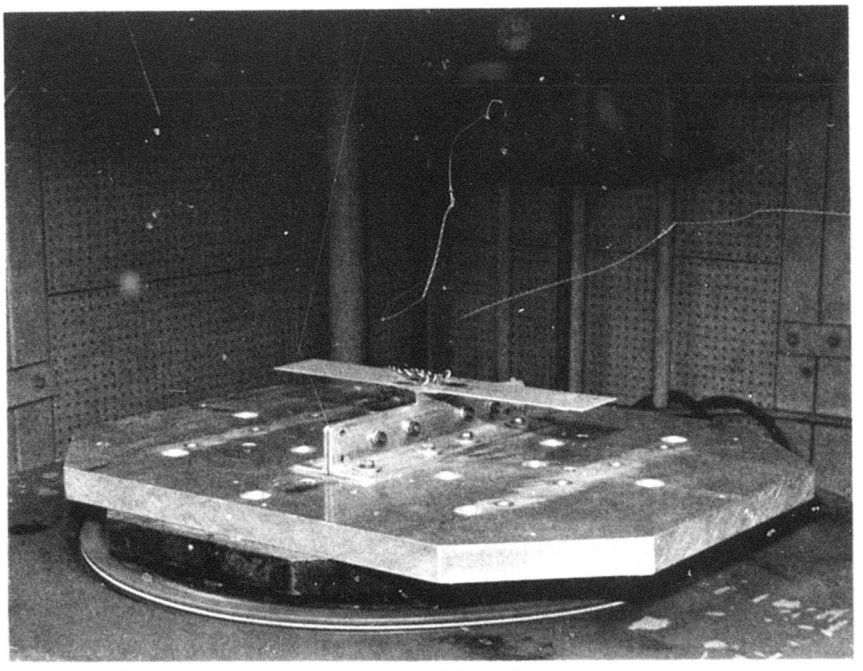

Figure 18. Clamping of Beam for Shaker Testing

2.8 Pressure Measurements During the Acoustic Tests Prior to the Conduct of This Test Program

Numerous tests were performed to determine the acoustic pressure distribution at various locations in the 24- by 24-inch test cell (e.g., Reference 3) and the 48- by 48-inch test cell (e.g., Reference 4) of the Northrop Progressive Wave Acoustic Test Chamber. During these tests, the pressure was recorded on magnetic tape and then analyzed to obtain the auto-correlation and cross-correlation functions. As a consequence of the experimental data, which showed a high degree of spatial uniformity, in this program Northrop measured the overall pressure at the center of the 24- by 24-inch test cell and the 48- by 48-inch test cell with concrete plugs in both cells to get a one-to-one relation - i.e., a calibration chart between the pressure at these two locations. Then during acoustic tests with panels in the 48- by 48-inch test cell (where all acoustic tests were performed), the pressure was measured at the center of the upstream 24- by 24-inch test cell to obtain the data that was then used with the calibration chart to obtain the pressure at the center of the 48- by 48-inch test cell.

2.9 Acoustic Test Procedure

The key aspects of the test procedure follow.

1. Instrumentation. The essential components of the instrumentation system employed in the program are shown schematically in Figure 19.

2. Recording and Data Analysis. All acoustic measurements were made with condenser microphones, with the associated carrier amplifiers and power supplies. Acoustic signals and displacement probe indications were analyzed and recorded by a B&K, Type 3315, Audio Frequency Spectrum Recorder System. A Spectral Dynamics Real Time Analyzer (SD 301 C) with its one-octave and 1/3-octave band converter, was also used to monitor the environment and the specimen responses. Strain gage outputs from selected runs were recorded on 1-inch magnetic tape and analysis of data was made by the B&K and by a constant bandwidth analyzer system for power spectral density.

3. Modal Surveys. Northrop conducted modal surveys on the panel using the "salt" pattern technique that has been often used in numerous experimental programs. The salt pattern technique consists of mounting a loudspeaker over the surface of a panel that is mounted in the fixture before the fixture is placed in the test cell of the progressive wave test chamber, sprinkling noncorrosive polyvinyl chloride pellets on the flat surface, and energizing the speaker with discrete frequency excitation. Using this well-known procedure, the nodal lines and experimentally determined natural frequencies were observed using acceleration and strain gage data.

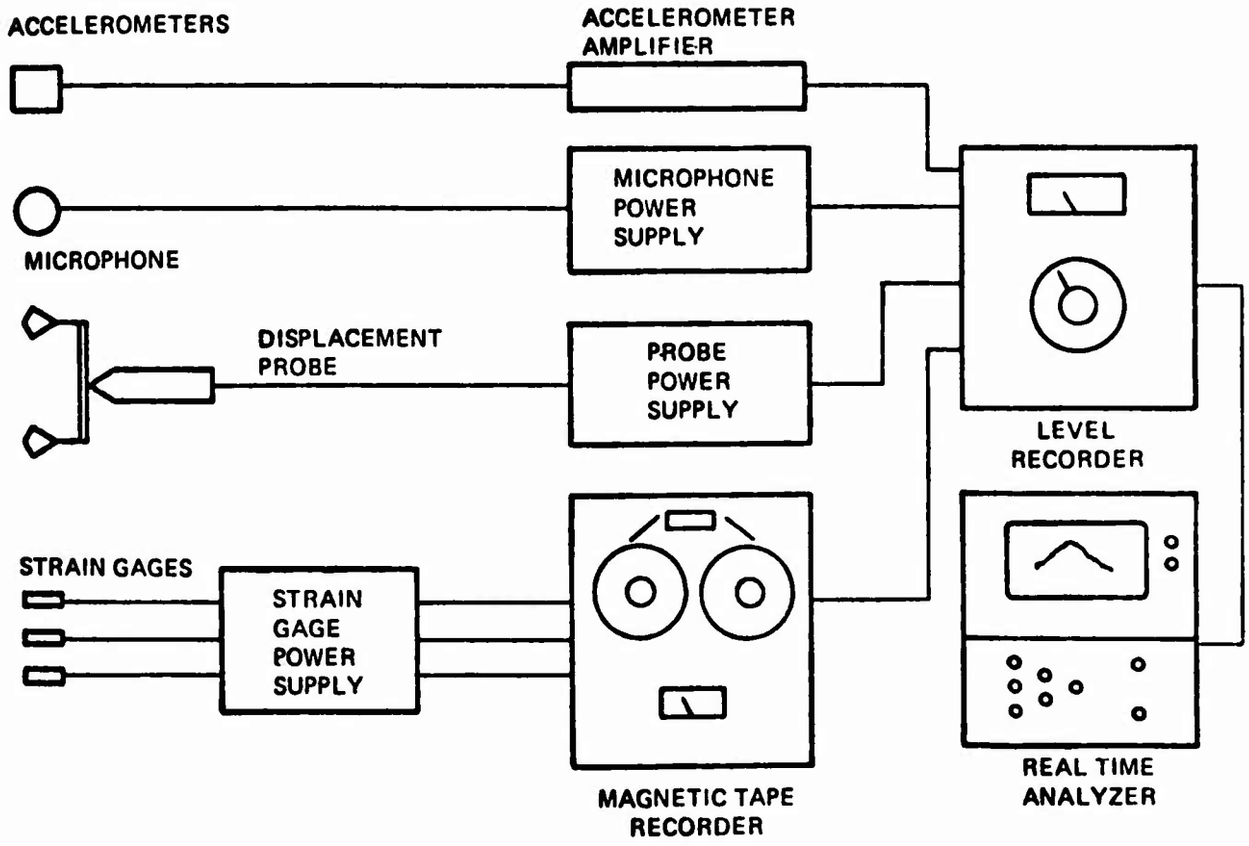

Figure 19. Instrumentation - Schematic Diagram

4. Panel Installations in the Acoustic Test Chamber. Figures 20 through 23 show different stages of the mounting of an acoustic panel on the jig plate and installation into the progressive wave test chamber. The panel attachment to the jig plate is shown in Figure 20. The attachment of wooden fillers to produce a relatively smooth surface for the acoustic flow is shown in Figure 21. The jig plate porting (venting) is shown in Figure 22. The termination box mounted over the vented jig plate is shown in Figure 23.

5. Damping Factors. Northrop obtained damping factors for the panels with the logarithmic decrement method utilizing the oscillograph decay record taken from the strain gage signals under loud speaker excitation and low level discrete frequency testing in the progressive wave test chamber. To obtain a resonant frequency, the SPL was held constant while the excitation frequency was varied to obtain the frequencies which produce the maximum quadrature voltage output from the strain gages. Damping decay records were made by sudden cessation of the excitation while tuned to each resonance of interest.

   To ascertain the degree which the jig plate and/or the blankets that have been used at Northrop to "seal off" the back surface of the jig plate in acoustic tests affects the apparent damping of the acoustic panel specimens, damping factors were obtained in some cases under loudspeaker excitation prior to and after the jig plate was connected to the panel specimen. Then, with the termination box and jig plate installed and the panel mounted in the progressive wave test chamber, damping factors were obtained for some panels under discrete frequency excitation. All discrete frequency excitation was of short duration and sufficiently low level to avoid producing any appreciable fatigue damage to the panel specimen.

6. Response and Fatigue Tests. After the modal surveys were completed and damping factors were obtained under low level discrete frequency excitation, the panel specimens were subjected to random acoustic loading at 136 db overall, and strain data were recorded. The sound pressure level was increased in increments of 3 db and data were recorded at each SPL until the level was reached for the sonic fatigue test. The SPL for the sonic fatigue test was the maximum SPL in the test cell. One purpose of the test procedure of increasing the SPL from 136 db to the final level was to observe if nonlinear effects were present. The testing at SPLs lower than the maximum test SPL was conducted rapidly in order to prevent undue exposure before the intended fatigue test commenced. Inspections were made as indicated under "Failure Detection" which follows, and the tests were halted once a fatigue crack was observed and recorded.

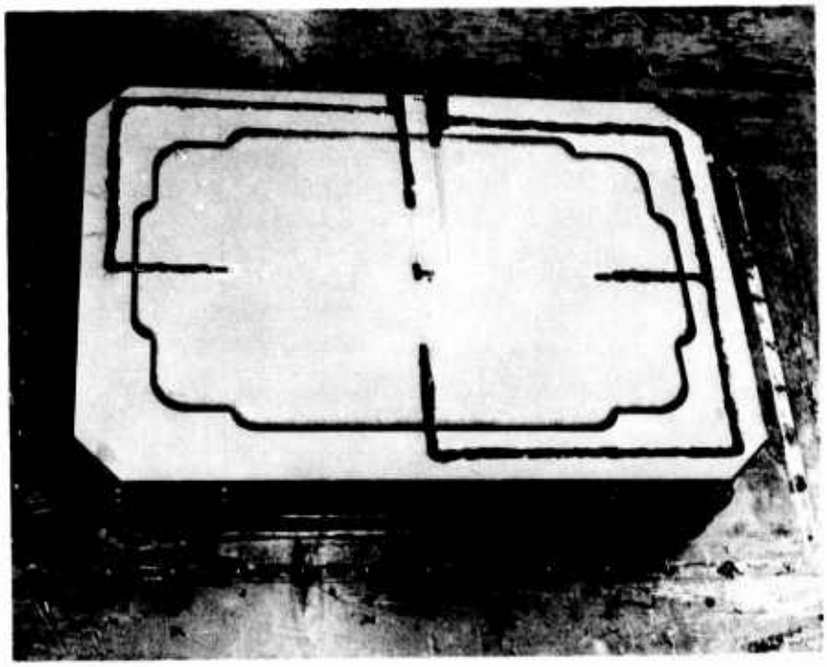

Figure 20. Acoustic Panel Attachment to Jig Plate

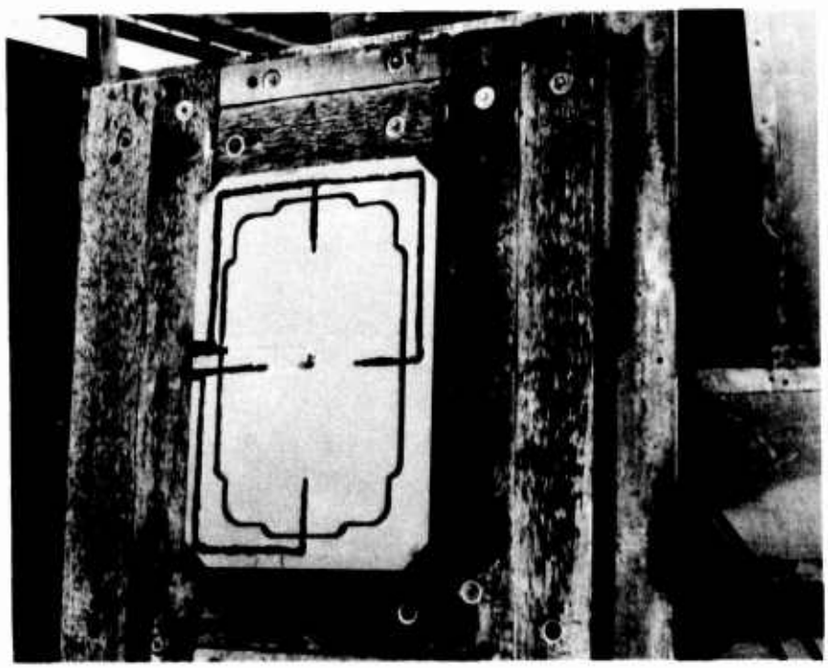

Figure 21. Attachment of Wooden Fillers to Jig Plate

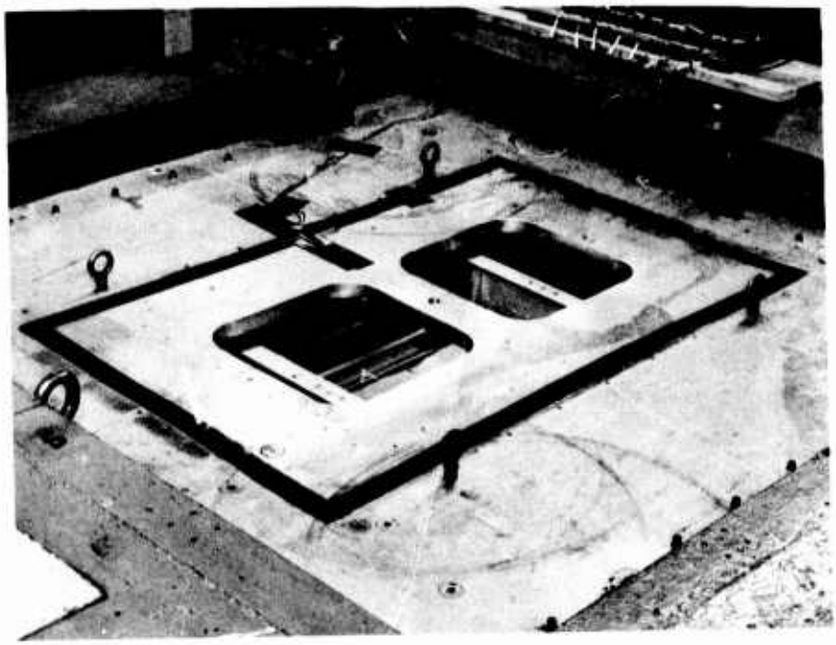

Figure 22. Jig Plate Porting

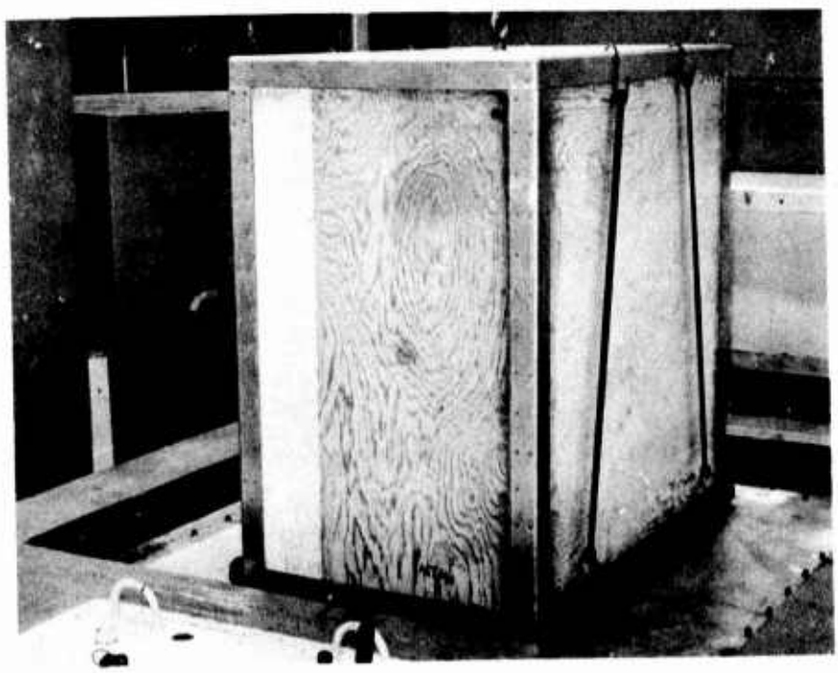

Figure 23. Acoustic Termination Box Installation

7. Failure Detection. Visual inspection was used as the primary determinant of fatigue failure. The visual inspections were conducted on a slicing schedule where the interval between inspections was related to accumulated test time. In addition, inspections were performed at any time in response to indicated changes noted in the response wave form or the spectral distribution of strain. Particular attention was given to tracking the predominant response frequency in the output of selected strain gages.

2.10 Shaker Test Procedure

Mechanical excitation of the beams was provided by mounting the specimens (singly) on a conventional laboratory shaker and applying narrow-band random vibration. Beam specimens V-3-6, V-3-7, and V-3-1 were tested to finalize the shaker test procedure and to obtain S-N data for determining the target strain level for the S-N tests of the remaining beam specimens. In addition to obtaining adhesive bond fatigue damage in the tests of the V-3-6 and V-3-7 beams, fatigue failures in the skin that originated in the longitudinal edges were experienced and attributed to notch effects along the edges of the skin. To prevent further fatigue failures from notch effects in shaker tests, all of the remaining beam specimens were ground throughout the length of all the longitudinal edges to obtain smooth edge surfaces.

The target strain in the fatigue tests was established on the basis of (1) the S-N data from specimens V-3-6, V-3-7, and V-3-1 and (2) the slope of an S-N curve obtained in shaker tests of bonded beams (without FM73 adhesive) under random excitation. From the S-N curve, it was surmised that a decrease in stress by 20 percent could lead to an increase in fatigue life by 3.8; conversely, insofar as producing fatigue failures were concerned, an increase in stress by 25 percent would lead to a decrease in fatigue life of 74 percent.

Specimens V-3-6 and V-3-7 were tested with measured rms strains maintained for 15 minute runs and increased from run to run in increments of 100 micro-inch per inch, rms to 1300 micro-inch per inch, rms. Based on the slope of the aforementioned S-N curve, the target strain of 1,000 micro-inch per inch, rms was selected for beam V-3-1 and the test life agreed satisfactorily

with the predicted life. The same method of predicting fatigue life was used in selecting the target strain (900 micro-inch per inch, rms) for specimens V-3-2, V-3-3, and V-3-4 and the test lives agreed satisfactorily with the predicted life.

Significant details of the shaker test procedure are described below:

1. Low level sinusoidal shaker excitation was applied to the specimen to determine (1) the resonant frequency (the second symmetrical bending natural frequency) for the fatigue test and (2) for the beam specimens with tee section stiffeners the higher of the rms strains at gages No. 3 and 5 (Figure 14). The higher strained gage of these two gages was then established as the control strain gage for the fatigue test of beams with tee sections. The control strain gage for the beams with angle section stiffeners was strain gage B (Figure 15).

2. Variable filters, band-limiting the white noise input signal, were adjusted to encompass 50 Hz and centered at the second symmetrical bending natural frequency of the beam. Test acceleration amplitudes were adjusted to produce the target strain response in the control strain gage at the beginning of the fatigue test.

3. After the target strain was reached for the S-N tests of the beam specimens in Table 2, the rms base acceleration excitation of the shaker was maintained for the remainder of the fatigue test (with the exception of shutdowns and restarts). Because the base acceleration was then the controlling factor in the S-N test, the strain in the control strain gage drifted from its initial value, because of fatigue damage in the FM73 adhesive bond and possibly elsewhere.

4. An accelerometer on the mounting fixture was used to servo-control the vibration amplitude. Strain gages and a noncontacting displacement probe were monitored to detect a change in the response of each specimen to warn of impending specimen failure.

5. During the fatigue tests, the rms strain of the strain gages and the frequency with the maximum power spectral density of strain of the control strain gage were recorded as a function of time. In general, the difference of rms strain between strain gages No. 3 and 5 of the beams with tee section stiffeners was less than six percent.

6. Changes in the character of the response natural frequency as shown on the real time analyzer were used to signal the operator to retune the input spectra to match the changing response characteristics of the specimen. In addition, on-line power spectral density plots of the input acceleration and response strain were monitored to ensure that the half power points of the response strain remained well encompassed by the 50 Hz bandwidth of the shaker excitation. A typical input and response PSD is shown in Figure 24. Note that the bandwidth of the strain response not only is significantly less than the bandwidth of the base acceleration imparted to the beam specimen, but also is included within the latter bandwidth.

7. Fatigue tests (excluding specimen V-3-6) were terminated when a fatigue failure in the bond was clearly visible as a separation between the skin and flange of the stiffener during the fatigue test.

2.11 One-Third Octave Band and Narrow Band Data Analysis

Narrow band strain and acoustic pressure plots were obtained from analyzing 32 ensemble averages of one second duration each with a 1.6 Hz bandwidth to 500 Hz. One-third octave band plots of strain and acoustic pressure were obtained from analyzing 32 ensemble averages of one second duration each to 500 Hz.

ENGINEER	Northrop Corporation Aircraft Division	PAGE
CHECKER 27 MAY 76		REPORT NO.

SPECIMEN .050 T SERIAL NO. V-3-7

TEST CONDITION

LOCATION G1 / BASE ANALYZER BANDWIDTH 1.6 HZ

AXIS OVERALL 1000 με 18.7 g RMS

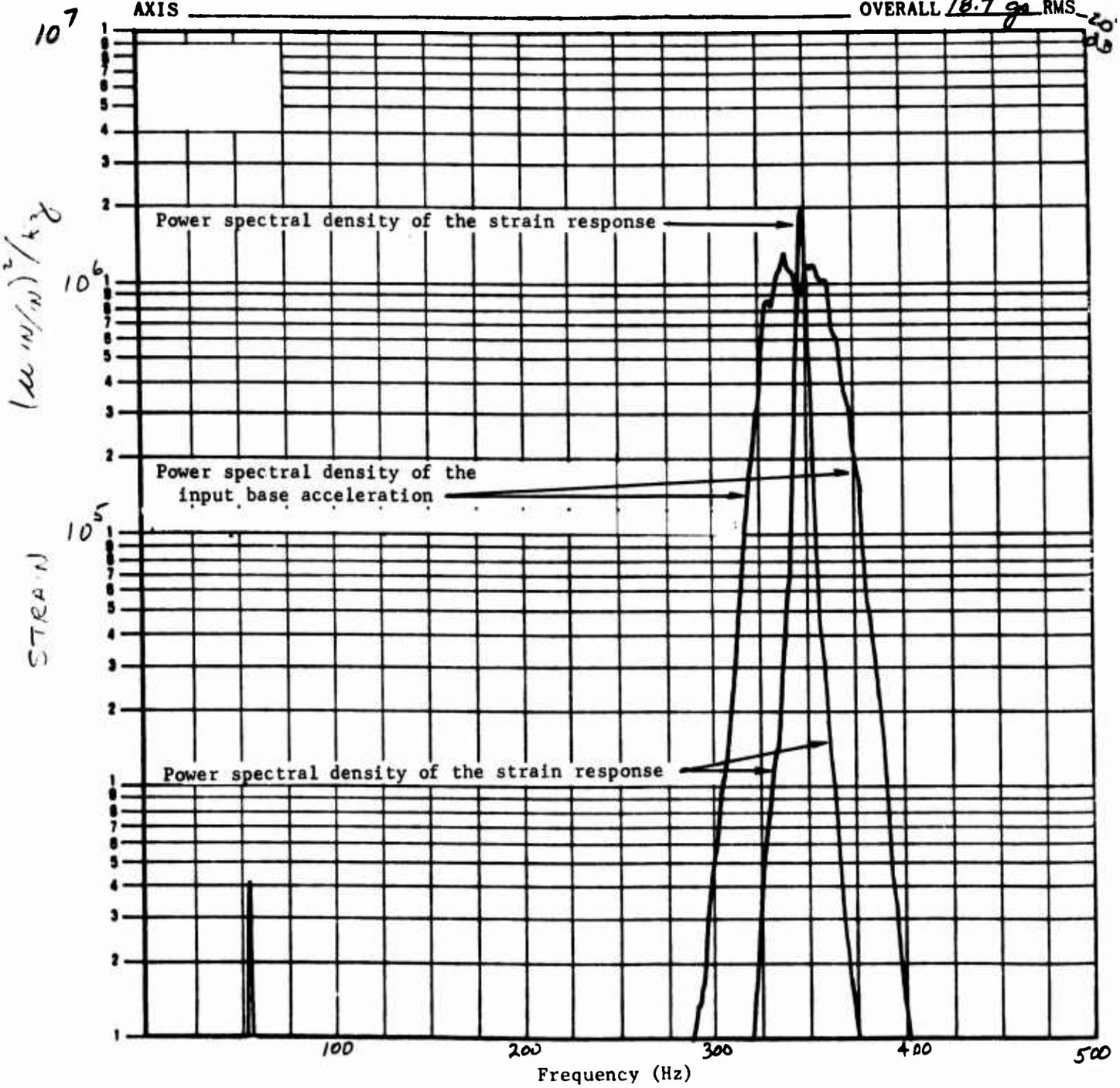

Figure 24. Typical Power Spectral Densities of Strain Response and Input Forcing Function for a Shaker Test Specimen

6

Form 21-143 (5-74)

SECTION III

SHAKER TEST RESULTS

3.1 Frequency and Strain Versus Time

During the shaker tests, the rms acceleration of the base of the shaker remained essentially constant throughout a fatigue test. During the initial portion of a fatigue test with a target rms strain of 900 micro-inch per inch, the strain at the control gage of the test beams increased from the target strain that existed at the beginning of the fatigue test. The rms strain at the control strain gage then peaked and decreased throughout the remainder of the fatigue test, excluding minor strain shifts resulting from occasional shutdowns and restarts. The increase in strain during the initial portion of the fatigue test was attributed to bond deterioration in the adhesive flash outboard of the strain gage elements. The subsequent decrease in rms strain was attributed principally to the adhesive bond deterioration between the stiffener and the flange.

A typical history of frequency and strain versus time (specimen V-3-4) is given in Table 6. The frequencies in Table 6 are the frequencies with the maximum power spectral density of the strain at the beginning of the incremental period of shaker excitation. A bond fatigue failure in specimen V-3-4 was experienced at 300 minutes of exposure. Strain readings were taken at regular intervals; however, the specimen was retuned at irregular intervals, namely, when the frequency shifted by approximately 3 Hz. As was the case of specimen V-3-4, a sharp drop in rms strain was noted near the end of the fatigue test of several beam specimens.

In the tests of beams with tee section stiffeners (i.e., the V-1 through V-5 sets of beams), the base acceleration of the shaker was set to produce 900 micro-inch per inch, rms strain at a strain gage on the beam and centered above an end of the flange of the tee section stiffener. Each specimen had more than one gage that fits the above description, and in general, the deviation in the strain readings from one gage to the other(s) differed by less than approximately six percent.

During the shaker excitation of the beam specimens, the observed response was always in the bending mode without twisting. Strain gage data from gages No. 2, 3, 4, 5, 9, and 10 (Figure 14) confirmed the visual observation.

TABLE 6. FREQUENCY AND STRAIN VERSUS TIME FOR SPECIMEN V-3-4

STRAIN	CUMULATED TEST TIME	FREQUENCY	TEST TIME	
			INCREMENTAL	CUMULATIVE
(micro-inch per inch, rms)	(min)	(Hz)	(min)	(min)
900	1	352	15	15
920	15	350	42	57
950	30	347	10	67
900	60	346	38	105
930	90	342	19	124
900	105	340	41	165
860	120	338	15	180
840	135	337	15	195
810	165	334	25	220
780	195	333	20	240
750	210	331	15	255
740	240	330	30	285
680	255	327	5	290
660	300	325	10	300
		325	0	300

At the beginning of the fatigue tests of a beam with an angle stiffener, the strain reading of Gage A (Figure 15) was significantly below the strain reading of Gage B. This indicated a significant stiffening effect by the adhesive in the flash area above the vertical leg of the angle. Strain readings that were recorded during the fatigue test of specimen V-6-3 are presented in Table 7. From the data, it is deduced that as the adhesive bond deteriorated in the flash zone, the beam at Gage A was subjected to increasing strains until 940 micro-inch per inch, rms was reached. The drop in strain thereafter was indicative of further bond deterioration between the flat surfaces of the beam and the flange of the stiffener.

TABLE 7. STRAINS IN SPECIMEN V-6-3

TIME	STRAIN	
	GAGE A	GAGE B
(min)	(micro-inch per inch, rms)	(micro-inch per inch, rms)
0	220	900
120	240	950
210	600	950
240	940	820
309	610	730

3.2 Fatigue Data from Beam Tests

Fatigue data obtained with the narrow band random shaker excitation are summarized in Table 8. The fatigue lives in the shaker tests were computed by two different methods that produced approximately the same lives for a particular specimen. In one method, the life was computed as

$$N = \Sigma f_i \Delta t_i \qquad (1)$$

with f_i being the predominant response frequency in the i^{th} time interval and t_i being the duration of the i^{th} interval. In the other method, the life was obtained as the product of the frequency at the midpoint of the test times the fatigue life. The fatigue lives in Table 8 were computed on the basis of the latter method.

The resonant frequencies of the beams being excited at the beginning of the fatigue tests are listed in Table 8; also listed is the percentage drop of that natural frequency that was experienced during the fatigue test. The tests were terminated when separation of the skin and stiffener was clearly visible while shaker excitation was in progress. Other definitions of failure (e.g., a five percent drop in the natural frequency) could have reduced the degree of arbitrariness in terminating the fatigue tests. Except for specimen V-3-1, the base acceleration of the shaker was chosen to produce a 900 micro-inch per inch, rms strain at one end of the bonded joint at the beginning of fatigue tests of specimens listed in Table 8.

3.3 Evaluation of Beam Fatigue Data

The fatigue lives versus skin thickness of some of the beams that were tested were unexpected. For example, it had been anticipated that as the skin thickness of the beams decreased, the fatigue life (i.e., cycles to failure) of the adhesive bonds would increase, because less bending moment, and hence less peel stress, would be transferred into the joint in the case of the thinner beams. However, these expected results were not always achieved.

Different explanations of the thicker beams having longer fatigue lives than the thinner beams were considered. One conceivable explanation was that the bonding was inferior in the thinner beams that failed sooner than were expected. However, that explanation was rejected, because all of the beam specimens were bonded at the same time in the same manner.

Another explanation relied heavily on the hypothesis that the combination of the skin thickness and the thickness of the scarfed flanges of the tee section stiffeners affects (i) the flexibility of the beams near the ends of the bonded joints and (ii) the ratio of bending moment to transverse shear that exists at the ends of the bonded joints during the shaker excitation. This explanation is discussed further in the following paragraphs.

TABLE 8. BEAM FATIGUE DATA RESULTING FROM SHAKER EXCITATION

BEAM DESCRIPTION		FREQUENCY		CONTROL STRAIN AT BEGINNING OF TEST BASE ACCELERATION	LIFE
IDENTIFICATION	SKIN THICKNESS	INITIAL	DROP		
	(inch)	(Hz)	(%)	(μ"/", rms)	(cycles)
V-1-1	0.032	228.4	6.3	900	7.0×10^6
V-1-2	0.032	230.2	8.3	900	5.2×10^6
V-1-3	0.032	231.0	6.5	900	3.8×10^6
Average	0.032	230.0	7.0	900	5.3×10^6
V-2-1	0.040	286.6	10.3	900	3.1×10^6
V-2-2	0.040	288.0	5.9	900	3.3×10^6
V-2-3	0.040	288.5	9.5	900	2.9×10^6
Average	0.040	287.7	8.6	900	3.1×10^6
V-3-2	0.050	350.4	6.4	900	6.0×10^6
V-3-3	0.050	351.0	8.0	900	7.0×10^6
V-3-4	0.050	351.4	7.8	900	6.1×10^6
Average	0.050	351.3	7.4	900	6.4×10^6
V-4-1	0.063	437.8	9.3	900	1.6×10^6
V-4-2	0.063	440.5	7.8	900	1.8×10^6
V-4-3	0.063	438.8	6.6	900	1.2×10^6
Average	0.063	439.0	8.2	900	1.5×10^6
V-5-1	0.050	356.4	7.7	900	4.0×10^6
V-5-2	0.050	356.6	8.0	900	6.0×10^6
V-5-3	0.050	357.0	8.0	900	4.8×10^6
Average	0.050	356.7	7.9	900	4.9×10^6
V-6-1	0.050	330.8	9.1	900	0.6×10^6
V-6-2	0.050	329.0	10.9	900	2.8×10^6
V-6-3	0.050	329.8	8.0	900	5.0×10^6
Average	0.050	329.9	9.3	900	2.8×10^6
V-3-1	0.050	349.5	5.4	1000	2.9×10^6

In the second symmetrical natural bending mode of the beam specimens bonded to a tee section stiffener and clamped at the outstanding leg of the stiffener, each half of the beam may be considered as a beam that is clamped at one end and free at the other end. The second natural bending frequency of a clamped-free beam of uniform thickness (Reference 10) is

$$f = \frac{1}{2\pi}\left(\frac{4.694}{L_o}\right)^2\left(\frac{EI}{\rho}\right)^{1/2} \qquad (2)$$

For rectangular beams of thickness h, length L_o, weight density of 0.100 lb/in^3, and Young's modulus of 10×10^6 psi, equation (2) may be cast into the following form for the natural frequency (in units of Hz)

$$f = \frac{19.89 \times 10^4\, h}{L_o^2} \qquad (3)$$

Because the deviation in the average value of Young's modulus (Table 1) of a particular set of tensile coupons (in this test program) of a given thickness from the average value of Young's modulus for all the coupons was less than 2.5 percent, only one value of Young's modulus was used in deriving Equation (3).

Using Equation (3), natural frequencies of beams of length 5.2 inches and 6.0 inches were calculated on the basis of skin thicknesses of 0.032 inch, 0.04 inch, 0.05 inch and 0.063 inch. The reasons for selecting lengths of 5.2 and 6.0 inches were that one-half of the length of the test beams with tee section stiffeners was 6.0 inches and the distance from the end of the skin of a beam with a tee section stiffener to the flange of the stiffener was 5.2 inches. The frequencies obtained with Equation (3) are in Table 9, which also includes the average initial test frequency of a set of specimens from Table 8 and the ratio of the average initial test frequency to the computed test frequency for beams with length equaling 5.2 inches. The test frequencies are considerably closer to the computed frequencies on the basis of a 5.2 inch length than a 6.0 inch length, which implies that the stiffener provides a large bending constraint to the unstiffened portion of the skin.

TABLE 9. COMPUTED AND TEST FREQUENCIES OF BEAMS

BEAM DIMENSIONS		FREQUENCIES		FREQUENCY RATIO
Thickness	Length	f_c = Computer	f_t = Test	f_c/f_t
(inch)	(inch)	(H_z)	(Hz)	
.032	5.2	235	230	1.02
.032	6.0	177	230	-
.040	5.2	294	288	1.02
.040	6.0	221	288	-
.050	5.2	368	351	1.05
.050	6.0	276	351	-
.063	5.2	463	439	1.05
.063	6.0	348	439	-

The stiffener flanges of the bonded beams with the thinner skins are somewhat more effective in producing a rotational constraint (for the unsupported skin) approaching the fully clamped condition than the flanges of the beams with the thicker skins. This is to be expected because the dynamic characteristics of the test beams with the thicker skins should be influenced the lesser amount by the presence of the flanges of the tee section stiffeners.

The implication from these considerations is that for the same target strain in all beam test specimens the radius of curvature and bending moment in the test beams are changing more rapidly in the vicinity of the end of bonded flanges of the thinner beams. Since transverse shear is

$$V' = \frac{dM'}{dx} \qquad (4)$$

the ratio of transverse shear effects to bending moment effects are probably greater at the ends of the bonded joints of the beams with the thinner skins. The transverse shear affects the peel stress at the end of the stiffener of the bonded joint because the adhesive flash outside the edge of the bonded flange was somewhat effective in transmitting load into the bonded joints. The principal tensile stress in the adhesive at the end of the stiffener flange depends both on the flatwise tensile stress and shear stress in the adhesive at that location and may be a more important parameter than the conventional peel stress (i.e., the extensional stress normal to the plane of the adhesive) in controlling the fatigue life of the bonded joint.

In view of all these factors, it may be deduced that at the edge of the bond between the skin and flange of the tee section stiffeners, the ratio of bending moment in the supported skin to the principal stress in the adhesive

may have been sufficiently different between the V-2 and V-3 sets of specimens to have resulted in shorter fatigue lives for the V-2 set of beam specimens even though the bending moment computed on the basis

$$M' = \frac{sh^2}{6} \qquad (5)$$

was less in the V-2 set of beams.

The fact that all natural frequencies (Table 8) of a given set of beam specimens at the beginning of the fatigue tests differ only slightly is indicative of the uniformity of the bonded joints of specimens within a set.

The average life (Table 8) of the V-3 set of beam specimens was higher (as expected) by approximately 30 percent than the average life of the V-5 set of beam specimens. The difference in the average fatigue lives of these two sets of specimens was attributed to stress concentration effects that resulted from the rectangular flanges of tee-section stiffeners in the V-5 set as opposed to tapered flanges of tee section stiffeners in the V-3 set.

The average frequency (Table 8) of the V-3 set of beam specimens was lower by approximately 2 percent than the average frequency of the V-5 set of beam specimens. This difference is also attributed to the difference in stiffener geometry between the two sets of beam specimens.

SECTION IV

ACOUSTIC TEST RESULTS AND MODAL DATA

4.1 Sonic Fatigue Failures in This Test Program

Sonic fatigue failures were obtained in the acoustic tests of all ten 9-bay acoustic test panels. The sonic fatigue tests were conducted with broad-band acoustic pressure at 166 dB overall SPL. The locations and modes of sonic fatigue failures are shown in the schematic drawings of Figure 25. The test lives and modes of failure are recorded in Table 10. All acoustic test panels except for panel A-3-1, which was the first acoustic panel tested, experienced bond failures. The cycles to failure were calculated as the product of the predominant response frequency and the acoustic exposure time at 166 dB overall SPL. The acoustic pressure spectrum level during the 166 dB runs are given in Table 10 and are based on one-third octave band acoustic pressure data and in some cases on narrow band data at the beginning of the sonic fatigue testing at 166 dB. Inasmuch as all strain gages did not have the same frequency for the occurrence of the peak in the strain PSD, the use of the spectrum level based on the 1/3 octave band acoustic pressure is recommended. Photographs of typical debond zones at the end of acoustic tests of two panels are shown in Figures 6 and 8.

The fatigue life data of the identical pairs of panels A-2-1 and A-2-2, panels A-4-1 and A-4-2 and panels A-5-1 and A-5-2 agree very well with each other. The absence of the -71 angles on panel A-3-1 may have been the principal cause of the different modes of sonic fatigue failures in panels A-3-1 and A-3-2. The difference in fatigue lives of panels A-1-1 and A-1-2 is not unusually large and may have resulted from differences in the coupling between the thin (0.032 inch thickness) skins of these panels with the substructure through the adhesive bonds.

TABLE 10. SONIC FATIGUE TEST LIVES AND FAILURE MODES

PANEL	SPECTRUM LEVEL[1]		TEST LIFE	MODE OF FAILURE
	"A"	"B"		
	(dB)	(dB)	(cycles)	
A-1-1	140	141	4.8×10^6	Bond
A-1-2	138	-	1.2×10^6	Bond
A-2-1	139	139	4.1×10^6	Bond
A-2-2	137	-	3.4×10^6	Bond
A-3-1	140	137	3.7×10^6	Stiffener at clip
A-3-2	138	-	10.5×10^6	Bond
A-4-1	141	141	2.5×10^6	Bond
A-4-2	140	-	2.5×10^6	Bond
A-5-1	140	140	6.3×10^6	Bond
A-5-2	140	-	5.3×10^6	Bond

(1) Spectrum level "A" is based on one-third octave band acoustic pressure data; spectrum level "B" is based on narrow band acoustic pressure data.

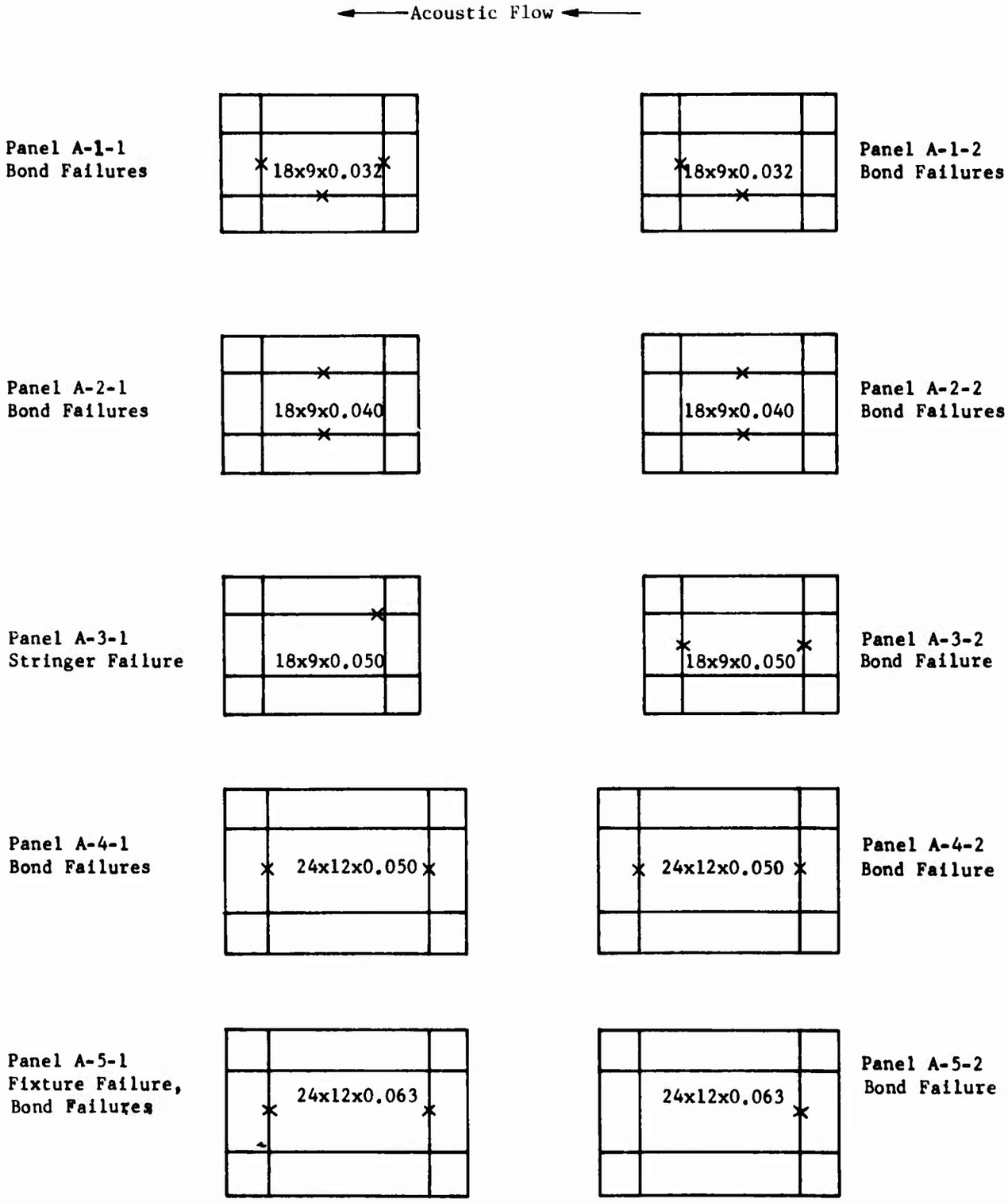

X denotes the general location of the sonic fatigue failure

Figure 25. Location and Mode of Sonic Fatigue Failures

The sonic fatigue failure obtained in the test of panel A-3-1 occurred in a J-section stiffener (Figure 26) and emanated from a rivet hole that was used in connecting the longeron to an angle clip that was riveted to an I-section frame. When the stiffener failure was detected, the sonic fatigue test of panel A-3-1 was halted in order to conduct first a harmonic bond inspection and then a C-scan inspection of the adhesive bonds. The NDI inspections disclosed no bond failures. Because the stiffener failure in panel A-3-1 may have been caused by the lack of the -71 stiffener on the I-section stiffeners, the -71 angle sections (Figure 2) were installed on all the remaining acoustic test panels with the 18 by 9 inch central bay. No further testing was performed with panel A-3-1.

The debond zones for all panels except panel A-5-1 were observed during an inspection period with the panel mounted on the jig plate. The method of inspecting for a debond zone was to press (by hand) against the unsupported skin of the central bay of the test panel in the absence of acoustic excitation to determine by eye if there was a separation between the stiffener and the skin at the bonded joint. Inspections with the harmonic bond tester were also made when the acoustic excitation was halted; however, no advance notice of a visible separation was obtained with the harmonic bond test method, although confirmation of a debond that was clearly visible with the unaided eye was obtained with harmonic bond tester.

The sonic fatigue test of panel A-5-1 was halted, primarily because of failures in the steel frame sections in the test fixture portion of the acoustic test panels. Furthermore, when the sonic fatigue test of panel A-5-1 was halted, there was reason to believe that there were impending sonic fatigue debond failures, because strains were drifting upwards in the sonic fatigue test. Contrary to the experience in the beam fatigue tests, it was observed in the acoustic panel tests that strains drifted upwards prior to a debond failure. This difference between beam and panel response may be attributable to the central bay of acoustic test panels being supported on all four edges, whereas the beams which were symmetric and clamped about the outstanding leg at the center of the beam had unsupported edges. It is to be noted that post-test calibrations (i.e., after the sonic fatigue tests) of the strain gages were not taken to compare with pre-test calibrations (i.e., before the acoustic loading), because the gages of interest were, in general, not functioning at the end of the tests.

After the sonic fatigue test of panel A-5-1 was halted, C-scan quality assurance tests with a Fokker Bond Tester (Mod 63), the Erdman Nanoscope, and a Holosonics Model 200 unit were performed to determine the quality of the adhesive bonds. The C-scan results were inconsistent in that no bond deterioration was detected with the Fokker and Erdman units, but bond deterioration was indicated by the Holosonics unit. Panel A-5-1 was then sectioned along its center lines into 4-sections. Visible separation between the skin and I-section stiffeners was then observed by pressing (by hand) the skin away from the I-section stiffeners to confirm the accuracy of the indications with the Holosonics unit. No debond between the J-section stiffeners and the skin were detected by the hand pressing or by any of the C-scan inspection methods.

The sonic fatigue test of panel A-1-1 was conducted at 166 dB overall SPL. During the sonic fatigue test in the 166 dB runs, visual inspections were made at the end of eight time intervals. At the last visual inspection in the acoustic testing, separation between the upstream I-section and the skin in the center bay was detected. The panel was removed from the test fixture and the bonded surfaces were then examined by the C-scan inspection and harmonic bond test inspection. These quality assurance tests produced evidence of substantial bond delamination in the central bay (only) between (i) the skin and the upstream I-section frame, (ii) the skin and the downstream I-section frame, and (iii) the skin and the longeron identified by strain gage No. 2 in Figure 13. Based on the 370 minutes of test life at 218 Hz, (i.e., the predominant response frequency during the acoustic test), 4.8×10^6 cycles to failure were computed. The fundamental frequency did not shift more than 2 Hz during the acoustic test.

During a visual inspection in the sonic fatigue test of panel A-2-2, it was observed that bond delamination had occurred along each J-section member in the central bay of the test panel, and the sonic fatigue failures were recorded. At that time the two bond delaminations were 3 and 6 inches in length. To obtain information on the debond propagation rate, the sonic fatigue test was then continued for another 60 minutes and the two bond delaminations each grew to 10 inches of visible length. The testing of the panel was then terminated.

The sonic fatigue test of panel A-5-2 was halted after 378 minutes of accumulated exposure at 166 dB overall SPL because a 6-inch long fatigue crack was observed emanating from an edge of the downstream section of the steel test fixture portion of the test panel. Approximately one-half of the length of the crack was at the radius connecting the two legs of the angle section and the remainder of the crack was approximately parallel to the width direction of the larger leg of the angle. All four 4130 alloy steel angle members were replaced with heat treated members (of the 4130 alloy) to 160 ksi ultimate tensile strength and with the radius connecting the two legs of the angle being increased to 0.25 inch. The panel was then mounted on the jig plate, reinstalled in the acoustic test fixture, and subjected to further sonic loading at 166 dB overall SPL.

At the time the sonic fatigue testing was resumed after the aforementioned repairs, Panel A-5-2 had accumulated 3.2×10^6 random cycles during 378 minutes of sonic exposure with the principal response frequency at 143 Hz. The panel was then subjected to 180 additional minutes of sonic exposure to bring the total time to 558 minutes with a total of 4.8×10^6 random cycles. The test was then halted, because a fatigue crack was observed in the downstream 4130 heat treated angle section and several bolts attaching the test panel to the jig plate were lost. The fatigue crack was repaired by welding and the damaged bolts were replaced. In addition, one-quarter inch thick steel radius strips were fabricated and installed (using a liquid shim) under the flanges of the 4130 steel angle frame members to decrease the likelihood of the occurrence of fatigue cracks during the remainder of the sonic fatigue test.

During the visual inspection following the 618 minutes of exposure, it was observed that (1) there was a slight adhesive bond fatigue failure in the central bay at the joint between the skin and the upstream I-section member (Figure 27), (2) insofar as the adhesive bond between the skin and downstream I-section member was concerned, there was a complete separation of adherends (Figure 28) throughout most of the entire length of the bonded joint, and (3) there were rivet failures at (i) the angle clip of the downstream I-section member and the steel frame (see the arrow on the web of the I-section member in Figures 28 and 29) and (ii) the angle clip and the J-section member on the south and north side of the test panel. No fatigue damage of the adhesive bond connecting the J-section members to the skin and frame portion of the test panel was observed.

The following sequence of events relating to the fatigue damage is believed to have occurred.

1. It was observed at the 558 minute inspection that the head of a rivet at an angle clip connecting the downstream I-section member to the south steel angle frame member had popped off. The damaged rivet connected the clip to the steel angle frame member and was one of four rivets through the clip transferring load to the frame. During the examination of the severed rivet head, it was concluded that the rivet head was damaged prior to the sonic fatigue loading. Therefore, it was decided to continue the sonic fatigue test without replacing the rivet, but to observe carefully the other rivets at that clip during subsequent visual inspections to determine the need, if any, for rivet repairs at that clip.

2. Probably, when the frequency shift at 608 minutes occurred, additional rivets failed and/or much of the bond between the downstream I-section member and the skin failed.

The events reported above were reviewed and the principal conclusion of importance to the test of panel A-5-2 was that the downstream bond failure did not drastically affect the sonic fatigue life of the upstream bond. The conclusion is based on the consideration that the lack of visible evidence of bond failure between the J-section stiffeners and the skin imply that the overall dimensions of the central bay did not increase substantially following the failure of the downstream bond. Consequently, the sonic loading which the upstream bond was resisting was not drastically increased after the downstream bond failure. The fact that the upstream bond was still effective during the final ten minutes of the sonic exposure also supports the conclusion, especially in view of a comparison of the sonic fatigue lives of panels, A-5-2, A-4-1, and A-4-2. The sonic fatigue lives of the upstream bonds of each of panels A-4-1 and A-4-2 (i.e., the panels with 36 x 24 inches overall dimensions with a 0.050 inch thick skin) was 2.5×10^6 random cycles.

Based on the above information, the fatigue life corresponding to 618 minutes of excitation (i.e., 5.3×10^6 random cycles at 143 Hz) was reported as the fatigue life of the upstream bond in the central bay of panel A-5-2.

Figure 26. Fatigue Failure in J-Section Stiffener of Panel A-3-1

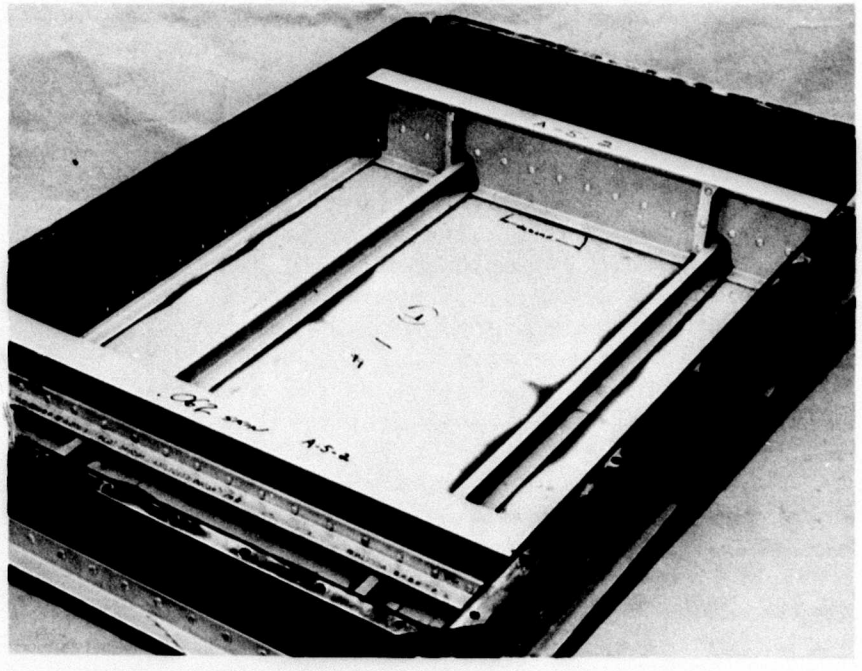

Figure 27. Bond Failure at Upstream I-Section Stiffener of Panel A-5-2

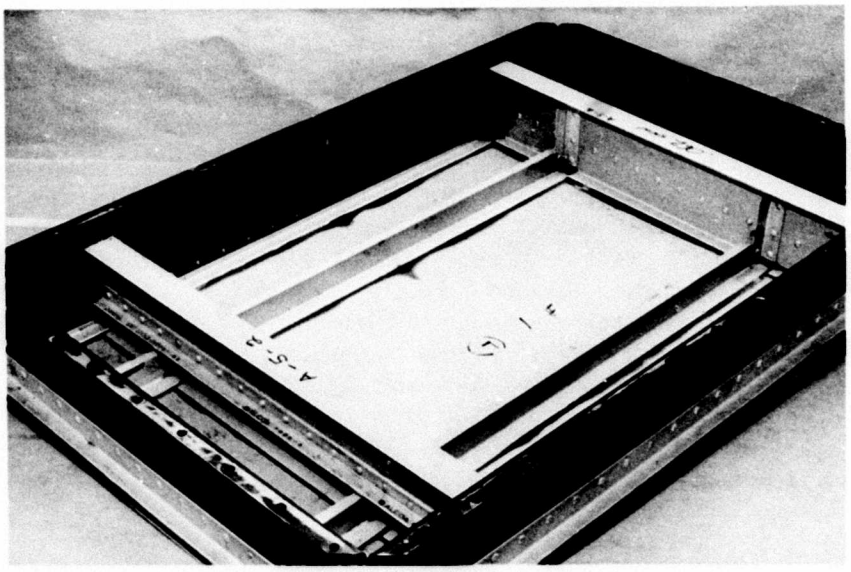

Figure 28. Bond and Rivet Failures at Downstream I-Section Stiffener of Panel A-5-2

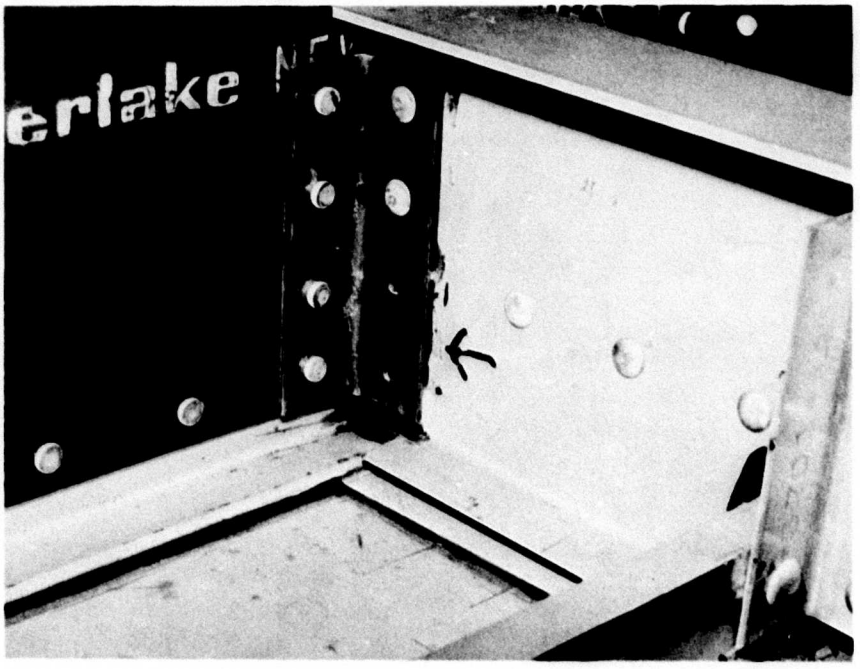

Figure 29. Angle Clip Failure at Steel Frame of Panel A-5-2

The sonic fatigue test of panel A-3-2 was halted with 390 minutes of accumulated sonic exposure at 166 dB overall SPL, because a fatigue crack approximately three inches in length was observed emanating from an edge at the radius of the downstream section of the steel test fixture portion of the test panel. The damage was similar to the initial sonic fatigue damage described for test panel A-5-2. Many of the corrective measures described for panel A-5-2 were also being applied to panel A-3-2.

The repair of panel A-3-2 consisted of replacing the downstream 4130 alloy steel section in the normalized condition with a 4130 alloy steel member of the same thickness but heat treated to a strength of approximately 160 ksi and with the radius connecting the two legs of the angle section increased to 0.25 inch. The panel was then mounted on the jig plate, reinstalled in the acoustic test chamber, and subjected to further sonic loading at 166 dB overall SPL. At the time the sonic fatigue testing was resumed, after the aforementioned repairs, panel A-3-2 had accumulated 4.8×10^6 random cycles during 390 minutes of exposure. The principal response frequency was 207 Hz. The panel was then subjected to 400 additional minutes of exposure to bring the total time to 790 minutes with a total of 9.8×10^6 random cycles.

The test was then halted for two reasons, namely, (1) a through-the-thickness fatigue crack approximately one inch in length occurred in an upstream angle clip connecting the J-section stiffener to the I-section frame (the crack was on the lower side of the lower rivet), and (2) the two 4130 steel angle frame members on the longer sides of the test panel, which had not been replaced, were fatigue damaged to the extent that repairs were necessary to permit continuation of the sonic fatigue test. In addition, both the heat treated 4130 steel angle frame member and the original 4130 steel angle frame member on the shorter sides of the test panel had experienced through-the-thickness fatigue cracks. The fatigue damage to the shorter sides of the panel was much less than to the longer sides.

Panel A-3-2 then underwent additional repairs prior to the resumption of the sonic fatigue testing. The repairs consisted of (1) replacing the three remaining original sides of the test panel with parts identical to the original parts, except that radius of the steel angles was increased to 0.25 inch, (2) welding the single fatigue crack in the heat treated angle, (3) replacing the damaged angle clip connecting the J-section member to the I-section member, and (4) installing (using a liquid shim) 1/4-inch thick steel radius strips under the flanges of the 4130 steel angle frame members to decrease the likelihood of the occurrence of fatigue cracks in the 4130 steel members during the remainder of the sonic fatigue test.

The fundamental frequency of panel A-3-2 was 193 Hz when the sonic fatigue test was resumed and dropped to 191 Hz near the end of the 60 minute run following the resumption of the test. At the visual inspection following

the 60 minute run, it was observed that the adhesive bond at the upstream I-section and downstream I-section had experienced a sonic fatigue failure. The total exposure time at 166 dB overall SPL was 850 minutes with the predominant frequency being 207 Hz during the first 790 minutes and 193 Hz during the last 60 minutes. Based on these frequencies and exposure times, the sonic fatigue life was computed and recorded as 10.5×10^6 random cycles.

4.2 Comparison of Sonic Fatigue Lives From This Test Program and Other Test Programs

A compilation of pertinent features of multibay panels tested under broadband sonic loading in completed test programs is given in Table 11 and the associated sonic fatigue test data are in Table 12. The last 9 panels in Tables 11 and 12 were 3-bay panels (References 11 and 12); all the other multibay panels in Table 11 and 12 were 9-bay panels. The substructure of panels B-1-1, B-1-2, B-1-3, T-1-1, T-1-2, and T-1-3 were bonded to the panel skin after the surfaces were treated with a Metalbond etch process. The substructure of all the other panels in Tables 11 and 12 was riveted to the panel skin.

Based on a comparison of spectrum level and cycles to failure in Table 10, with the corresponding data in Table 12, the bonded panels of Table 10 appear to be, in general, the more sonic fatigue resistant. The principal exception appears to be in connection with a comparison of the cycles to failure of panels A-3-1 and A-3-2 versus panels STR-30A and STR-30B. The longer lives of panels STR-30A and STR-30B may be attributed to (1) the smaller width and length of their central bay that increased the inherent stiffness of the central bay and (2) more flexibility in the stiffeners that decreased the skin stress at the stiffeners. It is somewhat surprising that the predominant response frequencies of panels STR-30A and STR-30B are somewhat less than the predominant response frequencies of panels STR-11A and STR-11B with thinner skins.

TABLE 11. 7075-T6 RIVETED ALUMINUM ALLOY PANELS FROM PREVIOUS ACOUSTIC FATIGUE TEST PROGRAMS

Reference	Panel No.	Central Bay Dimensions (inch)	Stiffener (inch)	Rib	Skin
3	STR-9A	18x9x.040	.040;extrusion;zee	zee	clad
3	STR-9B	18x9x.040	.040;extension;zee	zee	clad
3	STR-24A	18x9x.040	.040;extrusion;zee	zee	clad
3	STR-24B	18x9x.040	.040;extrusion;zee	zee	clad
3	STR-14A	18x9x.050	.050;extrusion;zee	zee	clad
3	STR-14B	18x9x.050	.050;extrusion;zee	zee	clad
3	STR-11A	16x8x.032	.032;extrusion;zee	zee	clad
3	STR-11B	16x8x.032	.032;extrusion;zee	zee	clad
3	STR-30A	16x8x.050	.050;extrusion;zee	zee	clad
3	STR-30B	16x8x.050	.050;extrusion;zee	zee	clad
6	A1-6A	18x9x.040	.050;hot formed;zee	ch	bare ?
6	A1-6B	18x9x.040	.050; hot formed;zee	ch	bare ?
4	STR-37A	18x9x.040	.040;formed;zee	.05ch	bare ?
4	STR-37B	18x9x.040	.040;formed;zee	.05ch	bare ?
4	STR-38A	18x9x.040	.040;formed;ch	.05ch	bare ?
4	STR-38B	18x9x.040	.040;formed;ch	.05ch	bare ?
4	STR-40A	18x9x.032	.032;formed;zee	.05ch	bare ?
4	STR-40B	18x9x.032	.032;formed;zee	.05ch	bare ?
10	R-1-1	18x6.7x.050	.050;formed;ch	--	bare
10	R-1-2	18x6.7x.050	.050;formed;ch	--	bare
10	R-1-3	18x6.7x.050	.050;formed;ch	--	bare
10	B-1-1(2)	18x6.7x.050	.050;formed;ch	--	bare
10	B-1-2(2)	18x6.7x.050	.050;formed;ch	--	bare
10	B-1-3(2)	18x6.7x.050	.050;formed;ch	--	bare
11	T-1-1(2)	18x6.7x.050	.078;extrusion(1);tee	--	bare
11	T-1-2(2)	18x6.7x.050	.078;extrusion(1);tee	--	bare
11	T-1-3(2)	18x6.7x.050	,078;extrusion(1);tee	--	bare

(1) The extrusion was machined down to 0.050 inch at the edges of the flange.

(2) For these panels, there were bonded joints in lieu of riveted joints.

TABLE 12. TEST PARAMETERS AND RESULTS FOR PANELS LISTED IN TABLE 11

Panel No.	Panel Dimensions	Overall SPL	Test Spectrum Level	Cycles to Failure	Frequency	Life	Skin Stress	Failure Type
	(inch)	(db)	(db)	(10^{-6})	(Hz)	(Hr)	(ksi-rms)	
STR-9A	18x9x.040	--	120	1.61	150	3.0	6.2	Skin
STR-9B	18x9x.040	--	120	1.51	150	2.8	6.5	Skin
STR-24A	18x9x.040	--	120	14.5	150	27.0	3.6	Skin
STR-24B	18x9x.040	--	119	16.2	145	31.0	4.6	Skin
STR-14A	18x9x.050	--	128	12.4	130	26.4	4.1	Skin
STR-14B	18x9x.050	--	126	14.9	150	27.6	5.0	Skin
STR-11A	16x8x.032	--	119	21.6	195	30.8	4.4	Skin
STR-11B	16x8x.032	--	118	22.0	200	30.6	5.1	Skin
STR-30A	16x8x.050	--	140	100.	165	166.0	3.1	Skin
STR-30B	16x8x.050	--	138	145.	165	244.0	2.8	Skin
A1-6A	18x9x.040	--	132	24.	200	33.4	2.1	None
A1-6B	18x9x.040	--	130	10.	132	21.2	2.1	None
STR-37A	18x9x.040	--	132	4.2	145	8.0	4.2(w)	Web
STR-37B	18x9x.040	--	132	1.4	140	2.8	1.2(w)	Web
STR-38A	18x9x.040	--	128	2.2	175	3.5	5.2(w)	Web
STR-38B	18x9x.040	--	128	1.0	140	2.0	4.2(w)	Web
STR-40A	18x9x.032	--	132	1.2	140	2.4	16.	Skin
STR-40B	18x9x.032	--	132	1.5	140	3.0	3.6(f)	Flange
R-1-1	18x6.7x.050	168	>140	--	--	0.03	--	Skin
R-1-2	18x6.7x.050	160	137	--	--	2.5	6.1	Skin
R-1-3	18x6.7x.050	160	137	--	--	3.0	6.1	Skin
B-1-1[1]	18x6.7x.050	166	139	--	--	0.0	5.0	Debond
B-1-2[1]	18x6.7x.050	166	139	--	--	0.1	4.5	Debond
B-1-3[1]	18x6.7x.050	160	137	--	--	0.7	5.0	Debond
T-1-1[1]	18x6.7x.050	166	139	--	--	1.0	6.5	Debond[2]
T-1-2[1]	18x6.7x.050	160	137	--	--	5.5	4.0	Debond[2]
T-1-3[1]	18x6.7x.050	166	139	--	--	2.0	<4.0	Edge clamp

(1) For these panels the substructure was bonded to the skin. In all the other panels, the substructure was riveted to the skin.

(2) In addition to the debonds between the stiffeners and the skins, skin cracks were observed at the clamps to the test fixture.

4.3 Experimental Strain and Acoustic Pressure Data

During the acoustic tests, the noise intensity was increased from 136 dB in increments of 3 dB until 166 dB was reached, and the rms strain versus overall SPL was recorded at each SPL. In order to avoid appreciable accumulation of fatigue damage at SPLs below 166 dB, the strain readings (Tables A-1 through A-5 in Appendix A) were taken rapidly and the panel exposure below 166 dB was limited to 3 to 6 minutes per SPL at which the strain readings were taken. The strain versus acoustic pressure data at increasing SPLs were taken to obtain a measure of the degree of linearity between the acoustic pressure and strain response.

In some runs, strain and pressure data at selected overall SPLs were recorded on magnetic tape for availability in subsequent analyses. Samples of the 1/3 octave band and narrow band analyses of the acoustic pressure and strain data are given in Figures A-1 through A-8 of Appendix A. The one-third octave band containing the predominant response frequency, the SPL in that one-third octave band, and the magnitude of the predominant response frequency of strain gage No. 11 were tabulated (Table 13) in the acoustic tests of all ten panels. Spectrum levels obtained from

$$L_{SL} = L - 10 \text{ Log}_{10} (\Delta f) \qquad (6)$$

where L_{SL} is sound spectrum level in decibels and L is sound pressure level in a one-third octave band Δf wide were computed and converted to pressure density units of psi/Hz and power spectral density units of psi^2/Hz (Table 13).

TABLE 13. ACOUSTIC PRESSURE DATA IN SONIC FATIGUE TESTS

PANEL	OVERALL SPL	f_p, FREQUENCY OF PEAK STRAIN RESPONSE	SPL IN ONE-THIRD OCTAVE BAND CONTAINING f_p	SPECTRUM LEVEL(1)	PRESSURE CORRESPONDING TO SPECTRUM LEVEL(1)	ACOUSTIC PRESSURE PSD FOR THE ONE-THIRD OCTAVE BAND
	(dB)	(Hz)	(dB)	(dB)	(psi)	(psi^2/Hz)
A-1-1	166	218	157	140	.0290	8.4×10^{-4}
A-1-2	166	204	155	138	.0230	5.3×10^{-4}
A-2-1	166	200	156	139	.0258	6.7×10^{-4}
A-2-2	166	211	154	137	.0205	4.2×10^{-4}
A-3-1	166	200	157	140	.0290	8.4×10^{-4}
A-3-2	166	207	155	138	.0230	5.3×10^{-4}
A-4-1	166	140	157	141	.0324	10.5×10^{-4}
A-4-2	166	145	156	140	.0290	8.4×10^{-4}
A-5-1	166	150	156	140	.0290	8.4×10^{-4}
A-5-2	166	143	156	140	.0290	8.4×10^{-4}

(1) The spectrum level is the average spectrum based on one-third octave band acoustic pressure data.

4.4 Increase of Panel Stiffness with Increasing SPL

At the lowest overall SPL (i.e., 136 dB) used in the acoustic tests with broadband excitation, the fundamental frequency of the response was essentially the same as had been obtained in loudspeaker tests with low level, discrete frequency excitation. However, as the overall SPL was increased above 136 dB, the fundamental frequency of the panel increased and the rms strain response versus acoustic pressure loading relation, in general, exhibited an increasing non-linearity. The increase in fundamental frequency and nonlinear strain-pressure relation are indicative of panel stiffening with increasing overall SPL that is attributed to the following factors:

1. At the lower acoustic pressures, the mean acoustic pressure is approximately zero. At the higher acoustic pressures, the mean pressure has risen significantly.

2. At the higher acoustic pressures, the unsupported skin of the central bay tends to strain extensionally significantly greater than the skin which is in contact with the adhesive at the bonded joints. Hence, an effect of the stiffeners at the high acoustic pressures is to stretch the skins and produce a net tensile (membrane) stress which is reflected by an increasing fundamental frequency and structural stiffness of the panel and, in particular, the central bay.

Evidence of the increasing frequency of the predominant strain response with increasing SPL is given in Table 14 for five of the acoustic test panels. The sound pressure level (of four panels) in the one-third octave band containing the peak of the strain PSD is also in Table 14. In some cases, a new mode of response became the mode with the peak strain PSD as the overall SPL was increased.

TABLE 14. FREQUENCY AND ONE-THIRD OCTAVE BAND SPL VERSUS OVERALL SPL DATA

		Predominant Frequency					1/3 Octave SPL[1]			
Run No.	Overall SPL	Panel A-1-2	Panel A-2-2	Panel A-3-2	Panel A-4-2	Panel A-5-2	Panel A-2-2	Panel A-3-2	Panel A-4-2	Panel A-5-2
	(dB)	(Hz)	(Hz)	(Hz)	(Hz)	(Hz)	(dB)	(dB)	(dB)	(dB)
0	(2)	97	141	141	84	99	-	-	-	-
1	136	98	148	144	84	93	131	126	128	131
2	139	109	148	147	87	93	130	129	132	134
3	142	116	150	147	90	95	133	132	135	137
4	145	119	151	149	92	95	136	135	139	140
5	148	120	159	154	92	95	139	138	142	143
6	151	140	165	161	93	115[3]	142	141	145	144[3]
7	154	147	176	168	93	117	145	144	148	146
8	157	162	180	174	90	118	147	147	151	148
9	160	174	190	182	130[4]	130	150	150	154	151
10	163	185	200	192	130	137	152	152	157	153
11	166	204	211	207	145	143	154	155	156	156

(1) This is the one-third octave band obtained by tracking the predominant response frequency.

(2) Run No. 0 was the low level discrete frequency excitation prior to subjecting a panel to broadband progressive wave excitation.

(3) The 95 Hz mode was no longer the predominant response mode.

(4) The 90 Hz mode was no longer the predominant response mode.

4.5 Modal and Damping Data

Under loudspeaker excitation with the panel mounted on the jig plate for the acoustic tests, the four lowest natural frequencies (Table 15) were obtained for all acoustic test panels except panel A-3-1. The mode shapes corresponding to the four lowest natural frequencies consisted of one-half wave in the width direction of the central bay and from one to four half waves in the length direction of the central bay. In other words, the natural modes (of the 9-bay panels) with the four lowest natural frequencies were characterized as the 1-1, 2-1, 3-1, and 4-1 modes in the central bay.

The ratio of the fundamental frequency obtained under the loudspeaker excitation to the frequency at which the peak strain PSD occurred in the sonic fatigue test at 166 dB overall SPL is f_1/f_{166} in Table 15. This ratio is a measure of the panel stiffening resulting from the high intensity noise excitation. The predominant response frequency at 166 dB overall SPL was obtained by tracking the low-level fundamental frequency through increasing levels.

All the damping factors listed in Table 15 were obtained under loudspeaker excitation, except for panels A-2-1 and A-3-1 for which progressive wave excitation was used. The damping factors were obtained by the log decrement method.

The damping factor of panel A-3-1 was obtained in the presence and in the absence of the termination box (Figure 17); the variation in the damping factor was 0.001, which is insignificant.

The average of the ten damping factors in Table 15 is 0.0134, whereas the average of thirty damping factors was 0.0145 with substructure riveted to skin and reported in Table VII of Reference 3. The difference in the average damping factors between the bonded versus riveted panels is not large. Therefore, no change in damping factor is recommended for bonded structures in lieu of riveted structures.

The modal data as well as the fatigue life data of the identical pairs of panels A-2-1 and A-2-2; of panels A-4-1 and A-4-2; and of A-5-1 and A-5-2 (Tables 10 and 15) agree very well with each other. The absence of the -71 angles on panel A-3-1 may have been the principal cause between the differences in modal data and the modes of fatigue failure between panels A-3-1 and A-3-2. The differences in modal data and fatigue lives between panels A-1-1 and A-1-2 may have been caused principally by the differences in the coupling of the thin skins (0.032 inch) of these panels with the substructure through the adhesive bonding.

TABLE 15. FREQUENCY AND DAMPING DATA

PANEL	DAMPING FACTOR(1)	NATURAL FREQUENCIES				f_{166} (2)	$\frac{f_1}{f_{166}}$
		$f_1 \equiv$ FIRST MODE	$f_2 \equiv$ SECOND MODE	$f_3 \equiv$ THIRD MODE	$f_4 \equiv$ FOURTH MODE		
		(Hz)	(Hz)	(Hz)	(Hz)	(Hz)	
A-1-1	0.018	137	189	265	340	218	1.59
A-1-2	0.015	97	147	179	266	204	2.10
A-2-1	0.011	144	209	284	386	212	1.47
A-2-2	0.009	141	203	279	376	211	1.50
A-3-1	0.012	165	245	-	-	205	1.21
A-3-2	0.011	141	210	295	413	207	1.47
A-4-1	0.023	80	114	155	226	140	1.75
A-4-2	0.009	84	124	172	235	144	1.71
A-5-1	0.012	103	155	211	292	150	1.46
A-5-2	0.014	99	153	215	300	143	1.44
Average	0.0134						

(1) Nondimensional viscous damping factor, $\frac{c}{c_c}$ (Reference 14)

(2) The parameter f_{166} was the frequency of the predominant strain response at 166 dB overall SPL.

4.6 Boundary Conditions and Their Effects on Fundamental Frequency, Strain Response, and Sonic Fatigue Failures

Calculations were performed to determine if the acoustic strain response and fundamental frequency in free vibrations of the nine-bay test panels could be predicted accurately on the basis of equations that had been developed previously. Two different approaches were used. The first approach that is discussed immediately below is based on an analysis of flat, rectangular plates of uniform thickness that are fully clamped on all four edges (Reference 13). The second approach (see subsection 4.7) is based on a semi-empirical method for multibay panels with substructure riveted to the skin and reported in References 1 and 2.

In the first approach, which is discussed in this and the following paragraphs, the central bay of the multi-bay test panels was simulated by a flat, rectangular plate that was fully clamped on all four edges. The fundamental frequencies (Table 16 of the flat plates were calculated on the basis of the plate length and width being (1) the nominal dimensions of the central bay of the test panels (Type A in Table 16) and (2) the length and width of the unsupported skin (Type B in Table 16) in the central bay.

For the thicker skinned panels and panel A-1-2, the experimental fundamental frequency obtained under low level discrete frequency excitation was very much closer to the calculated frequency obtained with the use of the nominal dimensions of the central bay (i.e., the Type A geometry in Table 16). However, the central bay of the test panels did not respond to the acoustic excitation as though it were fully clamped on all four edges in the sense that the highest dynamic test strains and the sonic fatigue failures did not both occur, in general, at the center of the long edges (i.e., in the vicinity of strain gages No. 1 and 2). Furthermore, the analytic strain predictions (based on the clamped plate theory of Reference 13) that the rms strains at Gages No. 3 and 4 were one-fourth the rms strains at gages No. 1 and 2 were definitely not verified by the test data reported in Tables 12 through 16 and summarized in Table 17. The most plausible explanation for the predicted strains of gages No. 3 and 4 rather than of gages No. 1 and 2 agreeing better with the test data is that the heavy I-section stiffeners (at the shorter edges) produced a greater clamping constraint at the bonded joints. The equations from Reference 13 that were used for predicting the fundamental frequency and the mean square response (of the fully clamped plates) to white noise acoustic excitation are repeated below.

$$\overline{e_x^2} = \frac{h^2 \Gamma^2 \psi^2}{4K^2} \left(\frac{d^2\phi}{dx^2}\right)^2 \frac{\pi f S_p}{4\zeta} \tag{7}$$

and

$$\overline{e_y^2} = \frac{h^2 \Gamma^2 \phi^2}{4K^2} \left(\frac{d^2\psi}{dy^2}\right)^2 \frac{\pi f S_p}{4\zeta} \tag{8}$$

TABLE 16. PREDICTED AND TEST FUNDAMENTAL FREQUENCIES

PANEL DESIGNATION	GEOMETRY - TYPE A			GEOMETRY - TYPE B			TEST[1] FREQUENCY
	LENGTH	WIDTH	FRE-QUENCY	LENGTH	WIDTH	FRE-QUENCY	
	(inch)	(inch)	(Hz)	(inch)	(inch)	(Hz)	(Hz)
A-1-1	18	9	92	16.4	7.4	135	137
A-1-2	18	9	92	16.4	7.4	135	97
A-2-1	18	9	117	16.4	7.4	169	144
A-2-2	18	9	117	16.4	7.4	169	141
A-3-1	18	9	146	16.4	7.4	211	165
A-3-2	18	9	146	16.4	7.4	211	141
A-4-1	24	12	82	22.4	10.4	107	80
A-4-2	24	12	82	22.4	10.4	107	84
A-5-1	24	12	103	22.4	10.4	135	103
A-5-2	24	12	103	22.4	10.4	135	99

(1) The test frequencies in this column were the fundamental frequencies obtained under low level excitation tests.

TABLE 17. RMS STRAIN TEST DATA AT 136 dB OVERALL SPL

PANEL	RMS STRAIN			
	GAGE NO. 1	GAGE NO. 2	GAGE NO. 3	GAGE NO. 4
	(μ"/")	(μ"/")	(μ"/")	(μ"/")
A-1-1	23	19	14	9
A-1-2	20	26	12	13
A-2-1	15	16	10	14
A-2-2	16	24	9	9
A-3-1	20	40	28	22
A-3-2	12	18	8	20
A-4-1	52	38	18	37
A-4-2	48	54	32	64
A-5-1	19	32	22	14
A-5-2	38	26	19	30

with

$$K = D_{xx} b \beta^4 a + 2 H \alpha \beta \theta \gamma (2 - \alpha \beta a)(2 - \theta \gamma b) + D_{yy} a \gamma^4 b \tag{9}$$

$$M = a b M_o \tag{10}$$

$$\Gamma = \frac{16 \alpha \theta}{\beta \gamma} \tag{11}$$

$$D_{xx} = D_{yy} = H = \frac{Eh^3}{12 (1-\nu^2)} \tag{12}$$

$$\alpha = \theta = .983 \tag{13}$$

$$\beta a = \gamma b = 4.73 \tag{14}$$

$$\omega^2 = \frac{K}{M} \tag{15}$$

and

$$f = \frac{\omega}{2\pi} \tag{16}$$

For strain calculations at the center of an edge of the plate, the beam functions, ϕ and ψ, and the appropriate derivatives are given in Table 18.

TABLE 18. BEAM FUNCTIONS AND SECOND DERIVATIVES AT THE CENTERS OF THE EDGES

Location	ϕ	ψ	$\frac{d^2\phi}{dx^2}$	$\frac{d^2\psi}{dy^2}$
$x = \frac{a}{2}$, $y = 0$	1.588	0	$-1.216\beta^2$	$2.00\gamma^2$
$x = 0$, $y = \frac{b}{2}$	0	1.588	$2.00\beta^2$	$-1.216\gamma^2$

To obtain the ratio of rms strains at the centers of the edges of the plate, let

$$e_1 = \left| (e_x)\, x = o,\ y = \frac{b}{2} \right| \tag{17}$$

and

$$e_2 = \left| (e_y)\, y = o,\ x = \frac{a}{2} \right| \tag{18}$$

Upon dividing equation (17) by equation (18), one obtains

$$\frac{e_1}{e_2} = \frac{\beta^2}{\gamma^2} \tag{19}$$

which implies that the strain is larger at the center of the long edge than at the center of short edge as is the case for isotropic plates of uniform thickness.

The orientation of the x and y axes and the plate edge dimension parameters a and b are in Figure 30.

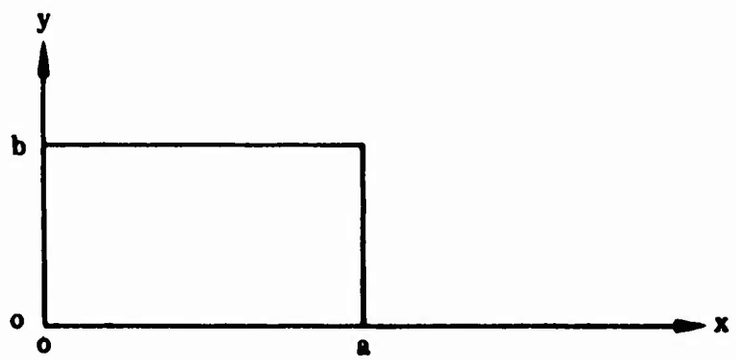

Figure 30. Geometry and Coordinate System of Rectangular Plate

Multi-modal response was believed to be of less significance than the ratio of torsional rigidities of the I-section and the J-section stiffeners, in obtaining closer agreement than was expected in test strains (e.g., between gages No. 1 and 3) at the long and short sides of the acoustic test panels. The belief that the multi-modal response was of lesser importance, in general, than the difference in stiffener torsional rigidities in affecting the strain ratios was arrived at after viewing strain PSD data such as shown in Figures A-5 and A-6 of Appendix A for strain gage No. 4 of panel A-4-1, of Figures A-9 and A-10 for strain gage No. 2 of panel A-4-1, and of Figures A-11 through A-14 for strain gages No. 2 and 4 of panel A-2-1.

In addition, it is noted that at the lower sound pressure levels with broadband random excitation that the strain at the panel center (gage No. 11 in Tables A-1 through A-5 of Appendix A) was in excess of the strain at gages No. 1 through 4 at the center of the sides. Inasmuch as strain predictions from Equations (7) and (8) are that the maximum strain response is at the panel edge rather than the panel center, the conclusion that may be reached (again) is that the unsupported skin in the central bay does not respond to acoustic excitation as though the bonded joints are totally rigid relative to the unsupported skin in the central bay.

4.7 Sonic Fatigue Life Predictions for Riveted Multibay Panels

Semi-empirical equations and a nomograph were presented in Reference 1 for predicting the stress response and sonic fatigue lives of multi-bay panels with the skin riveted to the substructure and subjected to acoustic excitation. The semi-empirical equation for predicting stress at the center of the long side of the stiffened bay of the acoustic panel is

$$\bar{\sigma}_s = \frac{0.072\, a^{1.25} S_p (f_{11}) (b/a)^{1.75}}{h^{1.75} \zeta^{0.56} [3(b/a)^2 + 3(a/b)^2 + 2]^{0.84}} \quad \text{ksi} \qquad (20)$$

The design nomograph for the riveted multibay panels based upon Equation (20) is presented in Figure 31. In Figure 31, "a" is the panel width.

Equation (20) has been applied to predict the stresses (Table 19) of the acoustic test panels with Spectrum Levels "A" of Table 10 in the 166 dB overall SPL runs using panel lengths and widths of Geometry A in Table 16 and damping factors from Table 15.

The lives (Table 19) of the riveted panels with nominal dimensions given by the Type A geometry (Table 16) and subjected to acoustic pressure with spectrum levels given in Table 10 were obtained using extrapolations of Figure 31.

Three principal differences in the dynamic behavior of bonded versus riveted multibay panels are summarized below. The riveted panels are, in general, expected to fail along the line of rivets of a long side of a panel bay, whereas the bonded panels are expected to fail at the edge of the bonded joints. The use of Equation (20) and Figure 31 for riveted panels implies sonic fatigue failures will occur in riveted panels along the line of rivets in the center of the long side of a bay; however, the bonded acoustic test panels experienced sonic fatigue failures at the edges of the bonded joints, mainly in the center of the short sides, but also in the center of the long sides. The fundamental frequency of many of the bonded panels agreed closely with predictions based on nominal dimensions of the central bay and fully clamped edge conditions, whereas the fundamental frequency of riveted test panels were shown (Figure AV-1 of Reference 1) to be intermediate between fully clamped and simply supported conditions. The difference in the fundamental frequencies between riveted and bonded panels may be attributed to the bonded joints producing a more effective rotational constraint to the unstiffened skin because the bonded joint has a positive method (i.e., the bonding) of ensuring surface contact in the region of the joint.

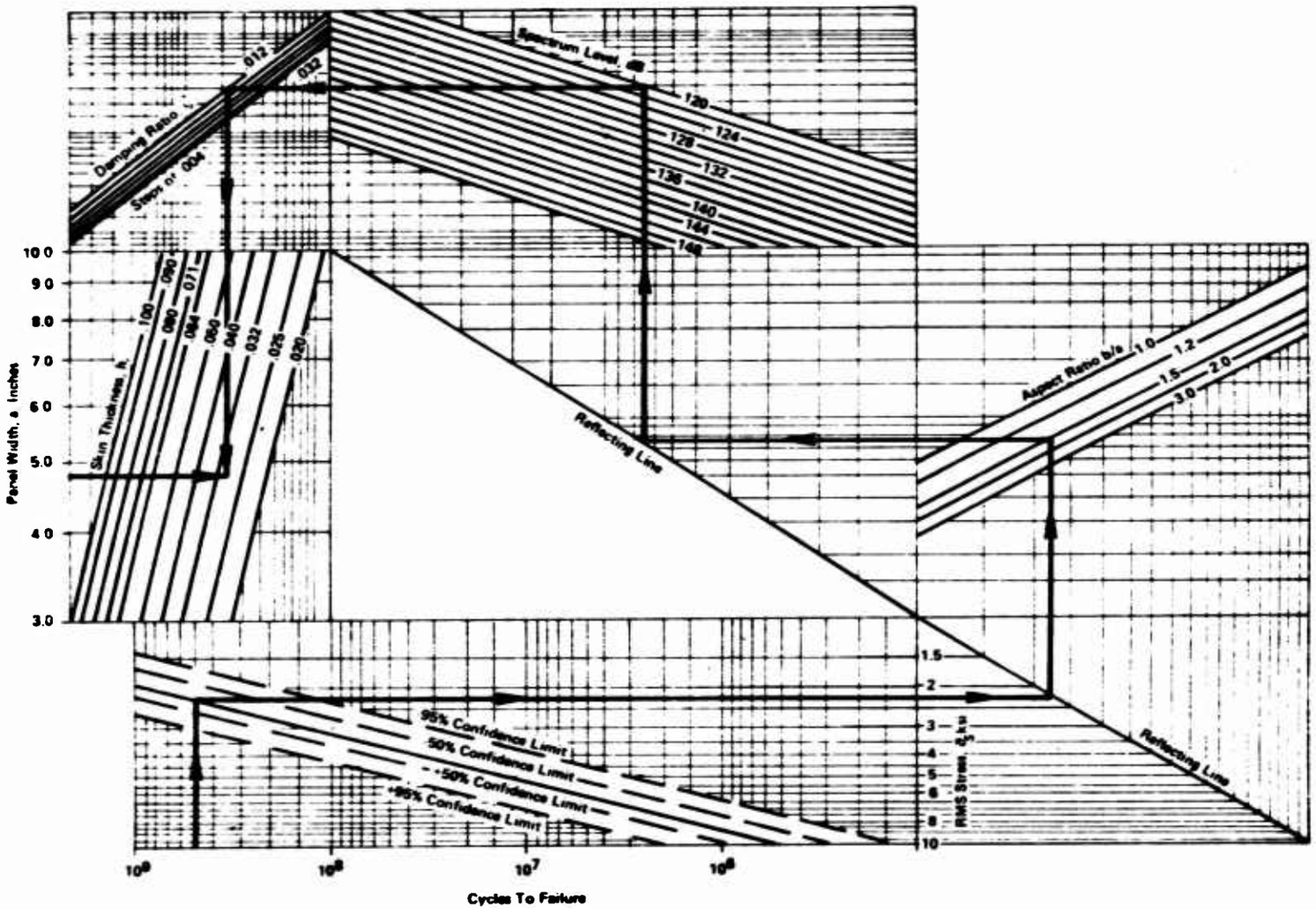

Figure 31. Nomograph for Stress and Fatigue Life for Stiffened Panel Skin with Riveted Joints Between Skin and Stiffeners at Ambient Temperature (Obtained from Figure 5.3.1-2 of Reference 1)

TABLE 19. PREDICTED SONIC FATIGUE LIVES OF MULTIBAY RIVETED PANELS

TEST PANEL BEING SIMULATED	$\bar{\sigma}_s$ FROM EQUATION (20)	PREDICTED SONIC FATIGUE LIFE FROM FIGURE 31
	(ksi-rms)	(cycles)
A-1-1	44.8	$<10^5$
A-1-2	39.3	$<10^5$
A-2-1	35.5	$<10^5$
A-2-2	31.6	$<10^5$
A-3-1	25.7	$<10^5$
A-3-2	21.4	$<10^5$
A-4-1	30.6	$<10^5$
A-4-2	43.3	$<10^5$
A-5-1	24.6	$<10^5$
A-5-2	22.5	$<10^5$

4.8 Sonic Fatigue Life Predictions for the Bonded Multibay Test Panels

The sonic fatigue lives of the bonded multibay panels of this acoustic test program could have been predicted with approximately the same accuracy expected in predicting the lives of the multibay riveted panels with the use of Figure 31 if $\bar{\sigma}_s$ in Figure 31 were replaced by an empirically obtained factor that is called σ' such that

$$\sigma' = 0.2 \ \bar{\sigma}_s \tag{21}$$

after $\bar{\sigma}_s$ is obtained from Equation (20). The computed stress parameter σ' for the acoustic test panels and the experimentally obtained sonic fatigue lives (N) are presented in Table 20. The σ'-N data of Table 20 are presented as solid circles in Figure 32. The dashed lines and solid line of Figure 32 resulted from drawing the corresponding lines of Figure 31 to a different scale and replacing the ordinate $\bar{\sigma}_s$ with the ordinate σ'. The computed parameter σ' may be thought of as a stress resulting from some undefined combination of bending stress, membrane stress, and transverse shear stress.

The factor of 0.2 in Equation (21) was obtained by a trial and error process that was performed to determine if a constant existed that would result in the σ'-N data (i.e., the solid circles of Figure 32) for the bonded panels fully within the $\pm$95 percent confidence limits for the riveted panels.

Notes: 1. The σ'-N curves in Figure 32 and the σ-N curve in Figure 31 are identical (but drawn to different scales) for a given confidence limit.

2. The solid circles shown in this figure depict the computed stress σ' and the sonic fatigue test lives N of the nine multibay panels that experienced sonic fatigue bond failures.

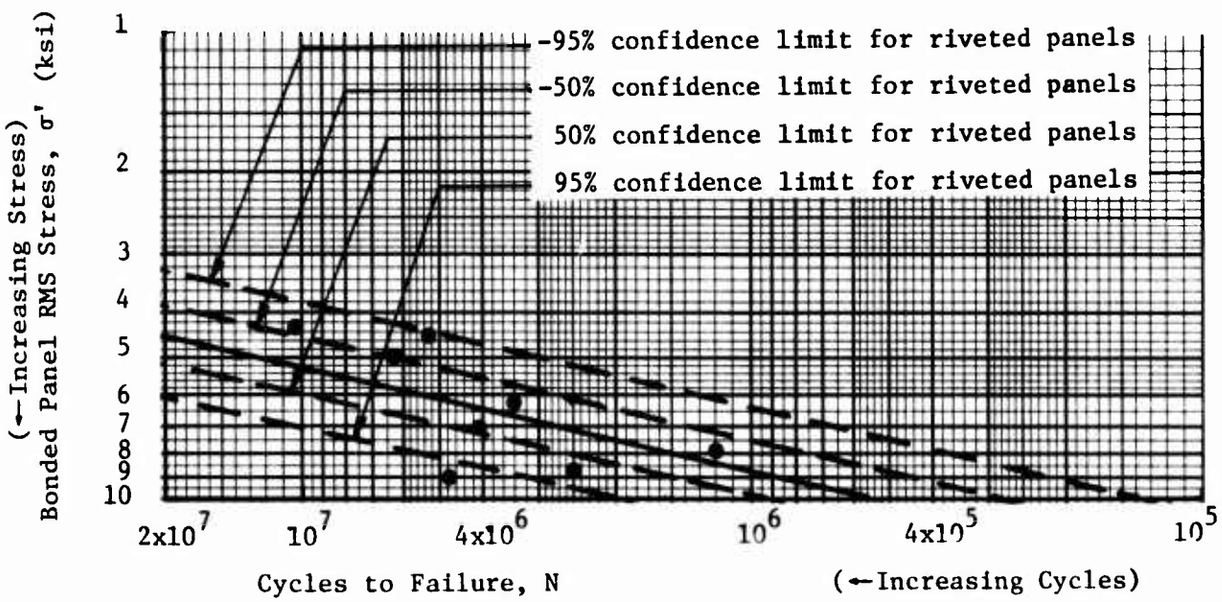

Figure 32. S-N Relations for the Bonded Acoustic Test Panels with the FM73/BR127 Adhesive System

TABLE 20. ACOUSTIC PANEL σ'-N DATA

PANEL	σ' FROM EQUATION (22)	EXPERIMENTAL LIFE (N)
	(ksi-rms)	(cycles)
A-1-1	9.0	4.8×10^6
A-1-2	7.9	1.2×10^6
A-2-1	7.1	4.1×10^6
A-2-2	6.3	3.4×10^6
A-3-1	5.1	3.7×10^6 (1)
A-3-2	4.3	10.5×10^6
A-4-1	6.1	2.5×10^6
A-4-2	8.7	2.5×10^6
A-5-1	4.9	6.3×10^6
A-5-2	4.5	5.3×10^6

(1) This sonic fatigue failure was in a simulated longeron at a clip to a simulated frame. All other sonic fatigue failures were bond failures.

4.9 Nonlinear Experimental Acoustic Pressure Versus Strain Response

In general, there was a nonlinear relation between the acoustic pressure and the overall rms dynamic strain response at each strain gage. The 1/3 octave band SPLs at the predominant response frequency of test panels A-2-2, A-3-2, A-4-2, and A-5-2 were tracked during the portion of the acoustic tests in which increasing SPLs from 136 dB to 166 dB overall SPL were applied. The resulting experimental relation between the 1/3 octave band SPL at the predominant response frequency versus the strain at a strain gage (Gage No. 2) is given in Figure 33 to illustrate the degrees of nonlinearity. The slope of reference curves for a linear and a cubic pressure-strain relation is shown in Figure 33.

It is noted in Figure 33 that the predominant mode of the response shifted at 154 dB for panel A-4-2 and at 144 dB for panel A-5-2. The slopes of the curves also shift in the region of the shift in the predominant response mode.

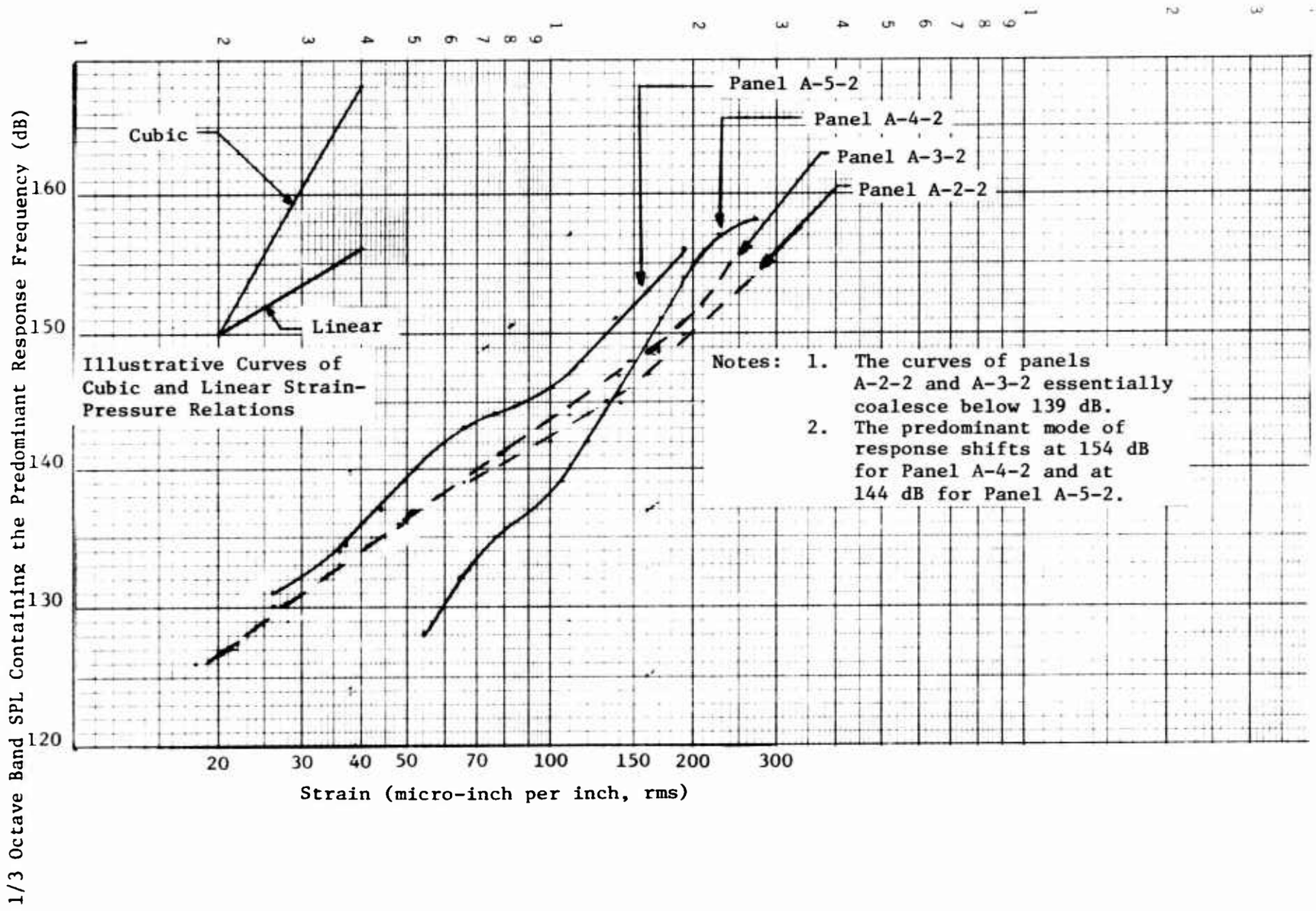

Figure 33. Strain-Pressure Relation of Strain Gage No. 2

4.10 Predictions of Strain Response of Plates Fully Clamped on All Edges

Equations (7) and (8) have been used to predict the strain response (Table 21) of flat plates simulating panels A-2-1 and A-4-1. The strain and acoustic pressure PSDs of panel A-4-1 are given in Figures A-1, A-3, A-5, and A-9 of Appendix A. Strains were predicted at the center of a long edge, the center of a short edge, and center of the plate, which were to simulate the locations of strain gages No. 2, 4, and 11 in Figure 13.

In the calculations, panel A-4-1 was simulated by a rectangular plate 24 x 12 x 0.063 inches and panel A-2-1 was simulated by a plate 18 x 9 x 0.040 inches. The damping factors were taken from Table 15.

The agreement between the test strains and the predicted strains in Table 21 is not good and in particular it is not good for strain gage No. 2. The analytic use of the plate that is fully clamped on all four edges to simulate the central bay of multibay panels results in an overprediction of strains and is not recommended other than to obtain an upper limit on the dynamic strain response that may be expected as a result of acoustic excitation.

TABLE 21. STRAIN PREDICTIONS BASED ON THE ASSUMPTION OF FULLY CLAMPED EDGES OF A PLATE

TEST PANEL BEING SIMULATED	OVERALL SPL	PRESSURE PSD	RMS STRAINS					
			GAGE NO. 2		GAGE NO. 4		GAGE NO. 11	
			TEST	PREDICTED	TEST	Pre-DICTED	TEST	Pre-DICTED
	(dB)	(psi^2/Hz)	(μ"/")	(μ"/")	(μ"/")	(μ"/")	(μ"/")	(μ"/")
A-2-1	142	5.0×10^{-6}	32	445	27	111	84	270
A-4-1	145	3.4×10^{-5}	75	766	110	192	178	466

SECTION V

SONIC FATIGUE DESIGN GUIDELINES FOR BONDED MULTIBAY AIRCRAFT PANELS

5.1 Sonic Fatigue Design Nomograph for Bonded Panels with the FM73/BR127 Adhesive System

A method was developed (see section 4.8) to use the sonic fatigue design nomograph for riveted panels in Figure 31 to predict the sonic fatigue lives of the bonded acoustic test panels of this program. The calculated parameter σ' of Equation (21)

$$\sigma' = 0.2 \ \bar{\sigma}_s \qquad \text{(21) repeated}$$

was postulated as the sole factor needed for predicting the sonic fatigue lives of the bonded multibay panels which experienced sonic fatigue bond failures. In a sense, σ' corresponds to the parameter $\bar{\sigma}_s$ that may be used with Figure 31 for predicting the sonic fatigue lives of riveted multibay panels.

The calculated stress parameters σ' as a function of test cycles to failure (N) of the bonded multibay test panels were shown as solid circles in Figure 32, which is repeated as Figure 34. Figure 35, which contains an extrapolation of the $\bar{\sigma}_s$ versus N curve of Figure 31 was developed as a sonic fatigue design nomograph for bonded multibay test panels featuring the FM73/BR127 adhesive system, the BAC-5555 phosphoric acid anodizing process, and 7075-T6 aluminum alloy skins and substructure. The weight density of the FM73 supported film adhesive of the acoustic test panels was 0.085 psf.

The design nomograph (using Figures 34 and Figure 35) is intended for use in the following manner:

1. Pick a sonic fatigue life, N.

2. Read σ' from the solid σ'-N curve in Figure 34 (or from the upper dashed curve of Figure 34 for more design conservatism).

3. Compute $\bar{\sigma}_s = 5\sigma'$ from Equation (21).

4. Enter Figure 35 with $\bar{\sigma} \equiv \bar{\sigma}_s$ and determine the panel dimensions corresponding to the acoustic pressure spectrum level and panel damping factor. (The dashed lines in Figures 34 and 35 are applicable to riveted panels of Figure 31 and are only reference lines in Figures 34 and 35.) Use 0.012 as a typical damping factor for the bonded panels.

Example problem No. 1 illustrating the use of Figures 34 and 35 and the four step method described above in the design of a panel to be subjected to a sonic environment is given below.

Step No. 1. Pick a life of 10.5×10^6 cycles (which applied to panel A-3-2).

Notes: 1. The σ'-N curves in Figure 34 and the σ-N curve in Figure 31 are identical (but drawn to different scales) for a given confidence limit.

2. The solid circles shown in this figure depict the computed stress σ' and the sonic fatigue test lives N of the nine multibay panels that experienced sonic fatigue bond failures.

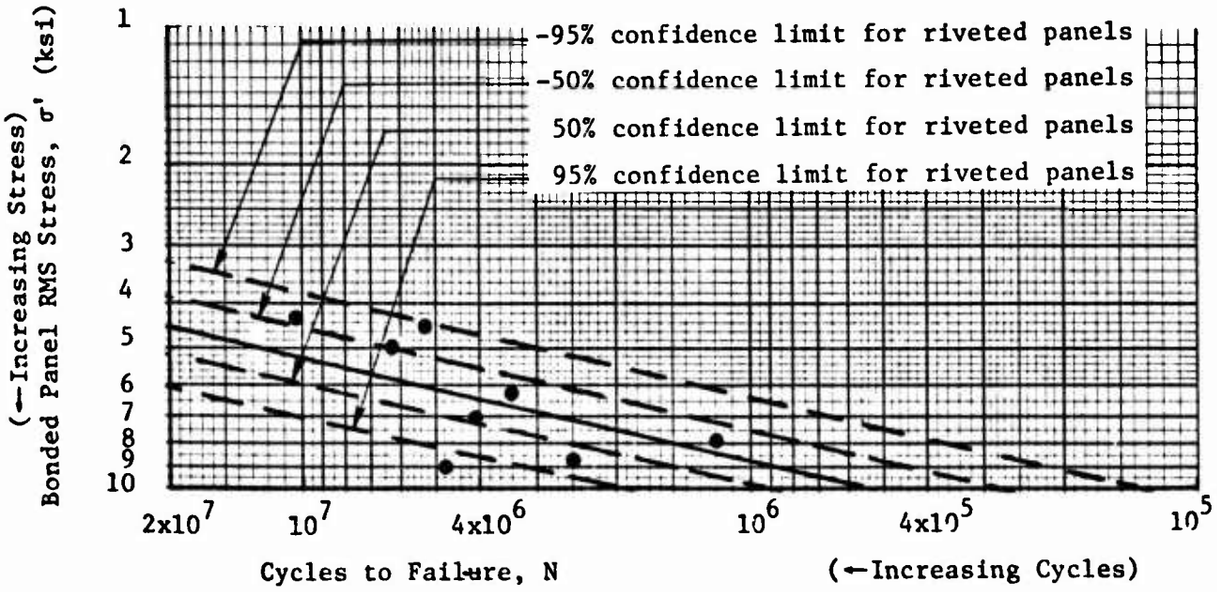

Figure 34. S-N Relations for the Bonded Acoustic Test Panels with the FM73/BR127 Adhesive System

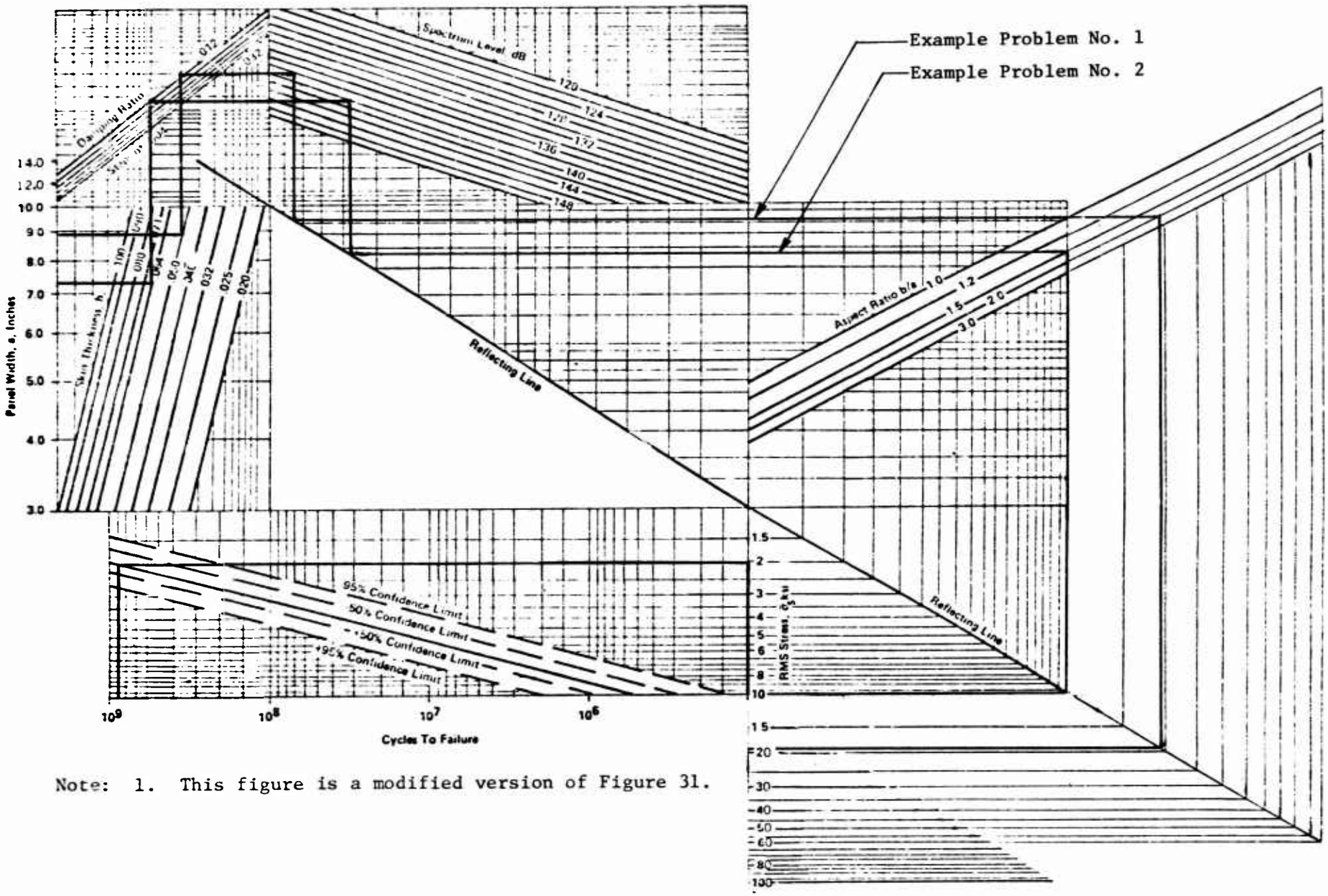

Note: 1. This figure is a modified version of Figure 31.

Figure 35. Nomograph for Sonic Fatigue Life of Bonded Multibay Panels Featuring the FM73/BR127 Adhesive System, the BAC-5555 Surface Preparation Method, and 7075-T6 Aluminum Alloy Skin and Substructure in a Room Temperature Sonic Environment

Step No. 2. σ' = 3.8 ksi-rms from the upper curve (for more conservatism) in Figure 34 using N = 10.5 x 10^6 cycles.

Step No. 3. $\bar{\sigma}_s = 5\ \sigma' = 19$ ksi-rms.

Step No. 4. By following the heavy line starting at $\bar{\sigma}_s$ = 19 ksi-rms in Figure 35, and accounting for an aspect ratio of 2.0, a spectrum level of 138 dB, a damping factor of 0.011, and a skin thickness of 0.050 inch, a panel width of 8.9 inch is obtained. The actual distance between center lines of the J-section stiffeners of the central bay of panel A-3-2 was 9 inches.

Steps No. 2', 3', and 4' that are described below may be substituted for steps 2, 3, and 4 that were previously described. (The limited range of the σ'-N curve of Figure 34 precludes its use in some problems for which steps No. 2', 3', and 4' may be used.)

2'. Read $\bar{\sigma}_s$ from the solid $\bar{\sigma}_s$-N curve in Figure 35 (or from the upper dashed curve of Figure 35 for more design conservatism). Let $\sigma' = \bar{\sigma}_s$.

3'. Compute $\bar{\sigma}_s = 5\ \sigma'$ from Equation (21).

4'. Enter Figure 35 with $\bar{\sigma}_s$ that was calculated in step No. 3' and determine the panel dimensions corresponding to the acoustic pressure spectrum level and panel damping factor. Use 0.012 as a typical damping factor.

Example problem No. 2 illustrating the use of steps No. 2', 3', and 4' and Figure 35 is given below.

Step No. 1. Pick a life of 9 x 10^8 cycles.

Step No. 2'. $\bar{\sigma}_s$ = 2 ksi-rms from the solid curve of Figure 35 using N^s= 9x10^8 cycles. Hence, $\sigma' = \bar{\sigma}_s$ = 2.0 ksi-rms.

Step No. 3'. A new value of $\bar{\sigma}_s$ is calculated: $\bar{\sigma}_s = 5\ \sigma' = 10$ ksi-rms.

Step No. 4'. Assume a panel aspect ratio of 1.5, a spectrum level of 140 dB, a damping factor of 0.012, and a skin thickness of 0.064 inch. By following the heavy line in Figure 35, starting at $\bar{\sigma}_s$ = 10 ksi-rms, a panel width of 7.2 inch is obtained.

Only nine multibay acoustic panel tests were performed to obtain data for the preparation of the design nomograph (Figure 35) for bonded multibay panels fabricated with the FM73/BR127 adhesive system and in accordance with the BAC-5555 process specification. Furthermore, the test data were obtained at only one overall SPL (namely 166 dB), with spectrum levels ranging only from 137

to 141 dB, with only one aspect ratio (namely 2), only two widths of the central bay of the test panels (namely 9 and 12 inches), with tapered flanges of the substructure to reduce stress concentrations and peel stresses, with a single design for stiffeners simulating longerons, and with a single design for stiffeners simulating frame sections. Therefore, the design nomograph (Figure 35) should be used with caution.

Other reasons for using Figure 35 with caution are that neither the modes of sonic fatigue failure nor the location of sonic fatigue failures are identified in Figure 35. All of the modes of the sonic fatigue failures of the test panels have not yet been identified (see Section VI). The location of the sonic fatigue failures in most instances were at the center of short sides of the central bay and in other instances were at the center of the long sides of the central bay (Figure 25). Until more sonic fatigue test data are available, it does not appear to be practical to develop S-N curves (or M-N curves as discussed in the following paragraphs) for different failure locations and modes of sonic fatigue failures of the multibay panels with the FM73/BR127 adhesive system and BAC-5555 surface preparation.

5.2 Comparison of S-N Data from Beam Tests with σ'-N Multibay Panel Data

At the beginning of the beam test program with shaker excitation, it was anticipated that the fatigue lives of the beams with tapered tee section flanges would exhibit some inverse relation with the thickness of the beams because (1) the target strain at the beginning of a fatigue test was the same (i.e., 900 micro-inches per inch, rms) for all beam specimens and (2) the fatigue life would be controlled by the peel stress which would be controlled by the bending moment in the skin at the end of the flange of the stiffener (Reference 15). However the test results (Table 8) did not verify the assumption that the fatigue lives would exhibit in all cases an inverse relation with the beam thicknesses. As expected, the fatigue lives of beam specimens of .050 inch thickness (the V-3 set) had greater fatigue lives than the beam specimens of .063 inch thickness (the V-4 set), and the fatigue lives of the beam specimens with 0.032 inch thickness (the V-1 set) had greater fatigue lives than the beam specimens with 0.040 inch thickness (the V-2 set). However, the V-3 set of beams had the highest average fatigue life of all the sets of beam specimens, and there are still uncertainties as to the reason.

The fact that an inverse relation between beam thickness and fatigue life was not developed in the shaker test program deterred the development of M-N data from the S-N data of the beam tests. M, the bending moment per inch of beam width in the skin at the end of the bonded stiffener, is calculated from

$$s = \frac{6M}{h^2} \tag{22}$$

with h being the skin thickness of the beam and s being the experimentally obtained stress from the one dimensional Hooke's law,

$$e = s/E \tag{23}$$

The M-N test data are presented in Figure 36 and M is the bending moment at the beginning of the fatigue test. The test data in Figure 36 does not lend itself to be represented accurately by a single M-N curve.

The lack of an experimentally derived M-N curve posed a problem in predicting the lives of the acoustic test panels from the use of beam fatigue test data, inasmuch as provisions had not been made for developing S-N curves for bond failures of beams with a constant skin thickness in the shaker test program.

A method described in the following paragraphs was explored to correlate the beam fatigue test and the sonic fatigue test data based on the observations that (1) in establishing the target strain in beam tests of V-3 specimens, the fatigue life appeared to increase by a factor of approximately 3.8 when the stress was lowered by 20 percent and (2) the parameter σ' of Equation (21) appeared useful in predicting the sonic fatigue test lives of the acoustic test panels.

The stress-life relations in the acoustic tests in terms of the parameter σ' and in the beam tests in terms of the target stress σ_v are summarized in Table 22. The target stress was calculated as 10^7 times the target strain of 0.0009 in./in., rms.

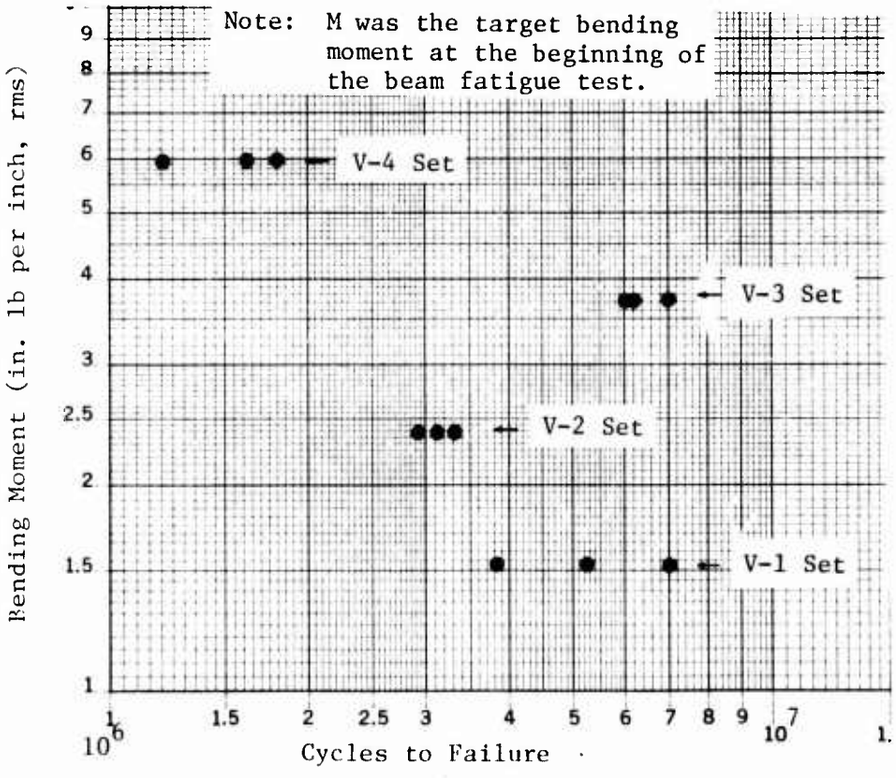

Figure 36. M-N Beam Test Data

TABLE 22. SUMMARY OF FATIGUE TEST DATA

SKIN THICKNESS	PANEL DATA			BEAM DATA		
	PANEL	CALCULATED STRESS σ'	TEST LIFE N	TARGET STRESS[1] S	TEST LIFE N_V	BEAM SET
(inch)		(ksi)	(cycles)	(ksi)	(cycles)	
.032	A-1-1	9.0	4.8×10^6	9.0	5.3×10^6	V-1
.032	A-1-2	7.9	1.2×10^6	9.0	5.3×10^6	V-1
.040	A-2-1	7.1	4.1×10^6	9.0	3.1×10^6	V-2
.040	A-2-2	6.3	3.4×10^6	9.0	3.1×10^6	V-2
.050	A-3-1[2]	5.1	3.7×10^6	9.0	6.4×10^6	V-3
.050	A-3-2	4.3	10.5×10^6	9.0	6.4×10^6	V-3
.050	A-4-1	6.1	2.5×10^6	9.0	6.4×10^6	V-3
.050	A-4-2	8.7	2.5×10^6	9.0	6.4×10^6	V-3
.063	A-5-1	4.9	6.3×10^6	9.0	1.5×10^6	V-4
.063	A-5-2	4.5	5.3×10^6	9.0	1.5×10^6	V-4

(1) σ_V was the target stress at the beginning of the beam fatigue tests. The excitation was maintained at a constant level during the tests and the strain drifted from the initial value.

(2) Panel A-3-1 experienced a sonic fatigue failure in a tee-section stiffener and not at a bonded joint.

Under the assumption that is not yet verified that the fatigue lives of all the beam specimens would have increased by a factor of 3.8 if the target stress in the skin of the beam had been reduced by 20 percent, S-N curves for each of the sets of beam specimens were prepared (Figures 37 through 40). The σ'-N data of Table 22 are also included as solid circles in the figures. The S-N curves in Figures 37 through 40 are shown with dashed lines to emphasize that the curves are tentative.

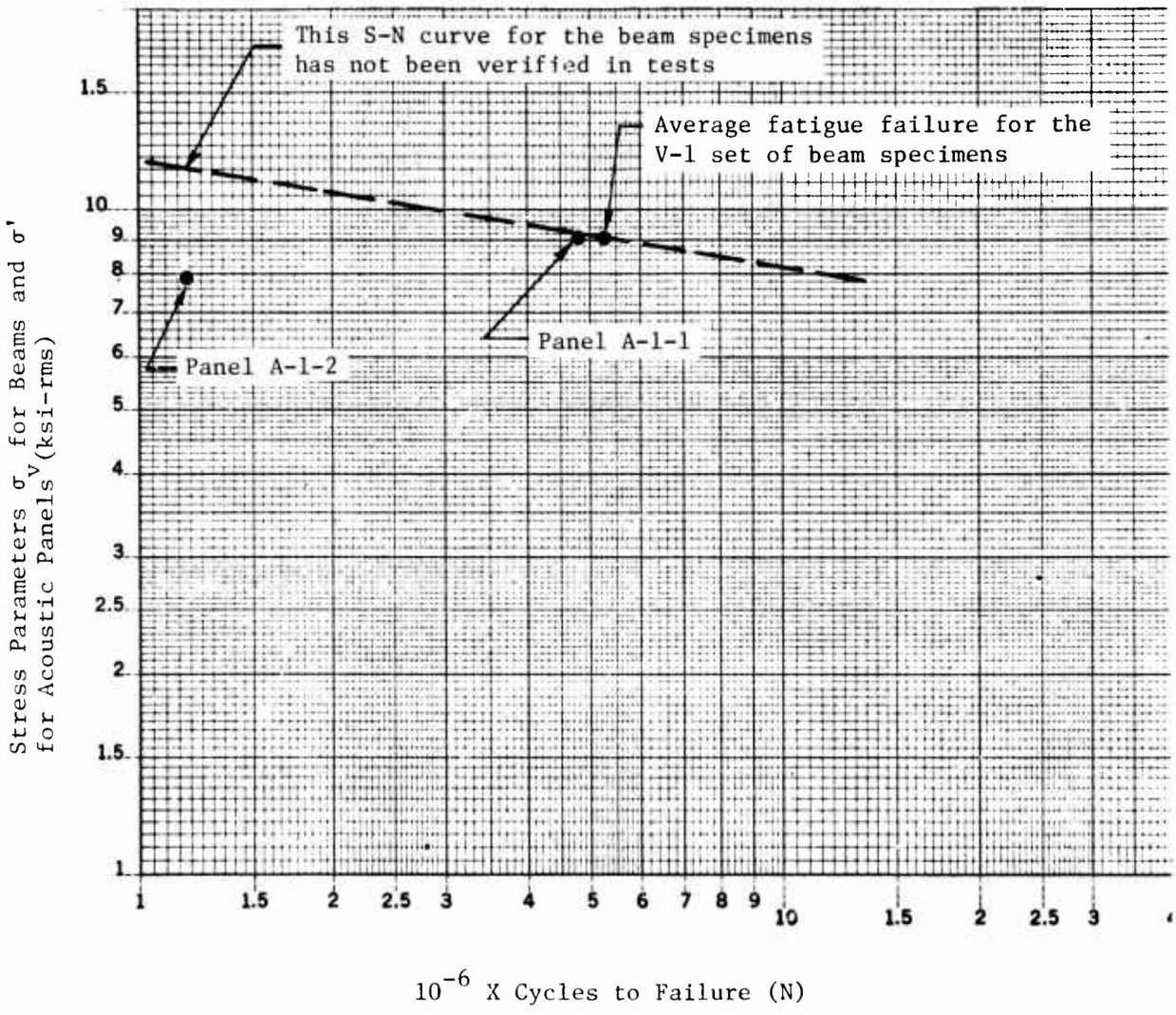

Figure 37. S-N Test Data for Specimens with Skin Thickness of 0.032 Inch

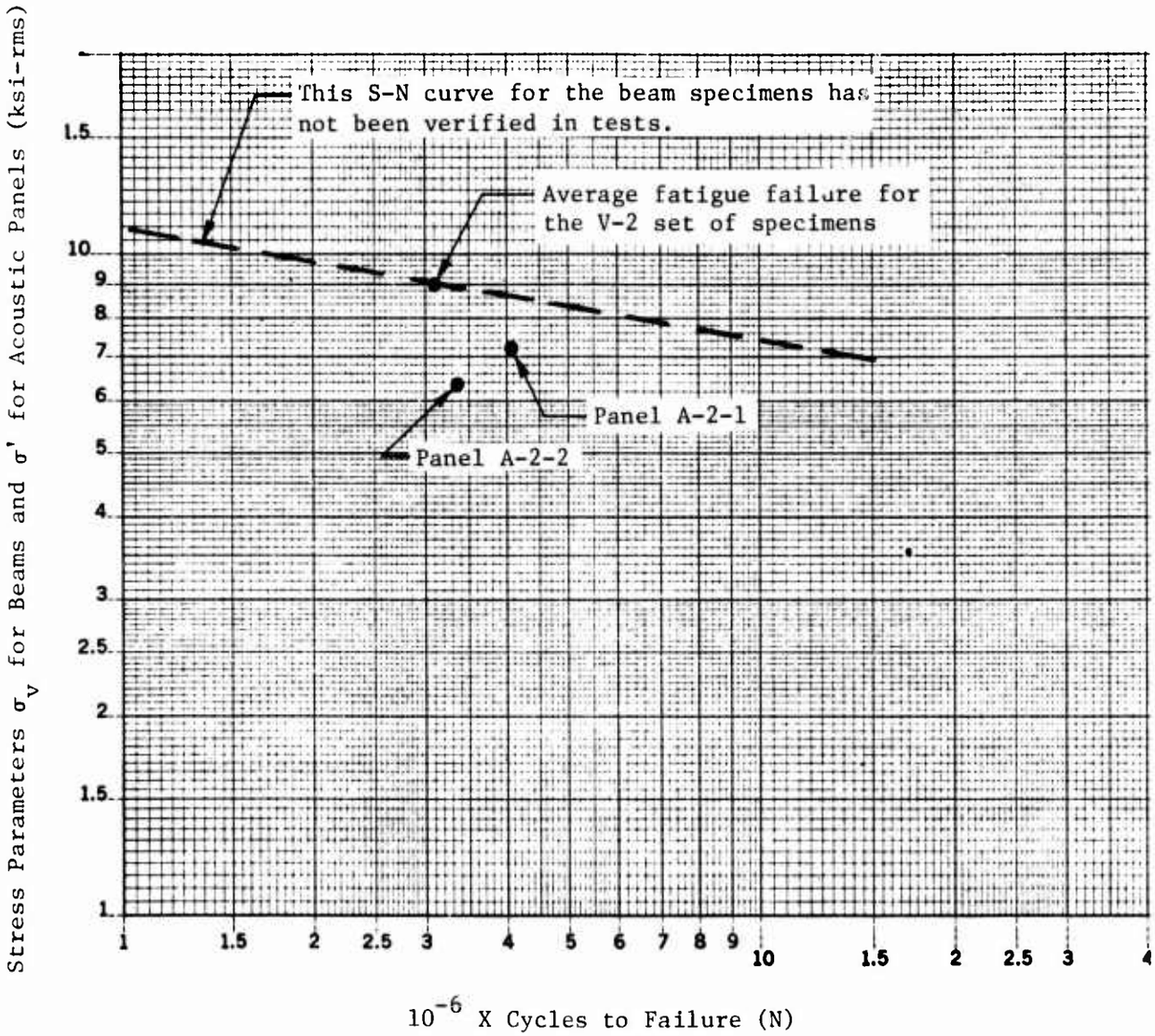

Figure 38. S-N Test Data for Specimens with Skin Thickness of 0.040 Inch

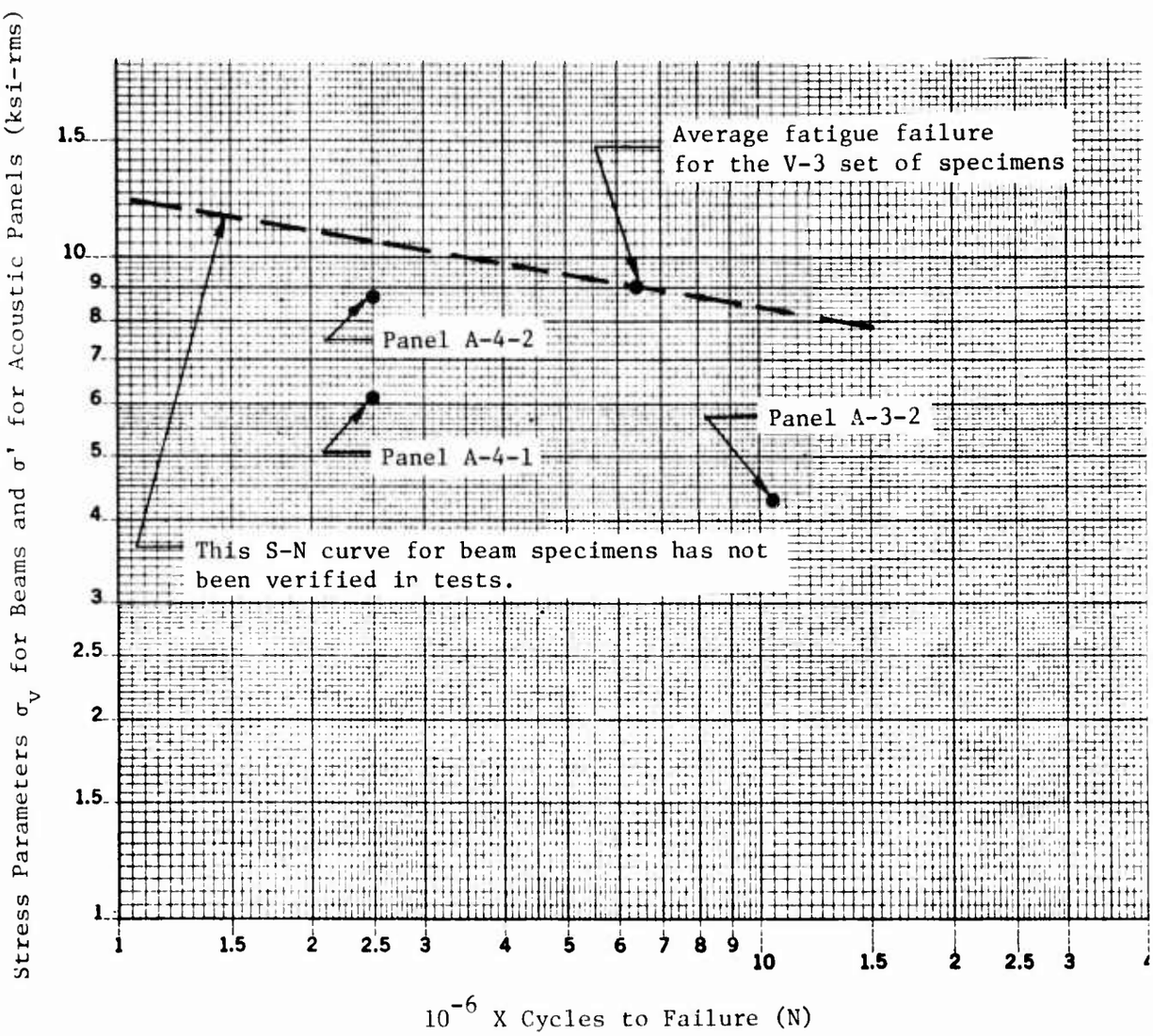

Figure 39. S-N Test Data for Specimens with Skin Thickness of 0.050 Inch

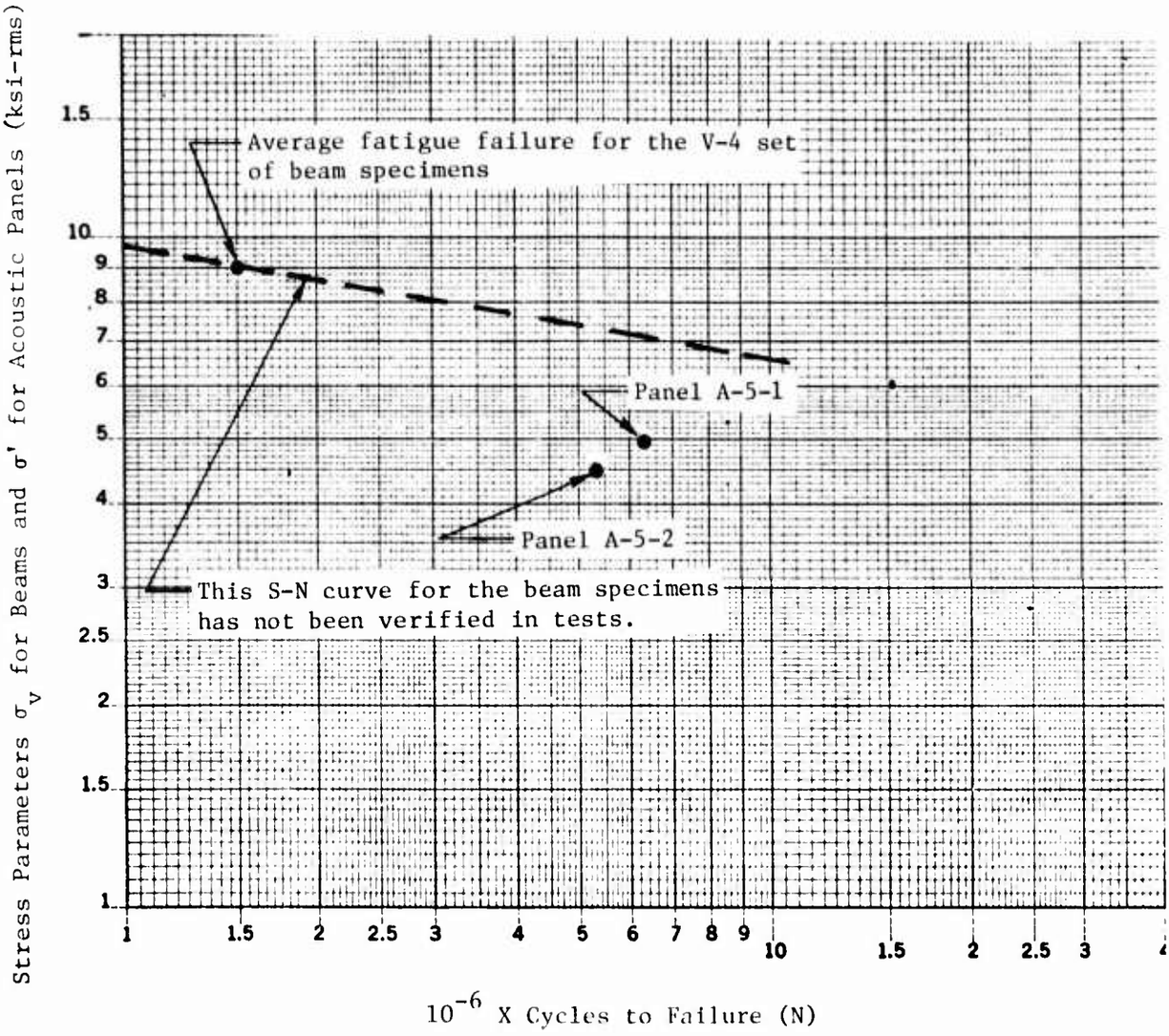

Figure 40. S-N Test Data for Specimens with Skin Thickness of 0.063 Inch

The stress σ_v in Figures 37 through 40 defined by the intersection of the dashed S-N curve and a vertical line through the appropriate solid circle with coordinates σ' and N for a particular acoustic test panel is presented in Table 23. Also in Table 23 are the values of σ' and the σ'/σ_v ratio for each of the acoustic test panels that experienced sonic fatigue properties. The ratio σ'/σ_v varied from a low of 52 percent to a high of 98 percent with an average of 74 percent. If through further beam and multibay panel testing that would produce even longer sonic fatigue lifetimes than were obtained in this test program, it could be shown that the ratio σ'/σ_v remains essentially constant, then the approach of using beam S-N tests to obtain fatigue data for predicting the sonic fatigue life of multibay panels would be further enhanced.

TABLE 23. RELATIONSHIP BETWEEN BEAM AND MULTIBAY PANELS FATIGUE STRENGTH PARAMETERS

PANEL	TEST LIFE	(1) σ_v BEAM DATA	σ' FROM CALCULATIONS	σ'/σ_v
	(Cycles)	(ksi-rms)	(ksi-rms)	(%)
A-1-1	4.8×10^6	9.2	9.0	98
A-1-2	1.2×10^6	10.1	7.9	78
A-2-1	4.1×10^6	8.6	7.1	83
A-2-2	3.4×10^6	8.8	6.3	72
A-3-2	10.5×10^6	8.3	4.3	52
A-4-1	2.5×10^6	10.0	6.1	61
A-4-2	2.5×10^6	10.0	8.7	87
A-5-1	6.3×10^6	7.1	4.9	69
A-5-2	5.3×10^6	7.3	4.5	62
Average				74

(1) σ_v is the stress obtained at the intersection of dashed S-N curve and a vertical line through the appropriate solid circle in Figures 37 through 40.

5.3 Prediction Method for the Predominant Response Frequency Versus Acoustic Pressure PSD

It was observed during the acoustic tests that the predominant response frequency often increased as the sound pressure level increased. Based on test data obtained in this program, Figure 41 was developed for predicting the predominant response frequency of multibay panels versus the acoustic pressure PSD. The ordinate in Figure 41 is a nondimensional frequency which is normalized to the fundamental frequency, $f_{L.S.}$, existing under low level discrete frequency excitation. (The subscript L.S. refers to loudspeaker.) In principle, $f_{L.S.}$ may be predicted by NASTRAN calculations (or by other suitable analytical methods) or obtained in tests under low level discrete frequency excitation. The abscissa in Figure 41 is a nondimensional acoustic pressure that accounts for the spectral density of the pressure, the predominant response frequency, and the damping factor.

Nondimensional response frequency versus nondimensional pressure curves (Figure 42) were developed for panels A-2-2, A-3-2, A-4-2, and A-5-2 on the basis of one-third octave band pressure data and predominant response frequency data in Table 14 and damping data in Table 15. The solid curve in Figure 41 represents an average of the curves in Figure 42. The dashed curves in Figure 41 represent limiting curves in Figure 42 with a minimum value of $f/f_{L.S.}$ equal to unity.

The curves in Figure 42 were developed as described below.

The acoustic spectrum level L_{SL} was computed from

$$L_{SL} = L_{1/3} - 10 \log_{10} (\Delta f) \tag{24}$$

with $L_{1/3}$ being the acoustic pressure in the 1/3 octave band containing the predominant response frequency of the panel and Δf being the 1/3 octave frequency band. The spectrum level was converted to pressure, p_{SL} (psi) from

$$L_{SL} = 20 \log_{10} \frac{p_{SL}}{2.9 \times 10^{-9}} \tag{25}$$

The acoustic pressure spectral density, S (psi^2/Hz), was computed from

$$S = (p_{SL})^2 \tag{26}$$

A pressure parameter P_{EQ} was computed from

$$P_{EQ} = \frac{\pi S f}{4 \zeta} \tag{27}$$

with f being the predominant response frequency in the test and ζ being the nondimensional viscous damping factor. (In the tests, the predominant response frequency coincided with the fundamental frequency unless otherwise noted.) A nondimensional pressure factor, P, was computed from

$$P = \frac{P_{EQ}}{E} \left(\frac{b}{t}\right)^4 \tag{28}$$

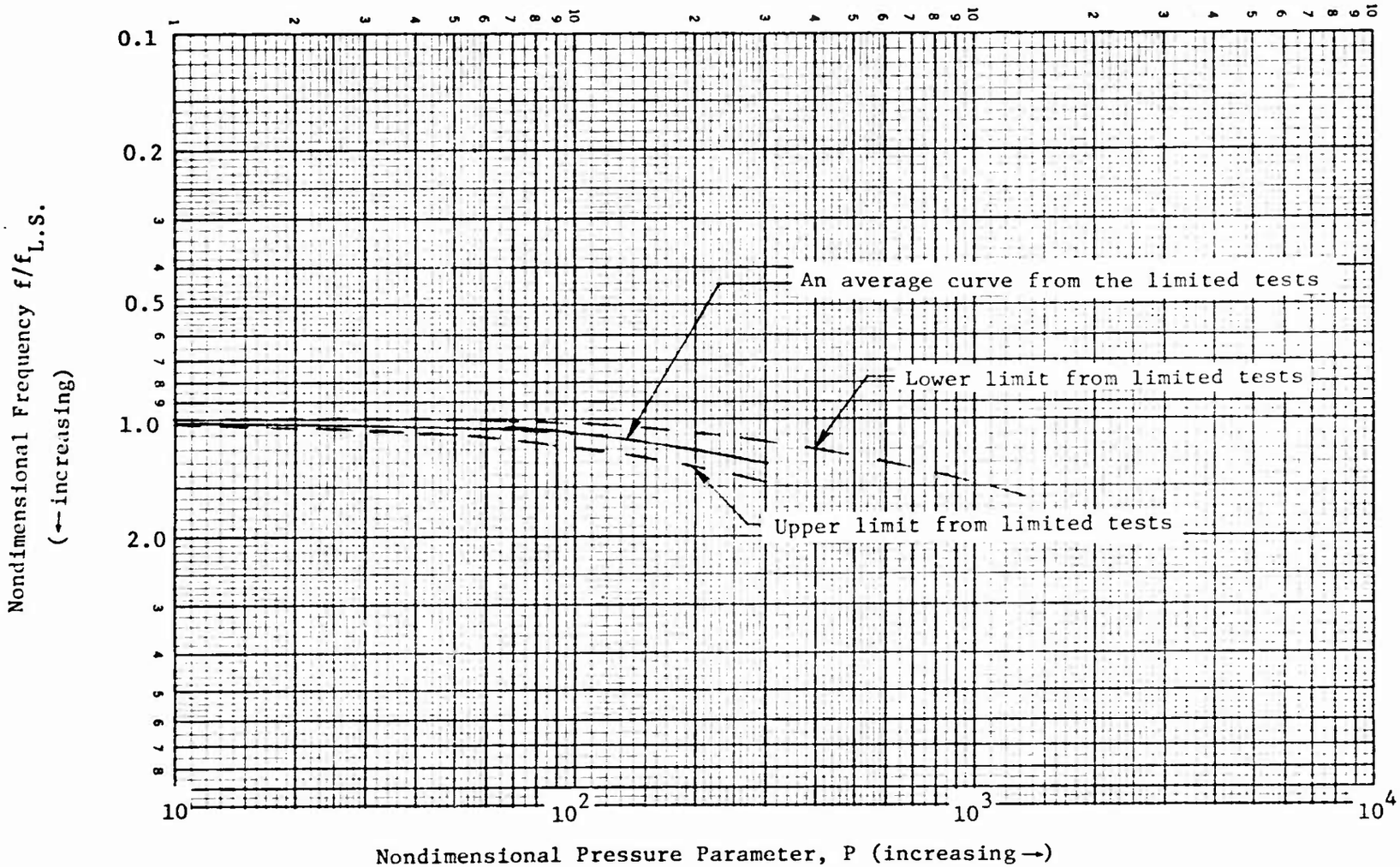

Figure 41. Average and Limiting Frequencies in Nonlinear Acoustic Response

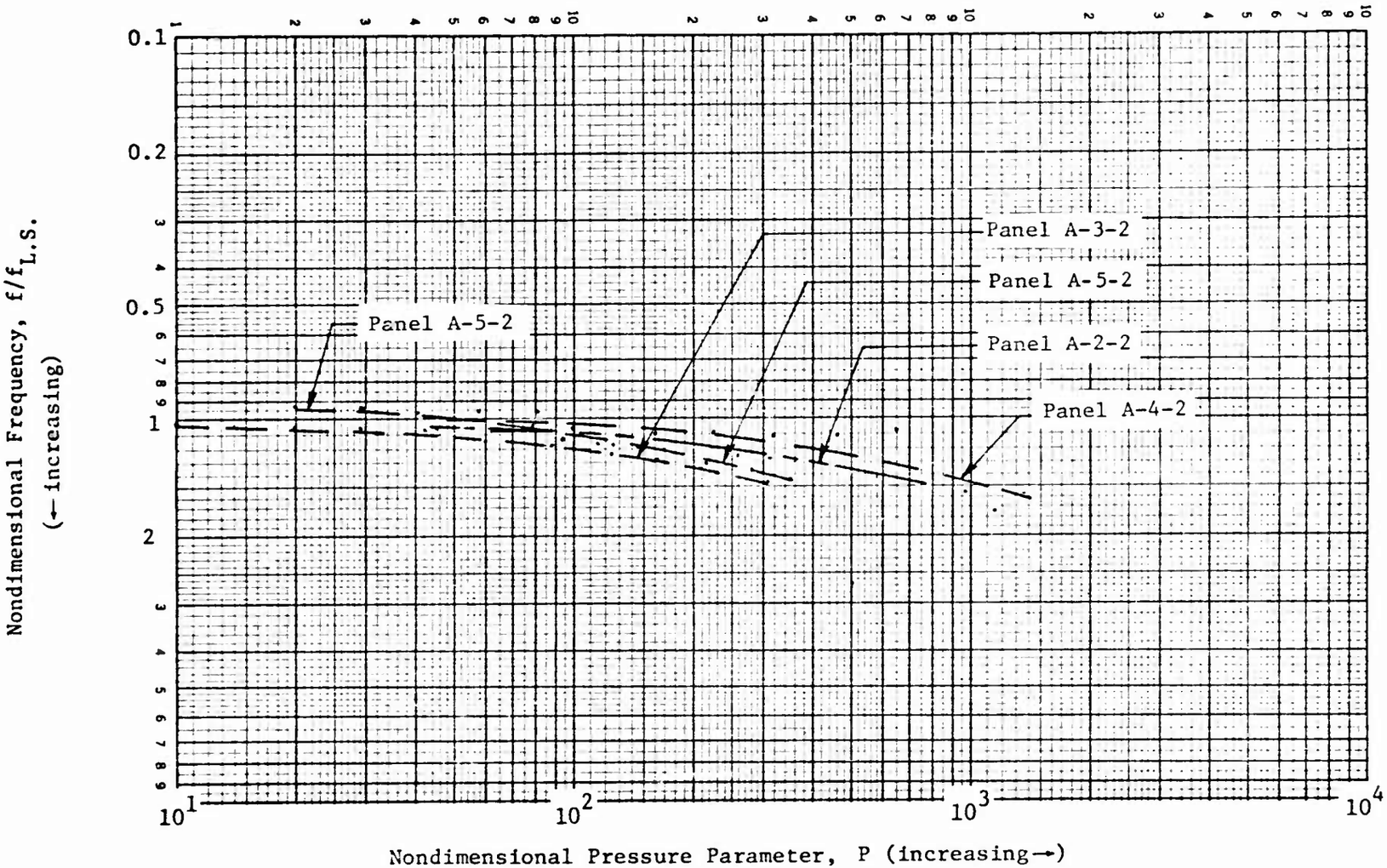

Figure 42. Frequencies in Nonlinear Acoustic Response

The right side of Equation (28) has been used in analyses of pressurized plates under static loading. Therefore, P_{EQ} may be considered as an equivalent static pressure.

The parameter f that is obtained from Figure 41 may be used to predict the fatigue life, t (with units of time), if the number of cycles (N) are prescribed, by using the relation

$$N = ft \tag{29}$$

It appears from Figure 42 that the onset of membrane stresses (from large deflections) are manifested by an increase in the fundamental frequency of the multi-bay panels when the parameter P reaches a value between 10 and 50, approximately. The fundamental frequency versus P does not increase rapidly with increasing P in the lower end of the nonlinear response range. Until more test data (and especially with different aspect ratios) are available, the solid curve in Figure 41 appears to be a useful tool for predicting the onset of the nonlinear acoustic response and the frequency at which fatigue damage is accumulating because of the application of a flat broadband acoustic spectrum. Because of the limited test data used in deriving the solid curve of Figure 41, the curve should be used with caution.

5.4 Comparison of S-N Data from Beam Tests with Experimental S-N Data from Acoustic Tests of Multibay Bonded Panels

The experimental sonic fatigue S-N data from the multibay panel tests are compared (in terms of strain) with the experimental beam fatigue S-N data in Figures 43 through 46. The multibay panel S-N data were obtained from Tables A-1 through A-5 of Appendix A and the beam S-N data were obtained from Figures 37 through 40 and then converted to strain with Equation (23). The lower strain of multibay panels relative to the target strain of beam specimens for a prescribed fatigue life is attributed principally to membrane and multimodal effects that were a factor in the multibay panel tests but not in the beam tests.

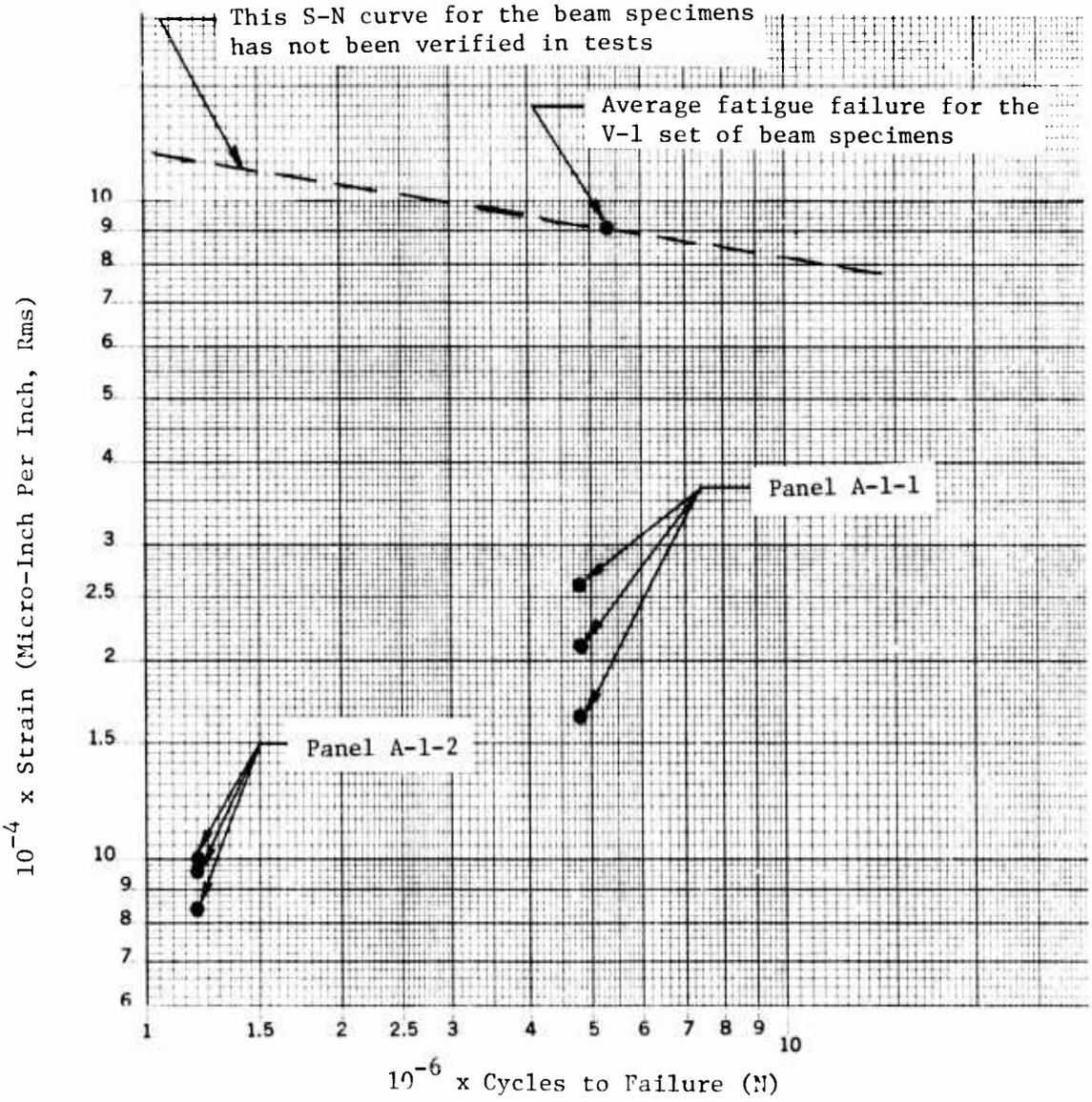

Figure 43. Experimental Strains in S-N Tests of Beams and Multibay Panels with Skin Thickness of 0.032 Inch

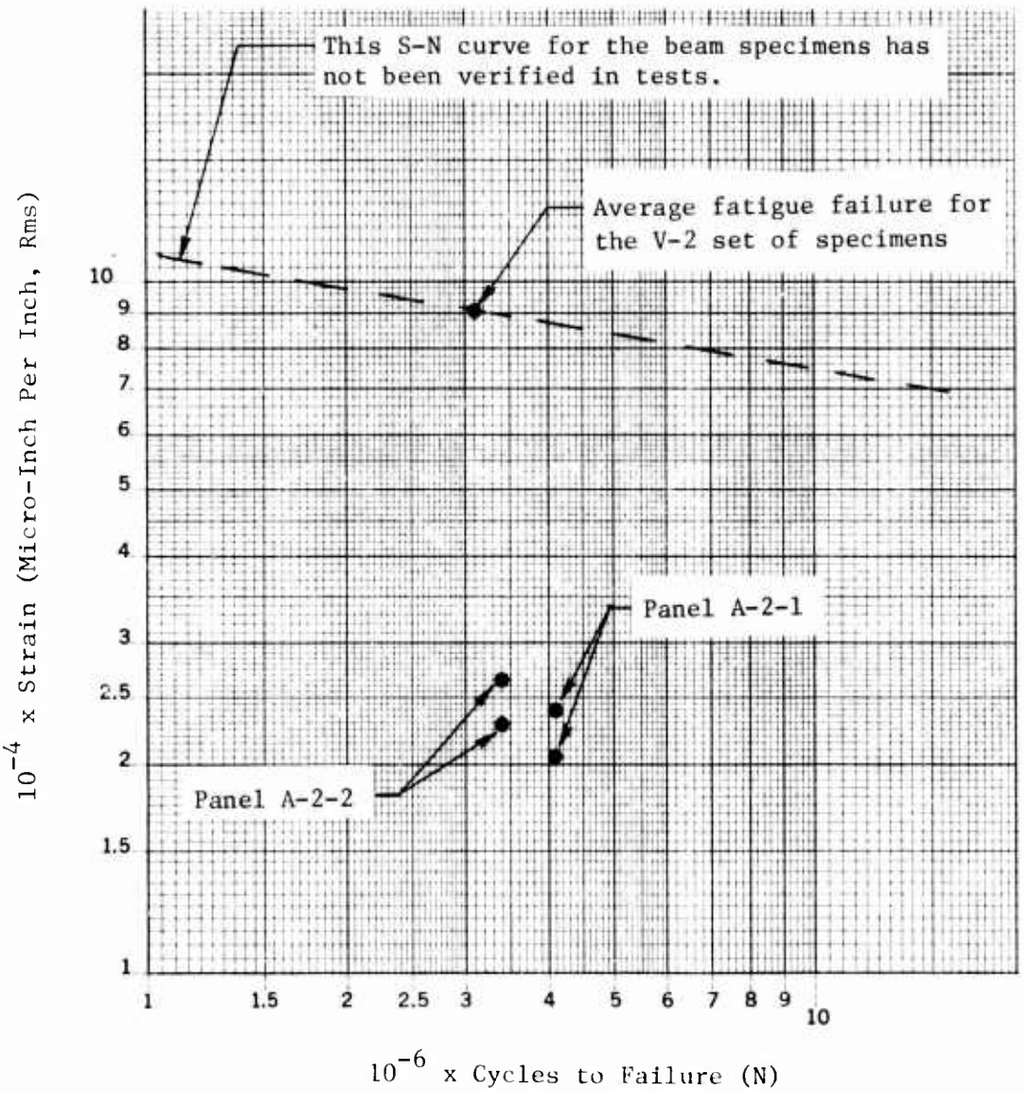

Figure 44. Experimental Strains in S-N Tests of Beams and Multibay Panels with Skin Thickness of 0.040 Inch

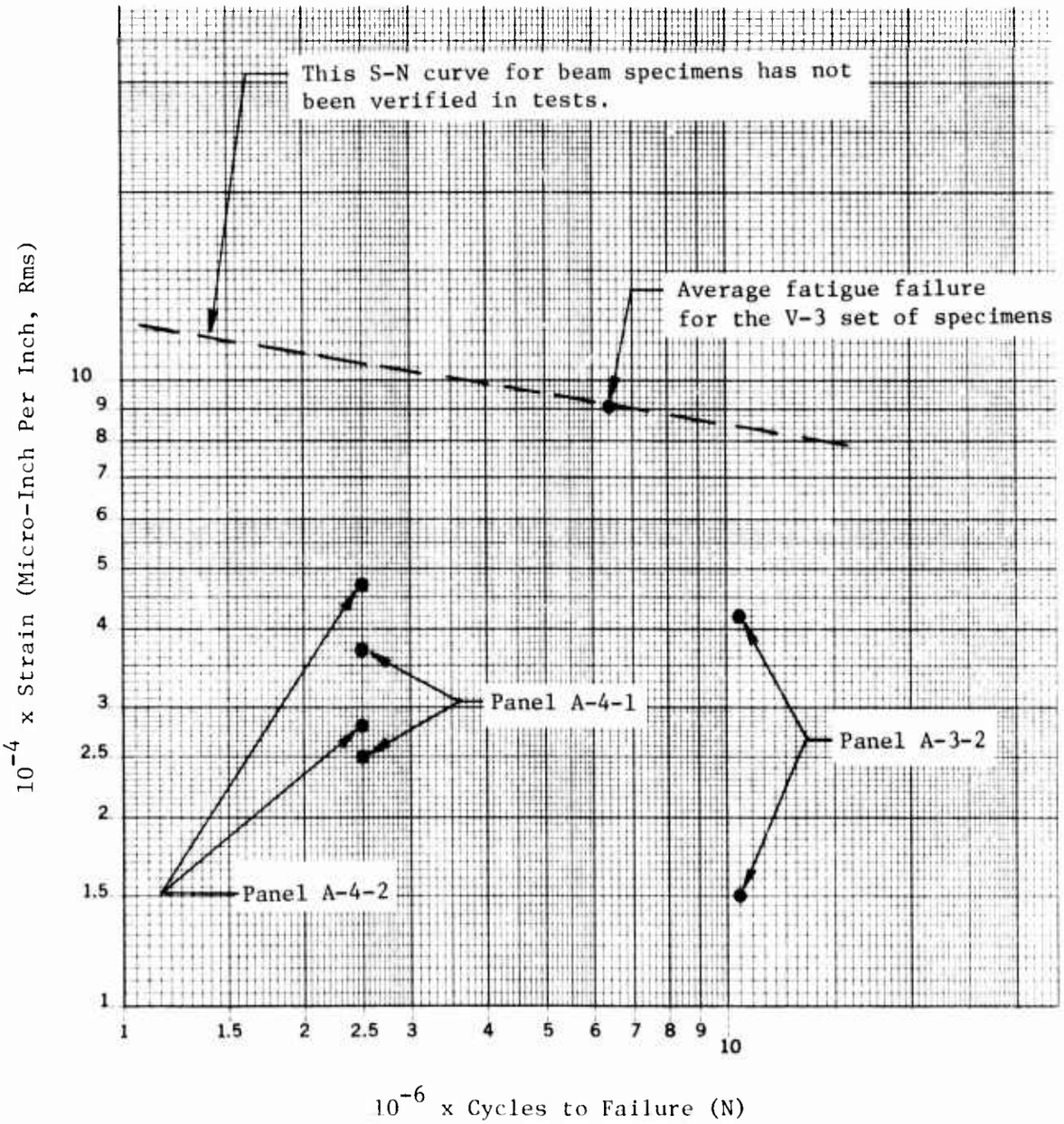

Figure 45. Experimental Strains in S-N Tests of Beams and Multibay Panels with Skin Thickness of 0.050 Inch

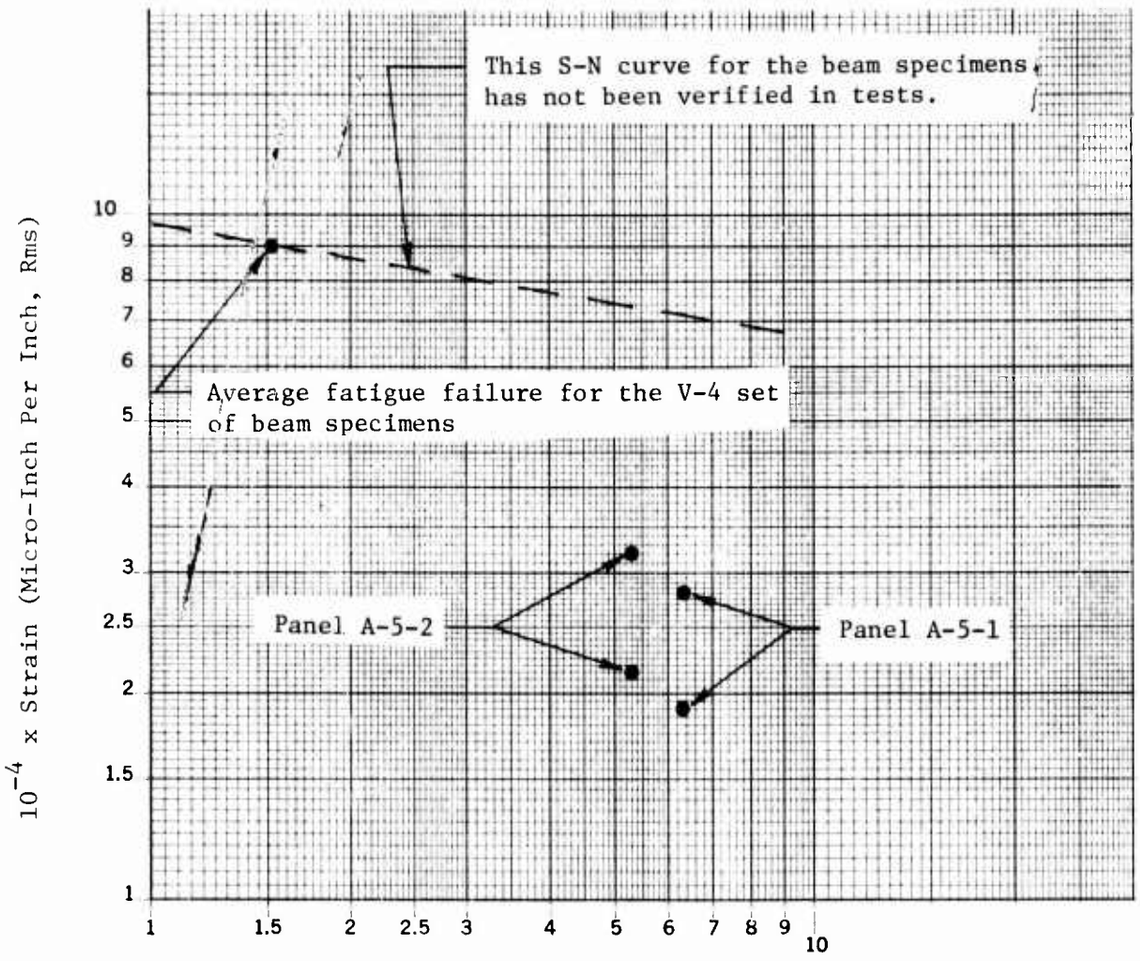

Figure 46. Experimental Strains in S-N Tests of Beams and Multibay Panels with Skin Thickness of 0.063 Inch

SECTION VI

MODES OF FATIGUE FAILURES

The skins of six of the beam specimens were peeled away from the substructure following the fatigue tests to investigate with the unaided eye the modes of fatigue failures, and the preliminary conclusion was that the fatigue damage was both adhesive and cohesive (Table 24), in contrast to only cohesive failures that were obtained in the adhesive in the static peel tests on the primed structure and the lap shear acceptance tests (Table 4). However, further investigation with scanning electron microscopy (SEM) techniques disclosed that the beam fatigue failures were cohesive failures in the BR127 primer near the surface of the adhesive in the stiffened beam assembly.

Panel A-5-1 was sectioned following the termination of the sonic fatigue test. The sonic fatigue failure observed by the unaided eye indicated that the primer in the sonic fatigue location of the bonded joint no longer adhered to the 7075-T6 aluminum alloy skin because the base metal of the skin was seen. However, as in the case of beam specimens, further investigation of the sonic fatigue failure mode of Panel A-5-1 with SEM analysis resulted in the conclusion that there was cohesive failure in the primer near the 7075-T6 aluminum skin rather than adhesive failure at the surface of the skin.

SEM analysis to investigate the beam and multibay panel failure modes was documented (Reference 16). The pressure of fatigue failure modes other than cohesive failures in the adhesive were unanticipated in this beam and multibay panel test program.

In principle, separate S-N or M-N curves should be prepared for each mode of failure that occurs such as the ones that are listed below.

- Cohesive failure of the FM73 adhesive
- Adhesive failure at the interface between the FM73 and the BR127 primer
- Failure in BR127 primer or its interface with the aluminum sheet
- Aluminum alloy sheet failures
- Aluminum alloy stiffener failures

However, in this program there were insufficient tests to investigate all of the failure modes that are listed above.

TABLE 24. ADHESIVE BOND DAMAGE DEVELOPED DURING BEAM FATIGUE TESTS

SPECIMEN DESIGNATION	TYPE OF FAILURE OBSERVED WITH THE UNAIDED EYE DURING THE FATIGUE TEST(1)
V-1-2	Fatigue failure on approximately 40 percent of the total bonded surface. The fatigue failure appeared to be 100 percent adhesive.
V-2-3	Fatigue failure on approximately 60 percent of the total bonded surface. The fatigue failure appeared to be 95 percent adhesive and 5 percent cohesive.
V-3-4	Fatigue failure on approximately 50 percent of the total bonded surface. The fatigue failure appeared to be 100 percent adhesive.
V-4-1	Fatigue failure on 50 percent of the total bonded surface. The fatigue failure appeared to be 70 percent adhesive and 30% cohesive.
V-5-3	Fatigue failure on approximately 40 percent of the total bonded surface. The fatigue failure appeared to be 80 percent adhesive and 20 percent cohesive.
V-6-3	Fatigue failure on less than approximately 5 percent of the total bonded flat metallic surfaces. The fatigue failure appeared to be 100 percent cohesive between the flat metallic surfaces and appeared to be 100 percent adhesive between the flash and the flat metallic surface.

(1) See the previous page for a discussion of the results of the SEM analysis that resulted in the conclusion that the beam fatigue failures were in the primer but near the surface of the adhesive. Therefore, although fatigue failures appeared to be adhesive, they are classified as cohesive failures.

SECTION VII

CONCLUSIONS

A few important conclusions were reached in evaluating the program results and they are listed below.

1. The sonic fatigue test lives versus spectrum level of the broadband acoustic excitation of the bonded test panels featuring the FM73/BR127 adhesive system, a phosphoric acid anodizing (BAC-5555) surface preparation treatment, and 7075-T6 aluminum alloy skins and substructure were greater (and substantially) in almost every case than the sonic fatigue lives of riveted multi-bay panels of 7075-T6 aluminum alloy skins and substructure having the same skin thickness and nominal dimensions of the central bay.

2. The adaption of a well-known sonic fatigue design nomograph for riveted multi-bay panels (Figure 31) produced a nomograph with satisfactory accuracy in predicting the sonic fatigue lives of the acoustic test panels.

3. More sonic fatigue test data of bonded aluminum alloy panels and failure mode identification are needed to determine the range of applicability of Figure 35 and the effects of changes in the design configurations and thicknesses of the substructure.

4. More beam fatigue data and failure mode identification are needed to determine the accuracy and usefulness of the S-N curves in Figures 37 through 40 and 43 through 46.

5. More finite element analysis is necessary to determine the best structural modeling to obtain natural frequencies and modal shapes of multibay acoustic panels in free vibrations and the rms strain response to the acoustic excitation when linear structural dynamics theory is applicable.

6. More finite element analysis is necessary to (1) determine the peel stresses, shear stresses, and principal stresses of the adhesive in tapered and untapered bonded joints of the beam specimens subjected to time-random excitation and (2) relate the effects of these stresses on the modes of fatigue failures.

7. More test data and analysis are needed to determine the nonlinear stress response to broadband acoustic excitation at sufficiently high intensity noise levels and the effects of the membrane stresses in the panel skins on the mode of sonic fatigue failure of bonded joints.

REFERENCES

1. F. F. Rudder, Jr. and H. E. Plumblee, Jr., "Sonic Fatigue Design Guide for Military Aircraft," Technical Report AFFDL-TR-74-112, May 1975.

2. "Structural Design for Acoustic Fatigue," Technical Documentary Report No. ASD-TDR-63-820, October 1963.

3. J. R. Ballentine, et al., "Refinement of Sonic Fatigue Structural Design Criteria," Technical Report AFFDL-TR-67-156, January 1968.

4. F. F. Rudder, Jr., "Acoustic Fatigue of Aircraft Structural Component Assemblies," Technical Report AFFDL-TR-71-107, February 1972.

5. A. G. R. Thomson and R. F. Lambert, "Acoustic Fatigue Design Data," AGARDograph No. 162, Parts I, II, and III.

6. C. W. Schneider, "Acoustic Fatigue of Aircraft Structures at Elevated Temperatures," Technical Report AFFDL-TR-73-155, Parts I and II, 1974.

7. T. F. Nelson, "An Investigation of the Effects of Surrounding Structure on Sonic Fatigue," NASA CR-1536, May 1970.

8. F. F. Rudder, Jr., "Study of Effects of Design Details on Structural Response to Acoustic Excitation," NASA CR-1959, March 1972.

9. M. J. Jacobson and P. E. Finwall, "Effects of Structural Heating on the Sonic Fatigue of Aerospace Vehicle Structures," Technical Report AFFDL-TR-73-56, January 1974.

10. W. C. Hurty and M. F. Rubinstein, "Dynamics of Structures," Prentice-Hall, Inc., Englewood Cliffs, New Jersey, 1964, p. 203.

11. M. J. Jacobson, "Acoustic Fatigue Design Information for Skin-Stiffened Metallic Panels," Northrop Report No. NOR-69-111, August 1969.

12. M. J. Jacobson, "Dynamic Response and Acoustic Fatigue Characteristics of Flat Skin-Stringer Aluminum Alloy Panels," Northrop Report No. NOR-70-22, February 1970.

13. M. J. Jacobson, "Advanced Composite Joints; Design and Acoustic Fatigue Characteristics," Technical Report AFFDL-TR-71-126, April 1972.

14. W. T. Thomson, "Mechanical Vibrations," Prentice Hall, New York, 1948, p. 45.

15. F. Sandow, Jr. and O. F. Maurer, "Random Vibration Fatigue Tests of Weldbonded and Bonded Joints," The Shock and Vibration Bulletin, Part 3, Aug. 1976, pp. 73-85.

16. Danforth, M.A., "Sonic Fatigue Metal Adhesive Failure Analysis," McDonnell Douglas Corporation (Long Beach, California) Report No. MDC J6071, May 1977.

APPENDIX A

ACOUSTIC PRESSURE AND STRAIN RESPONSE DATA

A.1 Rms Strain Response to Acoustic Excitation

During the acoustic tests, the noise intensity was increased from 136 dB in increments of 3 dB until 166 dB was reached. Strain readings (Table A-1 through A-5) were taken rapidly below the 166 dB overall SPL to avoid appreciable accumulation of fatigue damage prior to the sonic fatigue test at 166 dB.

A.2 One-Third Octave Band and Narrow Band Data

Samples of the 1/3 octave band and narrow band analyses of acoustic pressure and strain response obtained in the test of panel A-4-1 are given in Figures A-1 through A-14. One-third octave band analysis of acoustic pressure in the test of panel A-4-1 during the 145 dB run is in Figure A-1 and during the 166 dB run is in Figure A-2. Narrow band spectral analyses of the acoustic pressure during the 145 dB and 166 dB runs are in Figures A-3 and A-4, respectively. Narrow band and one-third octave band analyses of the strain response of strain gage No. 4 during the 145 dB and 166 dB runs are in Figures A-5 through A-8.

The pressure spectral density at 140 Hz obtained in the narrow band analysis of panel A-4-1 (Figure A-4) subjected to 166 dB overall SPL is approximately 10×10^{-4} psi^2/Hz and agrees well with the acoustic pressure PSD (10.5×10^{-4} psi^2/Hz) calculated on the basis of average pressure in the one-third octave band (Table 13).

The one-third octave band pressure distributions at 145 dB and 166 dB are very similar in shape (Figures A-1 and A-2), and the narrow band pressure distributions have many common characteristics (Figures A-3 and A-4). The peaks of the strain PSD of gage No. 4 are quite sharp at 145 dB (Figure A-5), whereas twin strain PSD peaks occur during the 166 dB run (Figure A-6) at approximately 140 Hz and below 80 Hz. The one-third octave distributions in Figures A-7 and A-8 depict the more peaked strain distribution in the 145 dB run as opposed to the 166 dB run.

From the strain PSD curves (Figures A-5 through A-7), it is deduced that although the predominant resonant response contribute considerably to the rms strain, the forced response at other frequencies also produce a significant portion of the overall rms strain response. For example, on the basis of comparisons of Figures A-4 and A-6, it appears that the strain response peak at approximately 140 Hz is a result of a response at a natural frequency, whereas the response in the 70 to 80 Hz range appears not to be occurring at a natural frequency. The response peak at approximately 70 Hz (Figure A-6) may be indicative of resonances of supporting structure that are transmitted into the central bay.

Narrow band analyses of the strain response of strain gage No. 2 of panel A-4-1 at 145 dB and 166 dB overall SPL are in Figures A-9 and A-10, respectively; of strain gage No. 2 of panel A-2-1 at 142 dB and 166 dB overall SPL are in Figures A-11 and A-13, respectively; and of strain gage No. 4 of panel A-2-1 at 142 dB and 166 dB overall SPL are in Figures A-12 and A-14, respectively.

TABLE A-1. OVERALL RMS STRAINS VERSUS OVERALL SPL'S FOR A-1 PANELS

PANEL A-1-1							PANEL A-1-2						
OVERALL SPL	TIME[1]	STRAIN					OVERALL SPL	TIME[1]	STRAIN				
		GAGE NO. 1	GAGE NO. 2	GAGE NO. 3	GAGE NO. 4	GAGE NO. 11			GAGE NO. 1	GAGE NO. 2	GAGE NO. 3	GAGE NO. 4	GAGE NO. 11
(dB)	(min)	(2)	(2)	(2)	(2)	(2)	(dB)	(min)	(2)	(2)	(2)	(2)	(2)
136		23	19	14	9	47	136[5]		20	26	12	13	68
139		30	25	17	12	60	139[5]		20	26	12	13	70
142		44	36	28	16	84	142		25	32	15	17	90
145		56	50	36	25	110	145		28	38	18	21	100
148		80	72	48	34	150	148		34	43	24	25	115
151		110	95	70	54	205	151		42	53	29	31	145
154		145	125	94	70	245	154		49	58	33	36	155
157		170	150	120	88	280	157		60	70	41	48	170
160		195	165	145	110	315	160		76	84	54	65	205
163		220	190	170	135	340	163		88	100	64	76	240
166	16	260	230	210	165	380	166	30	100	110	84	96	250
166	48	260	235	225	165	380	166	50	150	165	135	135	out
166	79	out	235	220	165	380	166[3]	95	230	290	450	170	out
166	140	out	240	220	280	out	166	(120)	(450)	(520)	(460)	(300)	out
166	200	out	250	230	out	out	166[4]	(132)	(460)	(420)	(460)	(420)	out
166	260	out	235	215	out	out							
166	314	out	230	245	480	out							
166	370	out	230	580	480	out							

(1) The accumulated time of exposure during the high intensity sonic fatigue test.
(2) The units of strain are micro-inch per inch, rms.
(3) A small bond delamination was observed at the end of this run (Run No. 13) in the vicinity of Gages No. 2 and 3.
(4) During Run No. 15, the value of the predominant response frequency dropped from 204 Hz to 190 Hz. At the end of this run (Run No. 15), it was noted that delamination, observed at the end of Run No. 13 had grown significantly and bond delamination at Gage No. 1 was visible. The parentheses enclosing the strains and exposure times in Runs No. 14 and 15 signify that the initial sonic fatigue failures were visibly detected at the end of Run No. 13.
(5) A possible explanation for the almost complete duplication of strains in Runs No. 1 and 2 is technician error. The electrical noise equivalent was approximately 1 micro-inch per inch, rms.

TABLE A-2. OVERALL RMS STRAINS VERSUS OVERALL SPL'S FOR A-2 PANELS

PANEL A-2-1							PANEL A-2-2						
OVERALL SPL	TIME[1]	STRAIN					OVERALL SPL	TIME[1]	STRAIN				
		GAGE NO. 1	GAGE NO. 2	GAGE NO. 3	GAGE NO. 4	GAGE NO. 11			GAGE NO. 1	GAGE NO. 2	GAGE NO. 3	GAGE NO. 4	GAGE NO. 11
(dB)	(min)	(2)	(2)	(2)	(2)	(2)	(dB)	(min)	(2)	(2)	(2)	(2)	(2)
136		15	16	10	14	40	136		16	24	9	9	42
139		28	25	15	21	75	139		19	26	11	12	52
142		34	32	17	26	84	142		27	36	15	16	66
145		40	40	22	30	100	145		38	48	24	26	95
148		56	58	30	44	140	148		52	66	30	33	125
151		74	78	40	62	180	151		78	100	56	60	180
154		92	105	56	88	220	154		100	140	74	84	230
157		125	135	80	140	300	157		120	160	95	105	270
160		155	175	110	175	370	160		150	190	120	140	320
163		180	205	130	215	395	163		180	230	155	180	380
166	10	205	240	175	260	420	166	60	230	265	200	220	430
166	30	215	245	175	265	out	166	100	200	260	190	210	out
166	62	210	240	165	280	out	166	160	out	350	170	220	out
166	122	210	255	165	280	out	166	205	out	480	250	310	out
166	182	215	500	165	300	out	166[3]	265	out	400	360	380	out
166	242	220	410	145	400	out	166	(325)	out	out	(430)	(440)	out
166	264	480	out	155	410	out							
166	324	450	out	155	430	out							

(1) The accumulated time of exposure during the high intensity sonic fatigue test.
(2) The units of strain are micro-inch per inch, rms.
(3) At the end of Run No. 15, separation between the J-section stiffeners and the skin was visible in the central bay. The sonic fatigue test was continued for one more run to observe the growth of the separation.

TABLE A-3. OVERALL RMS STRAINS VERSUS OVERALL SPL'S FOR A-3 PANELS

PANEL A-3-1							PANEL A-3-2						
OVERALL SPL	TIME[1]	STRAIN					OVERALL SPL	TIME[1]	STRAIN				
		GAGE NO. 1	GAGE NO. 2	GAGE NO. 3	GAGE NO. 4	GAGE NO. 11			GAGE NO. 1	GAGE NO. 2	GAGE NO. 3	GAGE NO. 4	GAGE NO. 11
(dB)	(min)	(2)	(2)	(2)	(2)	(2)	(dB)	(min)	(2)	(2)	(2)	(2)	(2)
136		20	40	28	22	35	136		12	18	8	20	42
139		30	52	44	30	48	139		18	28	10	28	56
142		40	75	60	42	70	142		24	36	14	38	72
145		60	110	85	60	95	145		30	42	18	50	100
148		80	152	125	90	145	148		40	58	24	68	130
151		125	225	200	135	210	151		56	78	34	105	180
154		148	270	250	185	240	154		72	110	52	150	230
157		180	320	290	240	300	157		100	140	68	190	280
160		200	380	350	280	340	160		120	170	84	240	340
163		240	450	400	350	380	163		145	210	120	320	400
165	15	280	480	500	375	400	166	60	160	240	150	420	430
166	30	275	out	520	380	400	166	120	150	380	160	480	out
166	60	280	out	520	430	420	166	180	150	out	200	540	out
166	120	260	out	530	410	410	166	220	150	out	260	560	out
166	180	280	out	550	420	out	166	280	150	out	320	560	out
166	240	280	out	570	460	out	166	305	150	out	380	560	out
166	300	280	out	590	490	out	166	330	150	out	420	560	out
							166[3]	390	150	out	440	560	out

(1) The accumulated time of exposure during the high intensity sonic fatigue test.
(2) The units of strain are micro-inches per inch, rms.
(3) Frame repairs were made after this run, and the sonic fatigue test was continued.

TABLE A-4. OVERALL RMS STRAINS VERSUS OVERALL SPL'S FOR A-4 PANELS

PANEL A-4-1							PANEL A-4-2						
OVERALL SPL	TIME[1]	STRAIN					OVERALL SPL	TIME[1]	STRAIN				
		GAGE NO. 1	GAGE NO. 2	GAGE NO. 3	GAGE NO. 4	GAGE NO. 11			GAGE NO. 1	GAGE NO. 2	GAGE NO. 3	GAGE NO. 4	GAGE NO. 11
(dB)	(min)	(2)	(2)	(2)	(2)	(2)	(dB)	(min)	(2)	(2)	(2)	(2)	(2)
136		52	38	18	37	98	136		48	54	32	64	120
139		66	48	28	54	140	139		50	64	36	78	130
142		82	68	34	68	160	142		60	76	46	110	160
145		91	78	42	86	178	145		72	105	60	140	190
148		108	83	57	106	195	148		100	120	?	165	210
151		122	98	74	134	220	151		115	130	100	185	220
154		157	132	105	175	265	154		130	145	115	210	245
157		183	159	128	215	300	157		150	170	140	250	270
160		205	178	150	245	338	160		175	190	170	280	330
163		245	215	190	290	390	163		210	225	210	390	390
166	10	300	265	248	370	440	166	60	260	270	280	470	470
166	40	290	255	250	380	425	166	105	250	330	540	660	460
166	70	out	255	360	530	415	166	165	250	380	600	560	out
166	115	out	270	580	640	out	166	225	270	440	560	out	out
166	150	out	out	600	600	out	166	285	300	480	550	out	out
166	182	out	out	600	580	out							
166	242	out	out	560	out	out							
166	302	out	out	out	out	out							

(1) The accumulated time of exposure during the high intensity sonic fatigue test.
(2) The units of strain are micro-inch per inch, rms.

TABLE A-5. OVERALL RMS STRAINS VERSUS OVERALL SPL'S FOR A-5 PANELS

PANEL A-5-1							PANEL A-5-2						
		STRAIN							STRAIN				
OVERALL SPL	TIME[1]	GAGE NO. 1	GAGE NO. 2	GAGE NO. 3	GAGE NO. 4	GAGE NO. 11	OVERALL SPL	TIME [1]	GAGE NO. 1	GAGE NO. 2	GAGE NO. 3	GAGE NO. 4	GAGE NO. 11
(dB)	(min)	(2)	(2)	(2)	(2)	(2)	(dB)	(min)	(2)	(2)	(2)	(2)	(2)
136		19	32	22	14	46	136		38	26	19	30	58
139		23	36	32	20	54	139		54	36	24	38	76
142		32	50	44	28	68	142		68	44	32	50	100
145		40	64	52	34	100	145		82	52	42	66	120
148		54	90	78	48	120	148		105	65	54	82	140
151		74	115	100	64	160	151		125	76	68	110	170
154		92	150	120	80	200	154		150	100	95	140	200
157		120	170	150	100	240	157		170	115	115	165	225
160		145	220	185	120	290	160		195	135	140	200	260
163		165	250	220	145	330	163		225	160	175	240	320
166	22	210	310	280	190	400	166	40	265	190	215	320	380
166	80	200	310	270	190	390	166	98	290	180	300	400	380
166	99	200	320	300	200	390	166	158	300	175	460	480	380
166	300	200	340	300	250	out	166	218	out	180	470	480	380
166	439	200	out	440	420	out	166	233	out	185	470	470	out
166	500	out	out	800	430	out	166	258	out	185	460	460	out
166	560	210	out	900	460	out	166	318	out	185	460	440	out
166	720	200	out	out	430	out	166[3]	378	out	190	out	420	out

(1) The accumulated time of exposure during the high intensity sonic fatigue test.
(2) The units of strain are micro-inch per inch, rms.
(3) At the end of this run, steel frame repairs were made and the sonic fatigue test was continued.

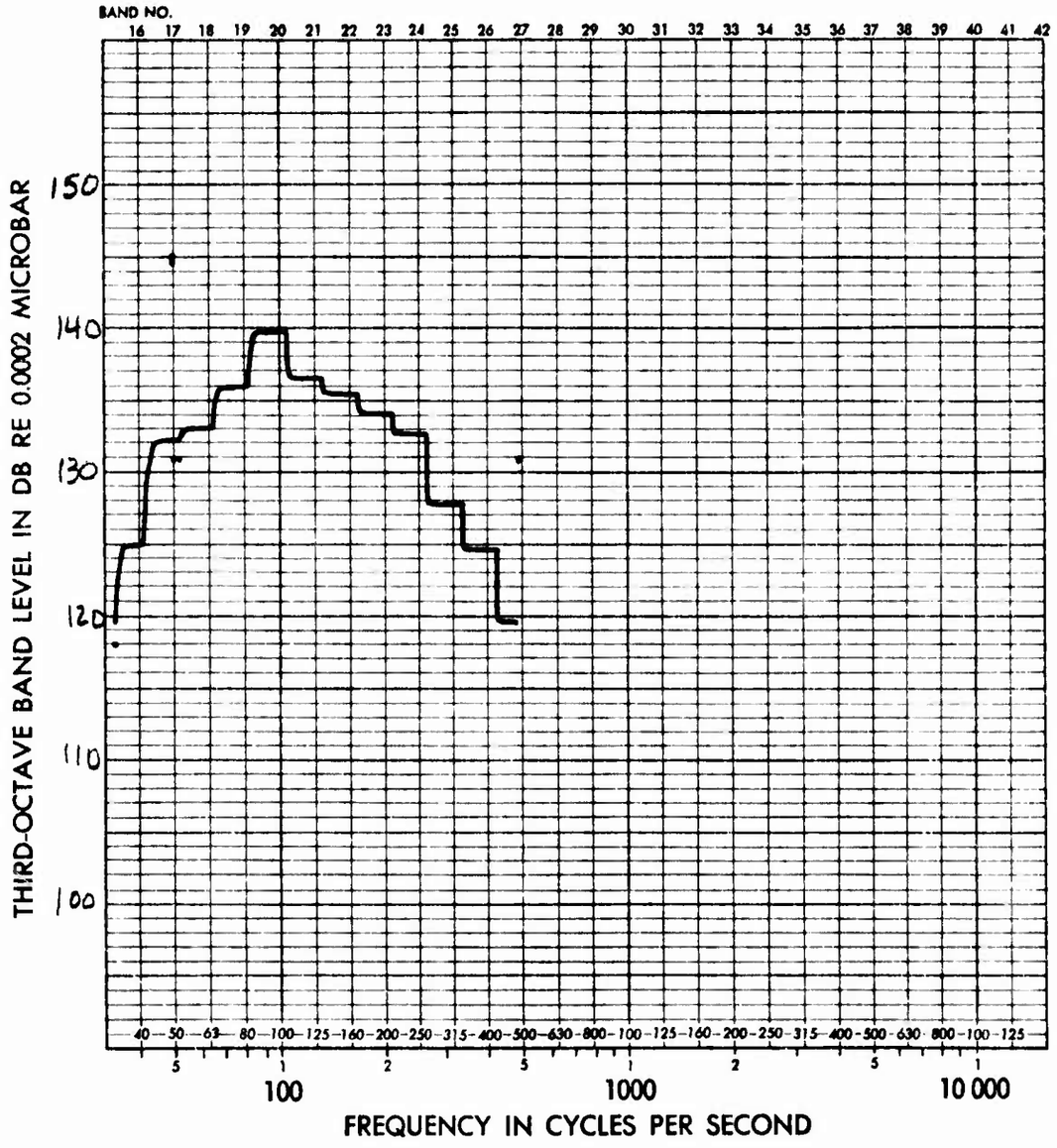

Panel A-4-1 Run 4
Microphone 145 dB OA 32 EA

Figure A-1. One-Third Octave Band Analysis of Acoustic Pressure at 145 dB in Test of Panel A-4-1

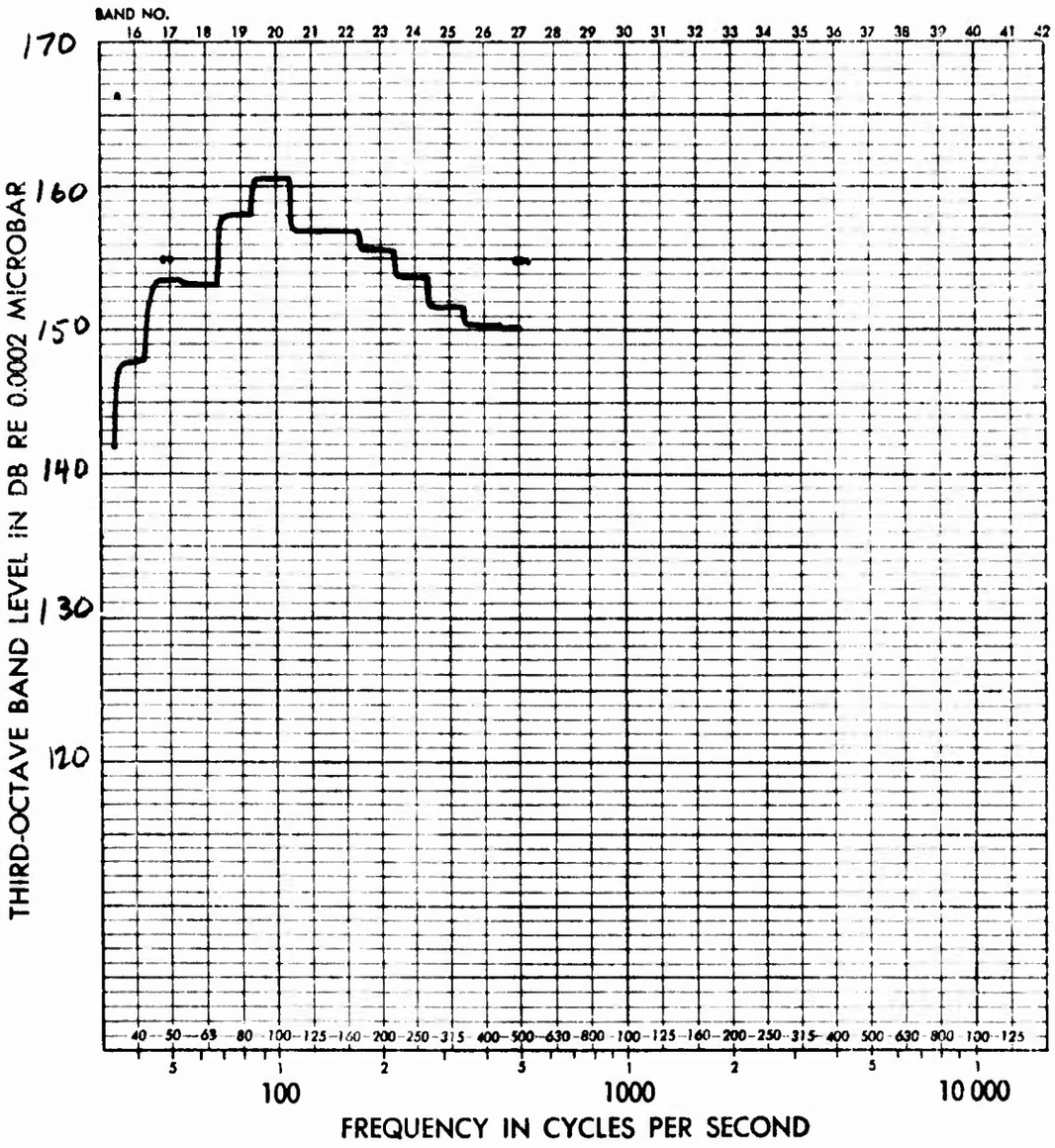

ADD 4.9 DB TO OBTAIN OCTAVE BAND LEVEL

CODEX BOOK COMPANY INC NORWOOD MASSACHUSETTS.
PRINTED IN U.S.A.

NC 31.462 SOUND ANALYSIS BY THIRD-OCTAVE BANDS.

Panel A-4-1 Run 11
Microphone 166 dB OA 32 EA

Figure A-2. One-Third Octave Band Analysis of Acoustic Pressure at 166 dB in Test of Panel A-4-1

TWO _____ DATE _____

VIBRATION TEST TITLE Panel A-4-1 RUN NO 4

Sine ☐ Random ☒ Transmissibility ☐ Input Axis vertical ☐ longitudinal ☐ lateral ☐ Response Axis ☐ ☐

Accelerometer – Control ☒ location 145 dB MIC

Response ☐ location _____

Remarks _____

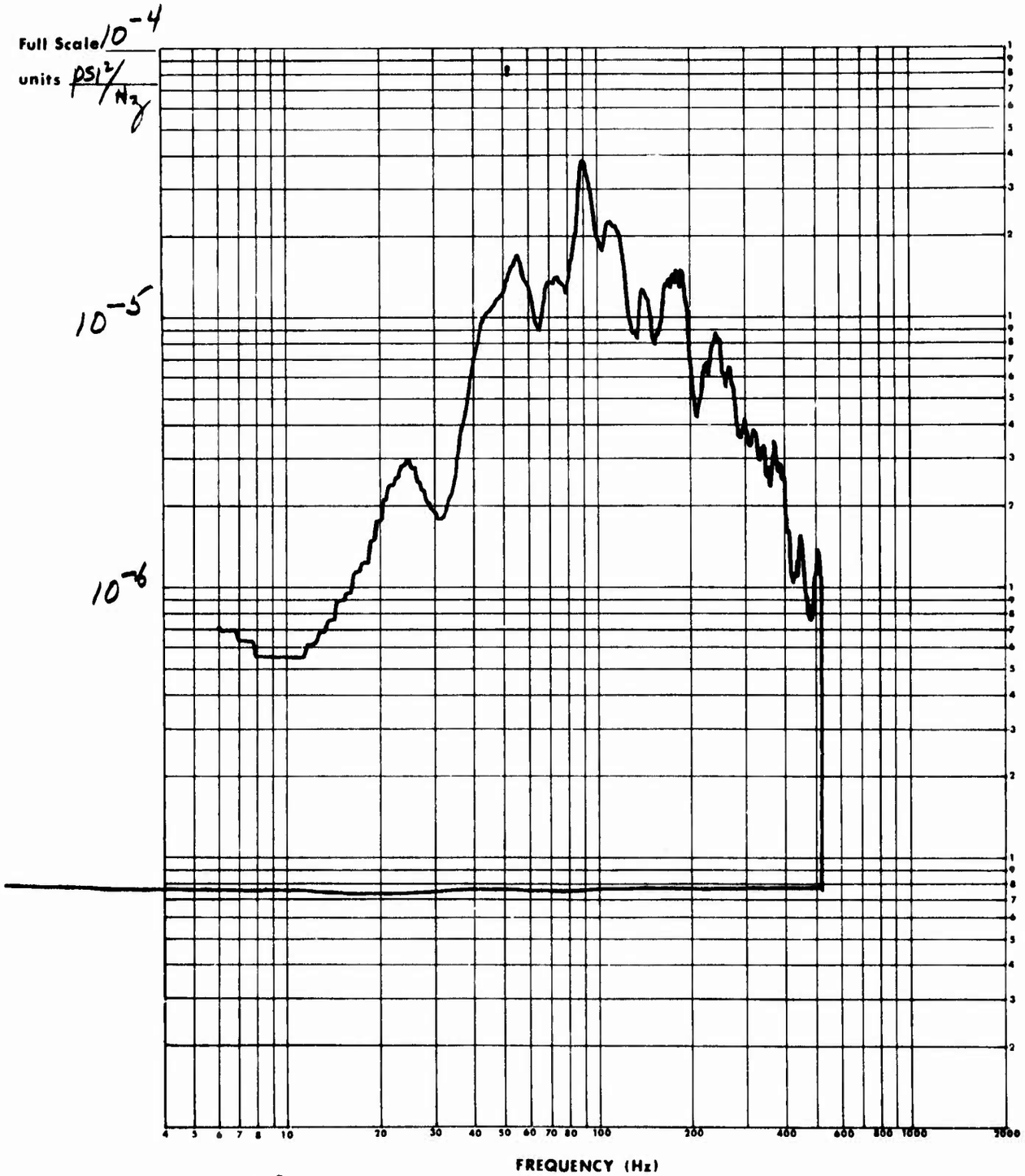

Form 21-56 (R9-75)

Figure A-3. Narrow Band Analysis of Acoustic Pressure at 145 dB in Test of Panel A-4-1

TWO _____ DATE _____

VIBRATION TEST TITLE Panel A-4-1 RUN NO 11

Sine ☐ Random ☐ Transmissibility ☐ Input Axis vertical ☐ longitudinal ☐ lateral ☐ Response Axis ☐ ☐ ☐

Accelerometer – Control ☐ location 1662B OA MIC

Response ☐ location _____

Remarks _____

Full Scale 10^{-2}

units PSI^2/Hz

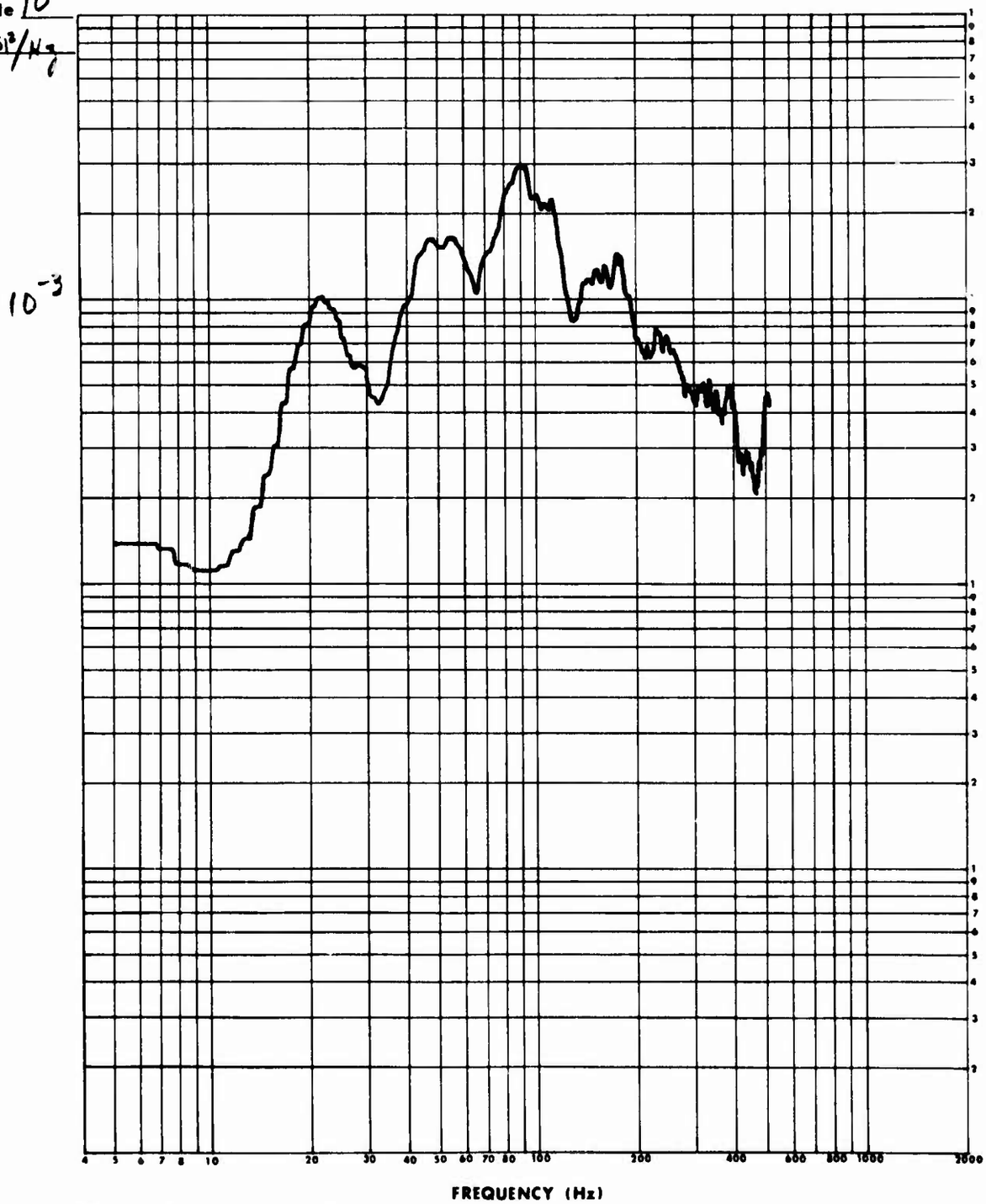

Form 21-56 (R9-75)

Figure A-4. Narrow Band Analysis of Acoustic Pressure at 166 dB in Test of Panel A-4-1

TWO 97244 DATE 4-1-77

VIBRATION TEST TITLE Gage 4 RUN NO 4

Sine ☐ Random ☐ Transmissibility ☐ Input Axis vertical ☐ longitudinal ☐ lateral ☐

Response Axis ☐ ☐ ☐

Accelerometer – Control ☐ location 145 dB M1e.

Response ☐ location 110 με RMS

Remarks Panel A-4-1

Full Scale 10^4

units $(\mu\epsilon)^2/Hz$

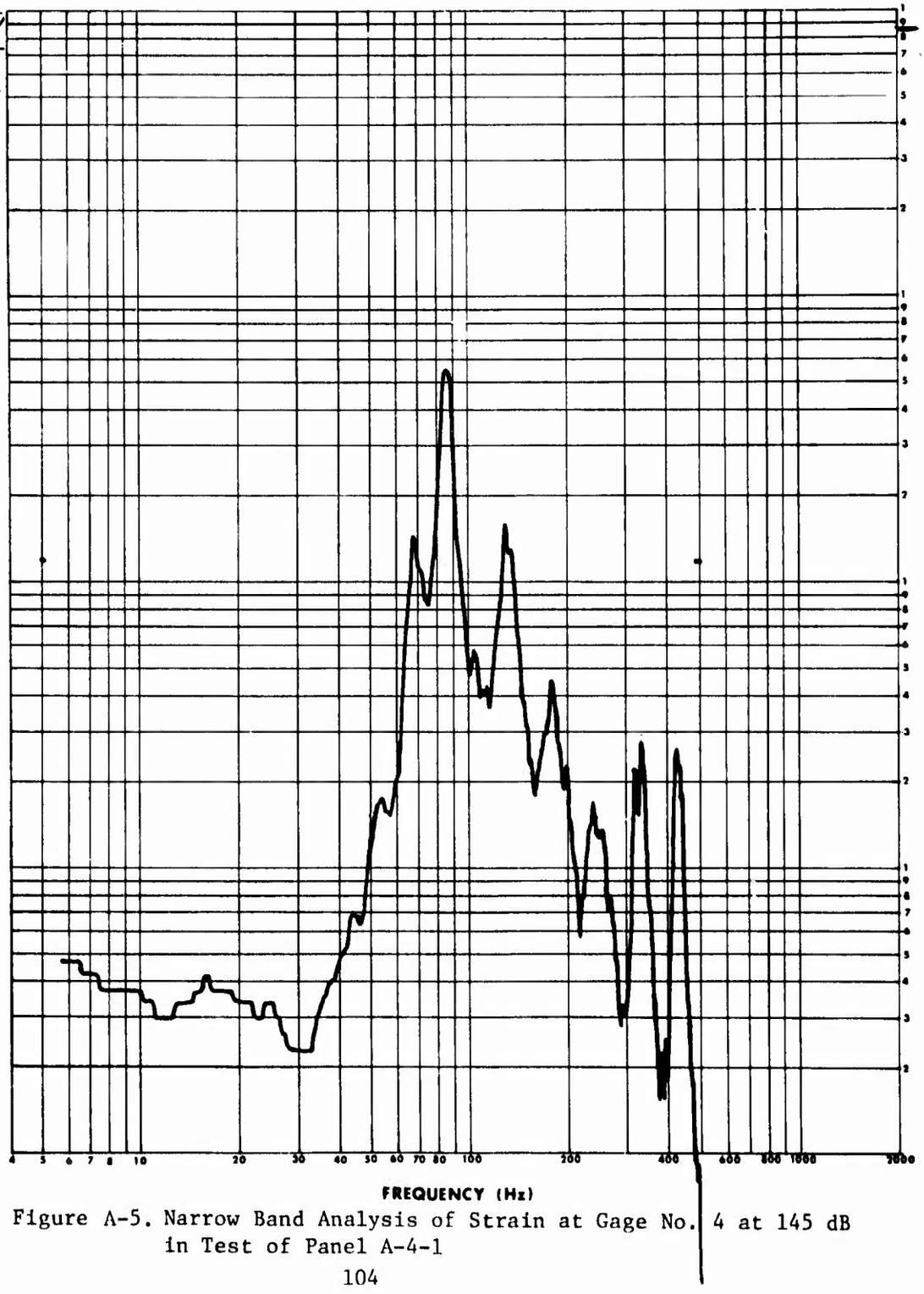

Form 21-56 (R9-75)

Figure A-5. Narrow Band Analysis of Strain at Gage No. 4 at 145 dB in Test of Panel A-4-1

TWO 97244 DATE 4-1-77

VIBRATION TEST TITLE GAGE # 4 166 db RUN NO 11

Sine ☐ Random ☐ Transmissibility ☐ Input Axis vertical ☐ longitudinal ☐ lateral ☐ Response Axis ☐ ☐ ☐

Accelerometer – Control ☐ location

Response ☐ location 380 μ IN/IN RMS

Remarks PANEL # A4-1

Full Scale 10^4

units

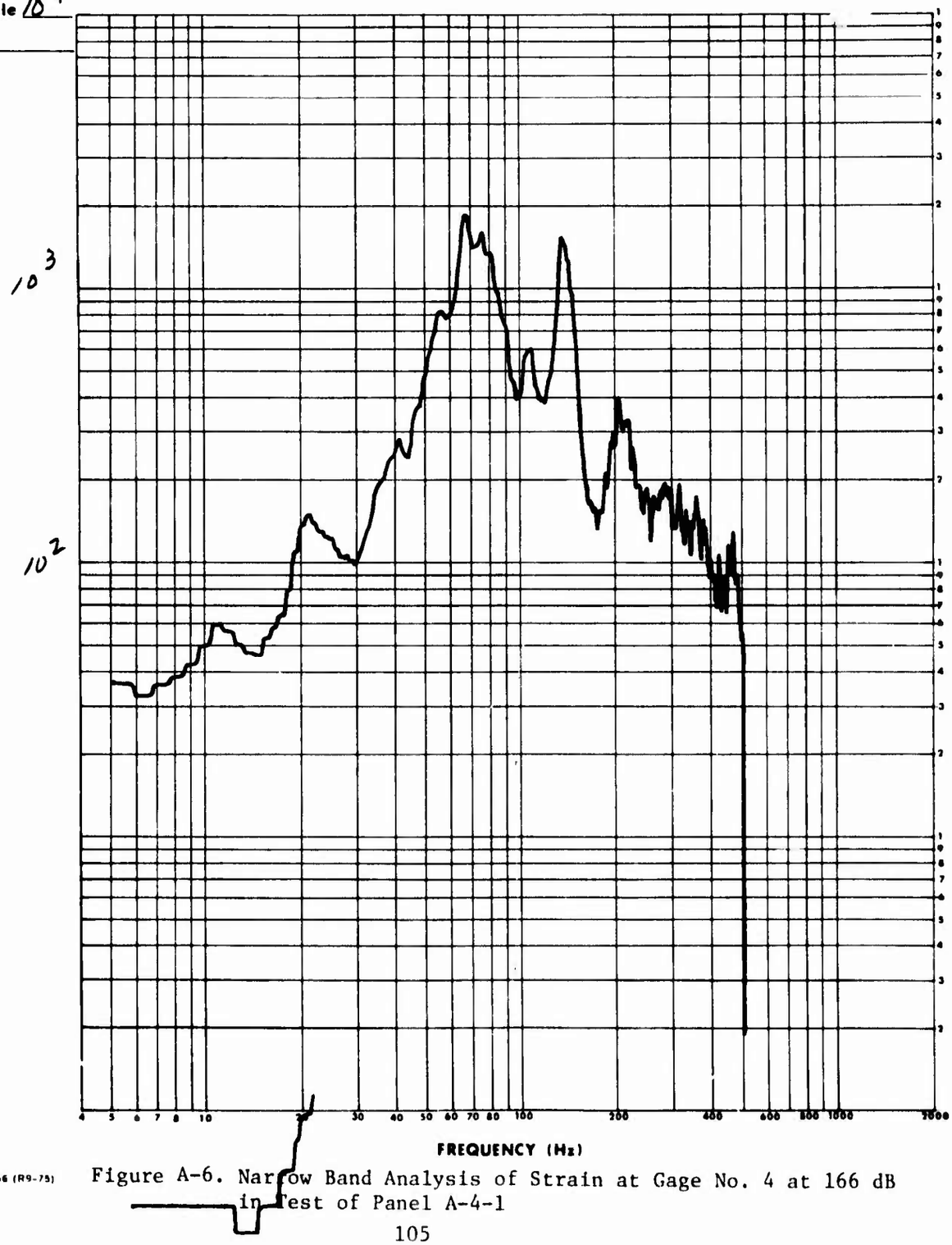

Form 21-56 (R9-75)

Figure A-6. Narrow Band Analysis of Strain at Gage No. 4 at 166 dB in Test of Panel A-4-1

TWO 97244 DATE 4-1-77

VIBRATION TEST TITLE GAGE # 4 RUN NO 4

Sine ☐ Random ☐ Transmissibility ☐ Input Axis vertical ☐ longitudinal ☐ lateral ☐ Response Axis ☐ ☐ ☐

Accelerometer – Control ☐ location 145 db

Response ☐ location 110 μIN/IN RMS

Remarks PANEL # A4-1 32 EA

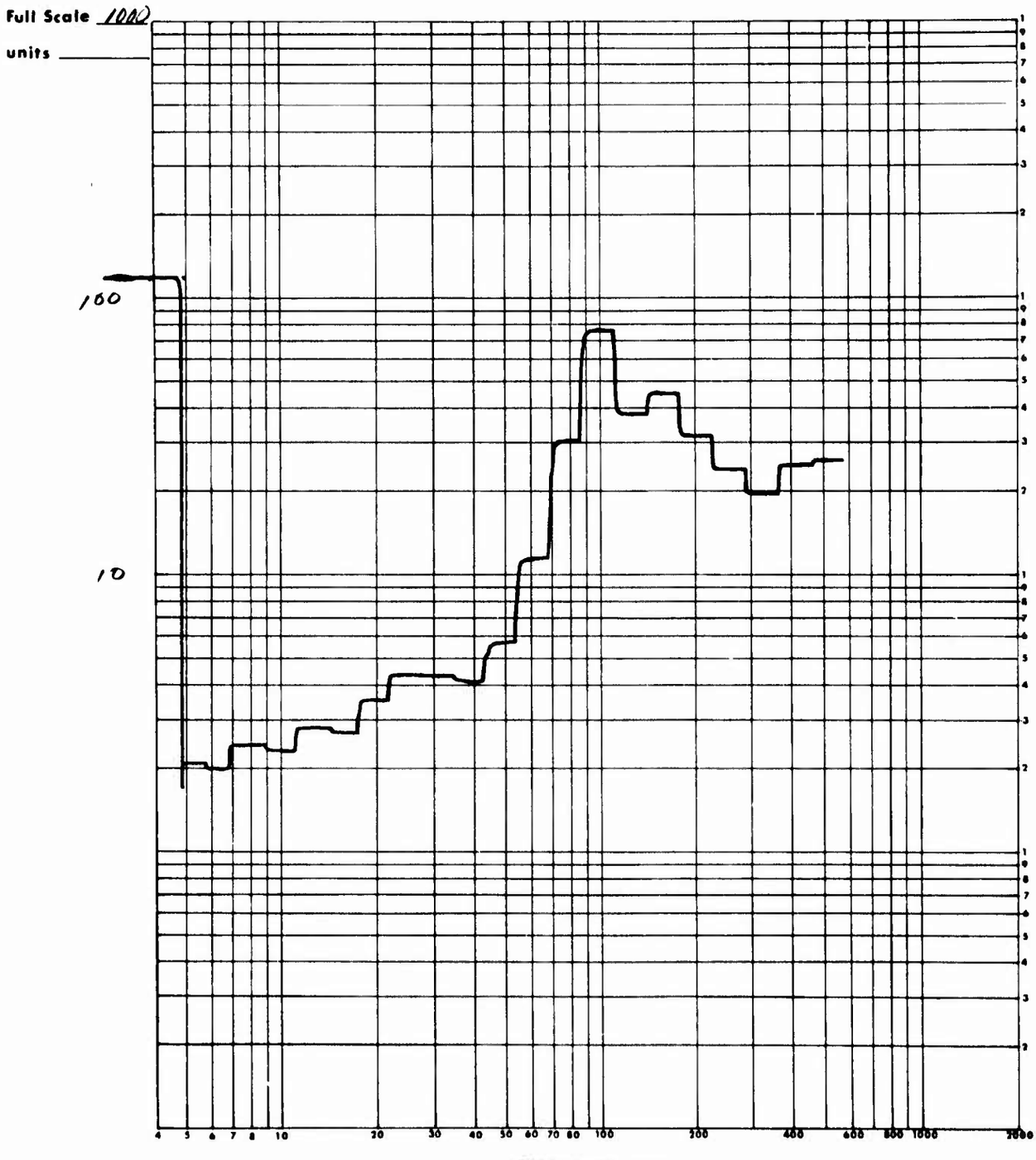

Form 21-56 (R9-75)

Figure A-7. One-Third Octave Band Analysis of Strain at Gage No. 4 at 145 dB in Test of Panel A-4-1

TWO 97244 DATE 4-1-77

VIBRATION TEST TITLE GAGE # 4 RUN NO 11

Sine ☐ Random ☐ Transmissibility ☐ Input Axis vertical ☐ longitudinal ☐ lateral ☐ Response Axis ☐ ☐ ☐

Accelerometer – Control ☐ location 166 db

Response ☐ location 380 MIN/IN RMS

Remarks PANEL # A4-1 32EA

Full Scale 1000

units

100

16

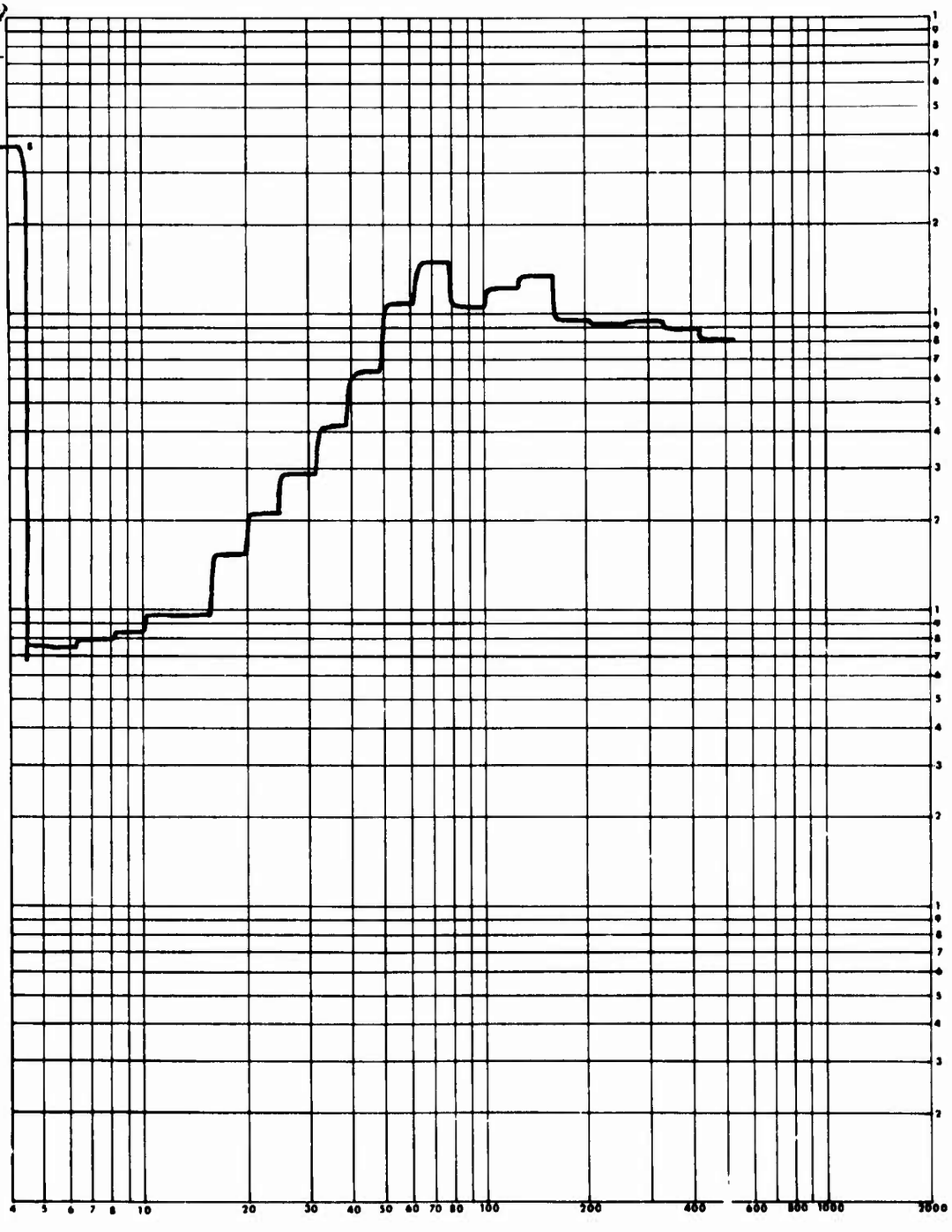

Form 21-56 (R9-75)

Figure A-8. One-Third Octave Band Analysis of Strain at Gage No. 4 at 166 dB in Test of Panel A-4-1

TWO 97244 DATE 4-1-77

VIBRATION TEST TITLE GAGE # 2 145 db RUN NO 4

Sine ☐ Random ☐ Transmissibility ☐ Input Axis vertical ☐ longitudinal ☐ lateral ☐ Response Axis ☐ ☐ ☐

Accelerometer – Control ☐ location

Response ☐ location 75 MIN/IN RMS

Remarks PANEL # A 4-1

Full Scale 10^4

units

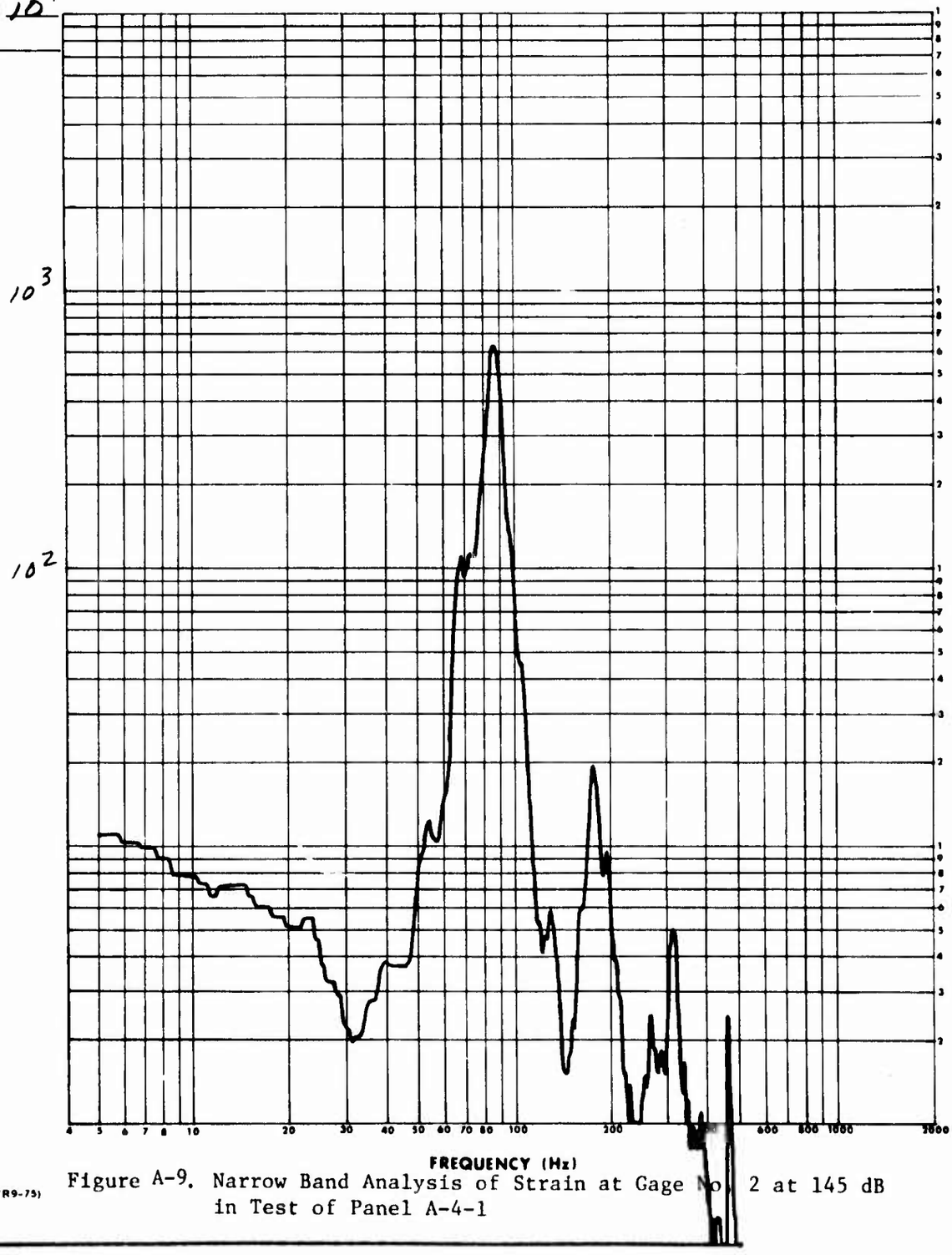

Form 21-56 (R9-75)

Figure A-9. Narrow Band Analysis of Strain at Gage No. 2 at 145 dB in Test of Panel A-4-1

TWO 97244 DATE 4-1-77

VIBRATION TEST TITLE GAGE # 2 166 db RUN NO 11

Sine ☐ Random ☐ Transmissibility ☐ Input Axis vertical ☐ longitudinal ☐ lateral ☐ Response Axis ☐ ☐ ☐

Accelerometer – Control ☐ location

Response ☐ location 260 MIN/IN RMS

Remarks PANEL # A4-1

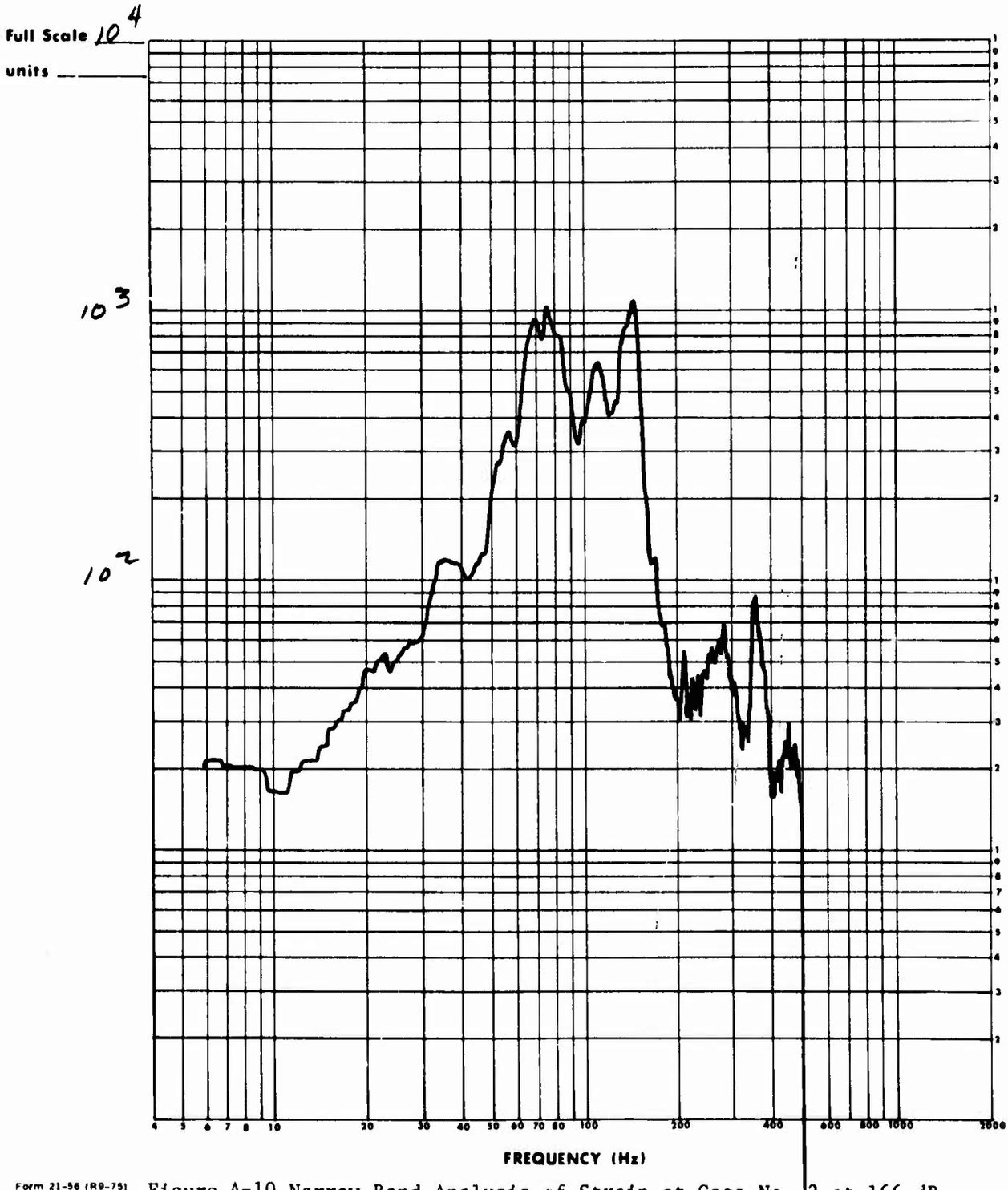

Form 21-56 (R9-75)

Figure A-10. Narrow Band Analysis of Strain at Gage No. 2 at 166 dB in Test of Panel A-4-1

TWO 97244 DATE 4-1-77

VIBRATION TEST TITLE GAGE #2 142 db RUN NO 3

Sine ☐ Random ☐ Transmissibility ☐ Input Axis vertical ☐ longitudinal ☐ lateral ☐ Response Axis ☐ ☐ ☐

Accelerometer – Control ☐ location

Response ☐ location 32 MIN/IN RMS

Remarks PANEL # AZ-1

Full Scale 10^3

units

10^2

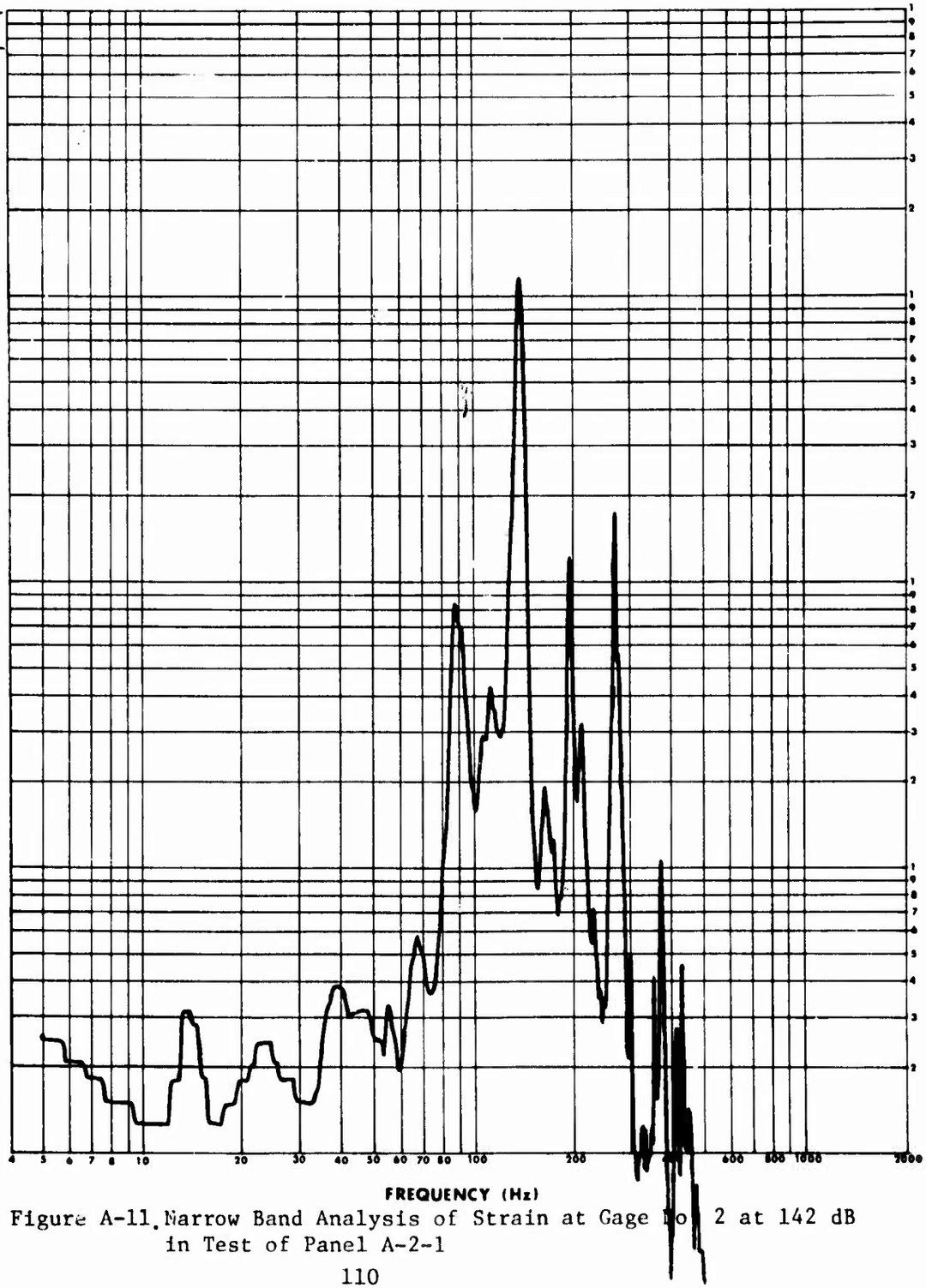

Form 21-56 (R9-75)

Figure A-11. Narrow Band Analysis of Strain at Gage No. 2 at 142 dB in Test of Panel A-2-1

TWO 97244 DATE 4-1-77

VIBRATION TEST TITLE GAGE # 4 142 db RUN NO 3

Sine ☐ Random ☐ Transmissibility ☐ Input Axis vertical ☐ longitudinal ☐ lateral ☐

Response Axis ☐ ☐ ☐

Accelerometer – Control ☐ location

Response ☐ location 27 μIN/IN RMS

Remarks PANEL # A2-1

Full Scale 10^{-3}

unit $(\mu\varepsilon)^2/Hz$

10^{-7}

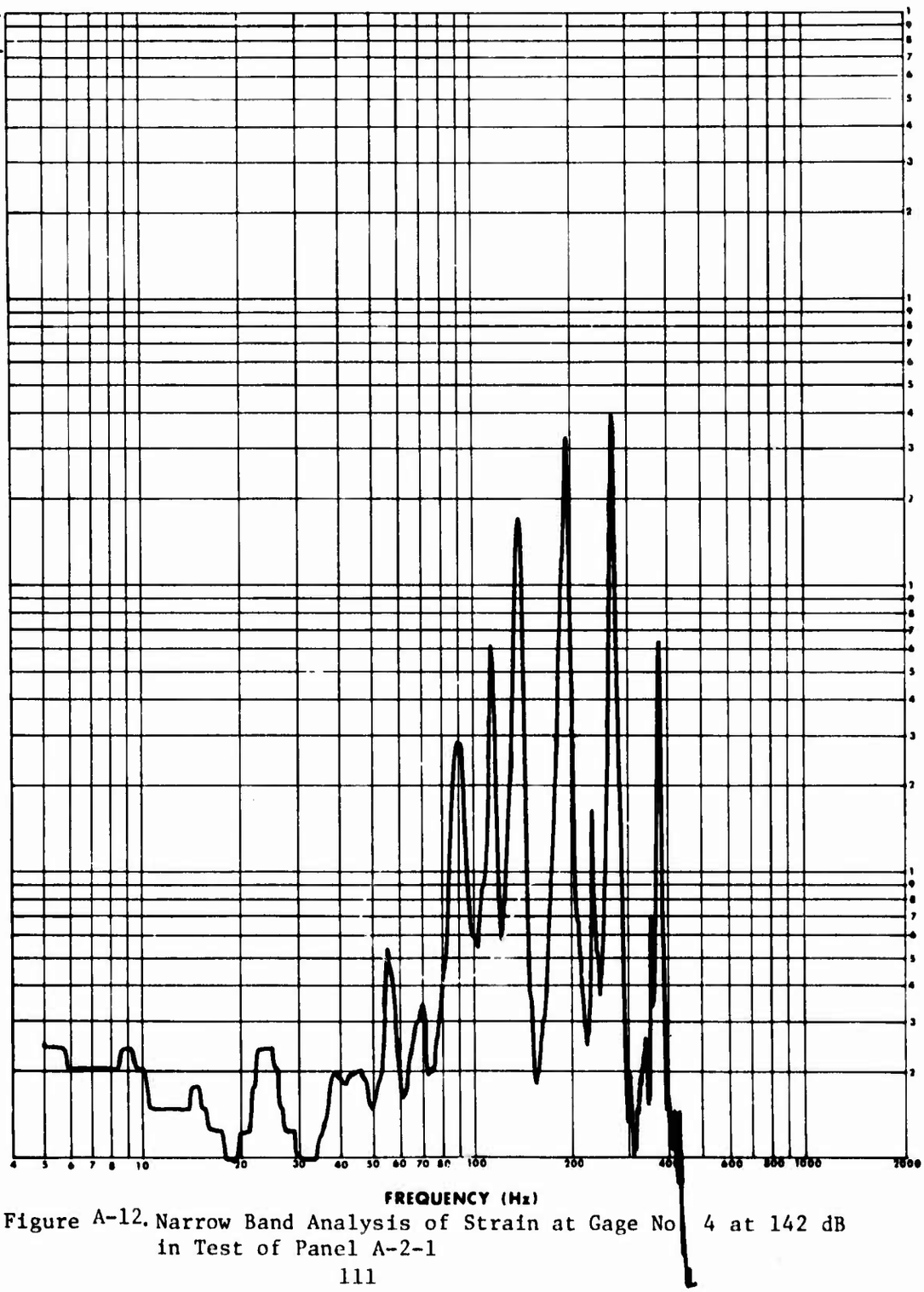

Form 21-56 (R9-75)

Figure A-12. Narrow Band Analysis of Strain at Gage No 4 at 142 dB in Test of Panel A-2-1

TWO 97244 DATE 4-1-77

VIBRATION TEST TITLE GAGE # 2 166 db RUN NO 11

Sine ☐ Random ☐ Transmissibility ☐ Input Axis vertical ☐ longitudinal ☐ lateral ☐

Response Axis ☐ ☐ ☐

Accelerometer – Control ☐ location

Response ☐ location 240 μ IN/IN RMS

Remarks PANEL # A2-1 1.5 Hz BW

Full Scale 10^4

units

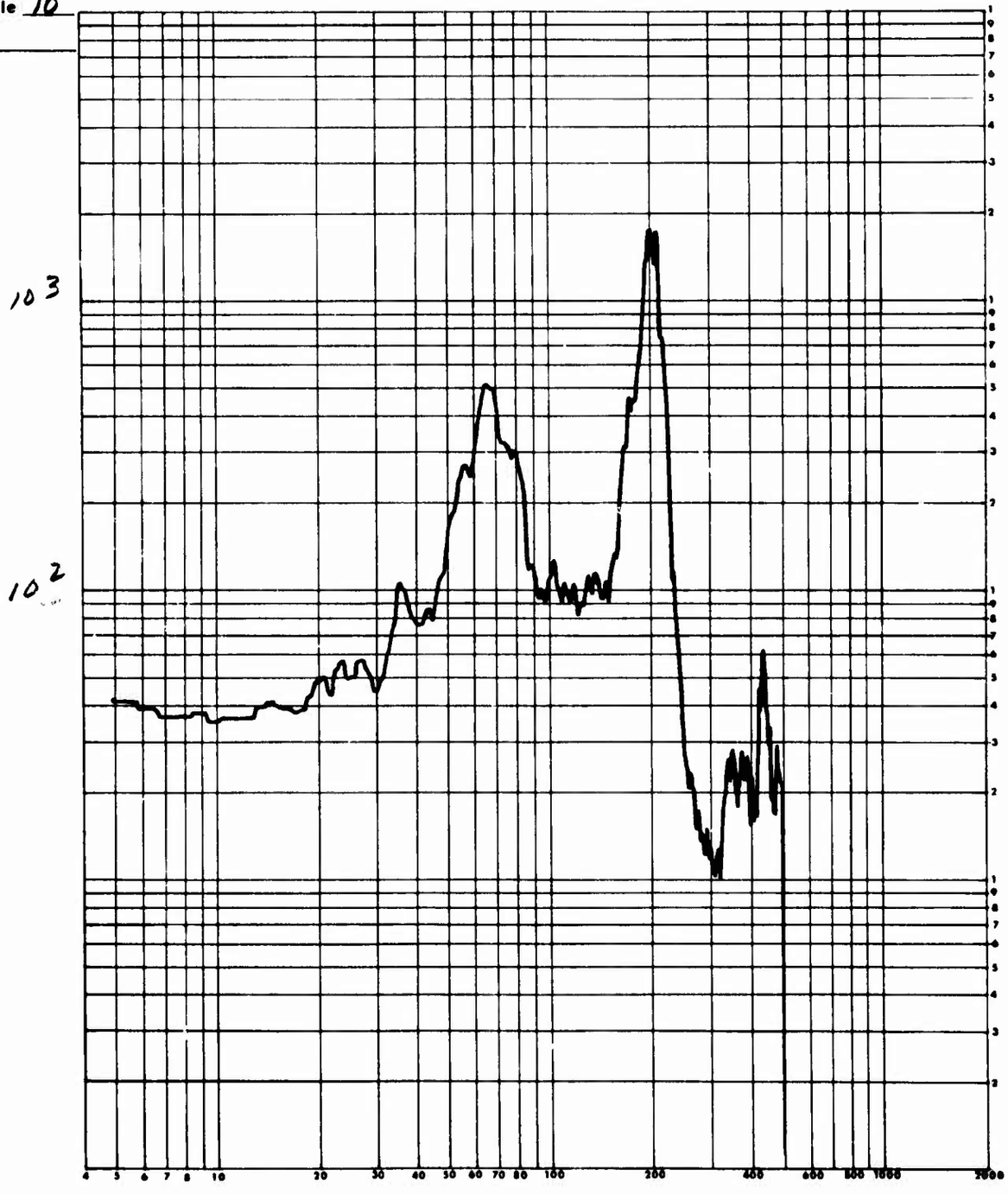

Form 21-56 (R9-75)

Figure A-13. Narrow Band Analysis of Strain at Gage No. 2 at 166 dB in Test of Panel A-2-1

TWO 97244 DATE 4-1-77

VIBRATION TEST TITLE GAGE #4 166 db RUN NO 11

Sine ☐ Random ☐ Transmissibility ☐ Input Axis vertical ☐ longitudinal ☐ lateral ☐ Response Axis ☐ ☐ ☐

Accelerometer – Control ☐ location

Response ☐ location 275 μ IN/IN RMS

Remarks PANEL A 2-1

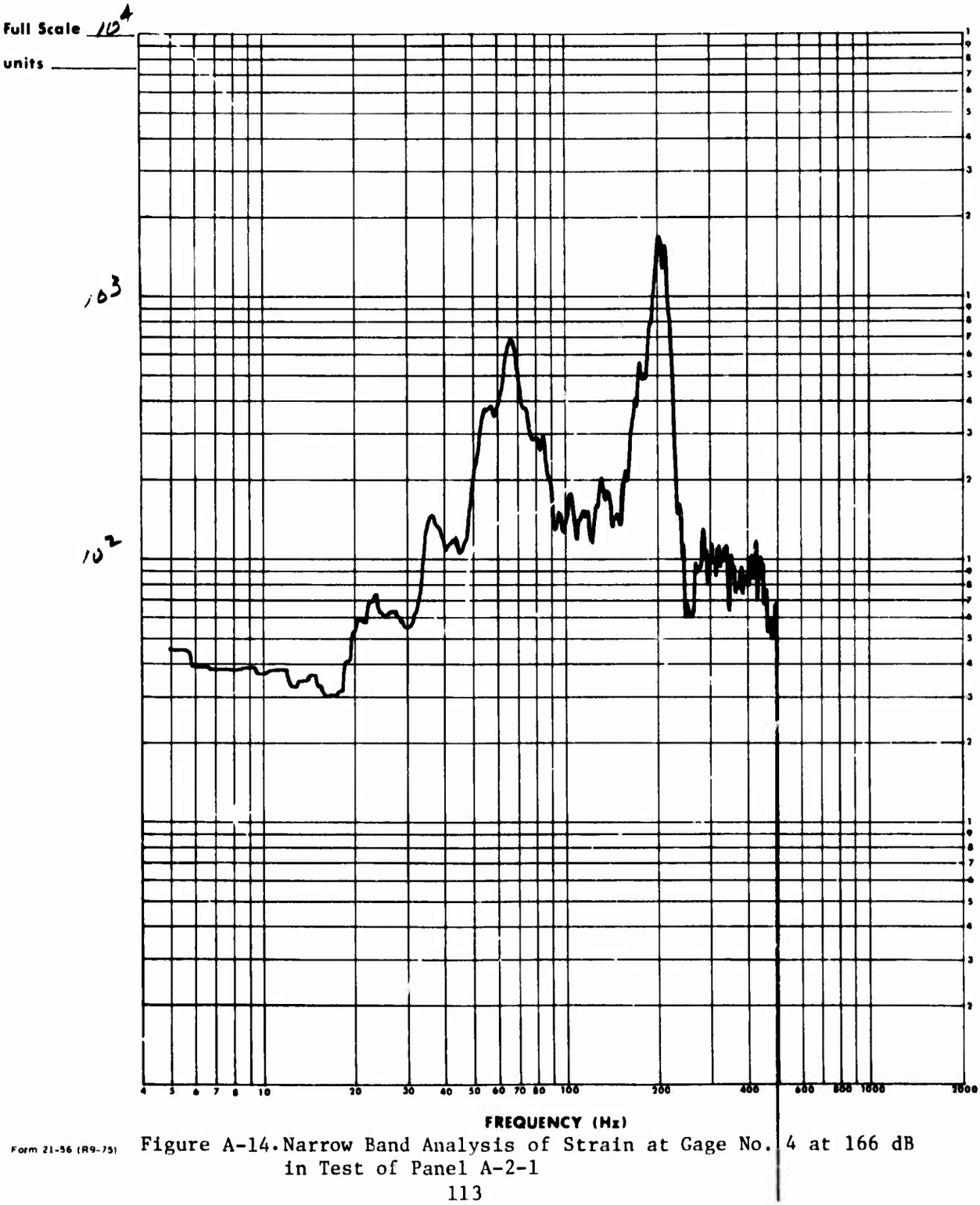

Form 21-56 (R9-75)

Figure A-14. Narrow Band Analysis of Strain at Gage No. 4 at 166 dB in Test of Panel A-2-1

APPENDIX B

FINITE ELEMENT MODELING

B.1 Computer Programs

Dynamic analyses with the REDYN (REdundant DYNamic) finite element computer program were conducted to obtain natural frequencies, modal shapes, and the acoustic response of the nine-bay panels. REDYN is a proprietary computer program developed by Northrop. Analytic predictions of dynamic response obtained with REDYN have agreed well with results obtained with STARDYNE and NASTRAN, two more well-known and widely-used computer programs. REDYN was successfully used in acoustic response analyses in Contract F33615-75-C-3144 that were documented in Reference B-1. The analytic work performed with REDYN is discussed in Section B.2 and the principal conclusions from comparisons of the analytic predictions with the test data indicate that (1) denser grids than were used are needed to predict stresses accurately in sonic fatigue sensitive locations of the skin and (2) surface contact rather than line contact between the stiffeners and skin is needed to predict accurately the natural frequencies and the stress response in the sonic fatigue sensitive locations of the skin. The REDYN computations were performed prior to the conduct of the test program.

Static stress analyses were conducted, prior to the conduct of any testing, with the NASTRAN finite element computer program to obtain predictions of stress in the adhesive, the skin, and the substructure of the bonded joints of the acoustic test panels. The principal conclusion that was reached was that the stress state in the adhesive at the end of the bonded joint was quite complex in that substantial flatwise tension (commonly referred to as peel stress) and in-plane shear were computed. It is believed that in the experiments the adhesive flash was effective in transferring a portion of the stress in the unsupported skin to the bonded joint. Therefore, the likelihood of a complex stress state in the adhesive at the edge of the bonded stiffener is likely.

B.2 Effect of Structural Modeling in Dynamic Analyses for Acoustic Response

The effect of using different finite element structural models in obtaining the dynamic response (with REDYN) of test panel A-3-1 was investigated prior to conducting the test program. The structural models are shown in Figures B-1 and B-2 and the features that differentiate the various models are described in Table B-1.

Prior to modeling the structure, it was assumed that the actual 9-bay test panels, which are rectangular and possess structural symmetry about both center lines, would be subjected to spatially uniform white noise. Inasmuch as the test panels are rectangular and possess structural symmetry about both center lines, the assumed spatially uniform acoustic loading will only excite modal shapes that contain symmetry about both center lines of the panel. Therefore, Models A, B, C, E and G consisting of only one quadrant of the test panels were developed since these one quadrant models can be used to generate all the response modes without anti-symmetry. Model F (with coarse grid spacing but with essentially the same number of degress of freedom as the one quadrant models) consisting of all four quadrants was developed to obtain natural frequencies of modes with anti-symmetry. Significant parameters in the modeling are presented in Tables B-2 through B-4.

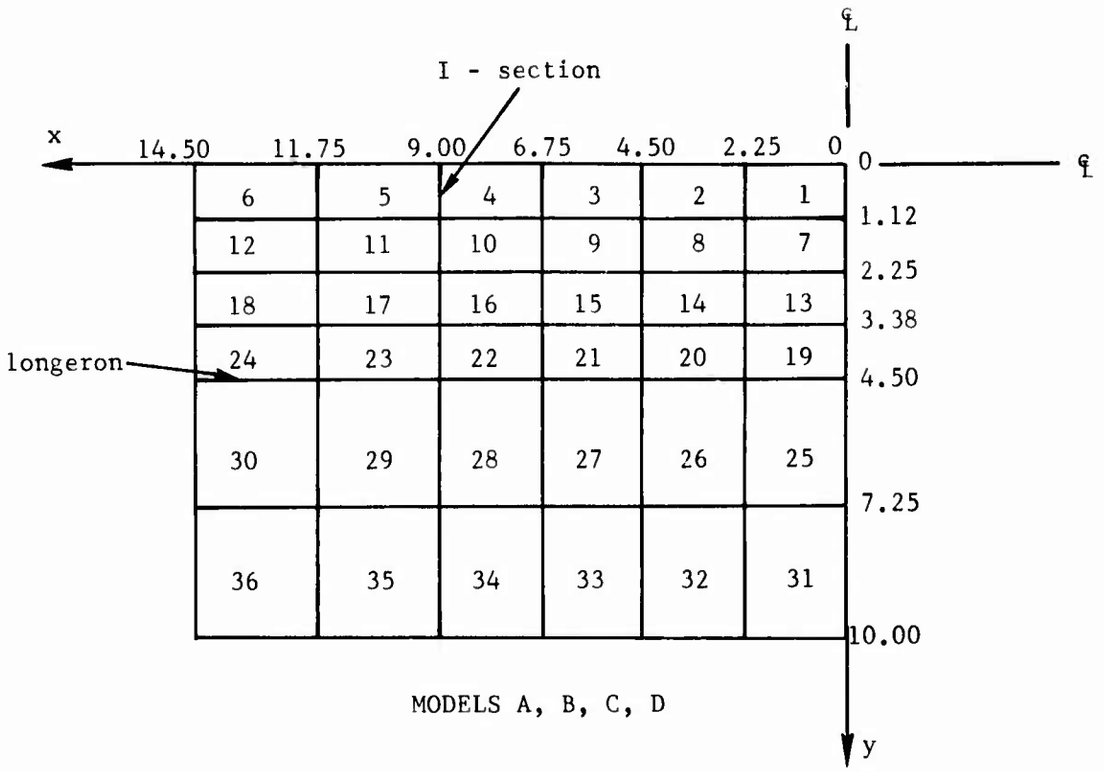

MODELS A, B, C, D

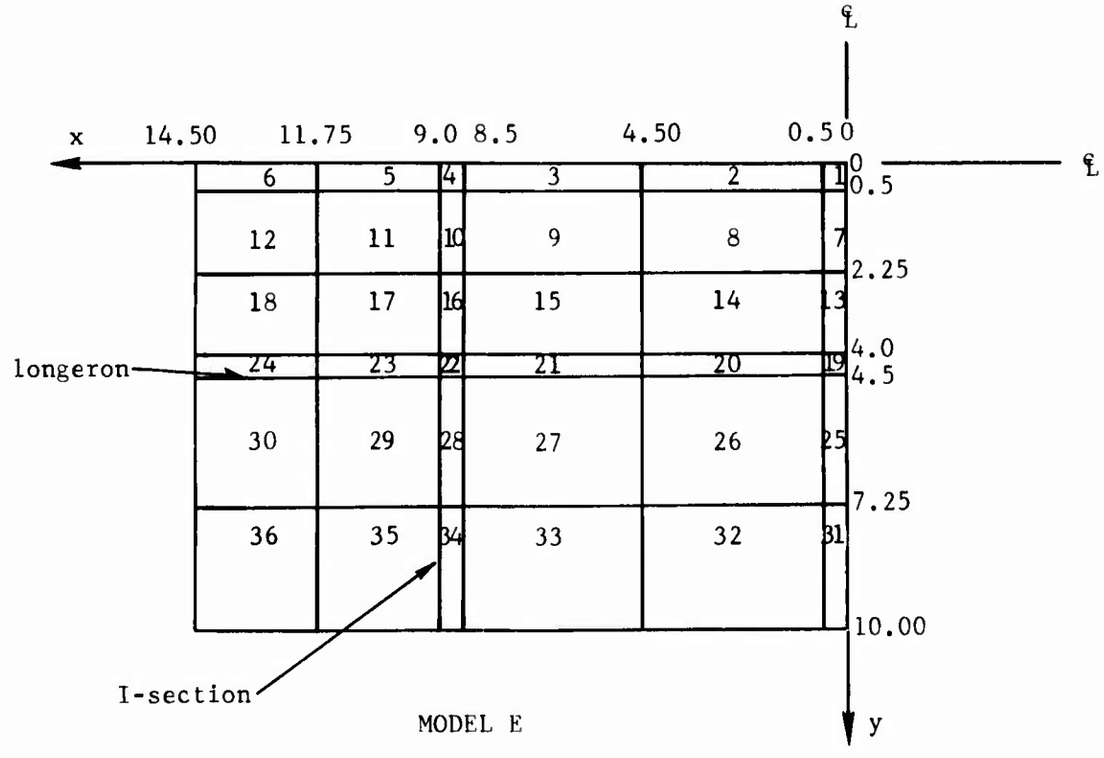

MODEL E

Figure B-1. Finite Element Models A Through E

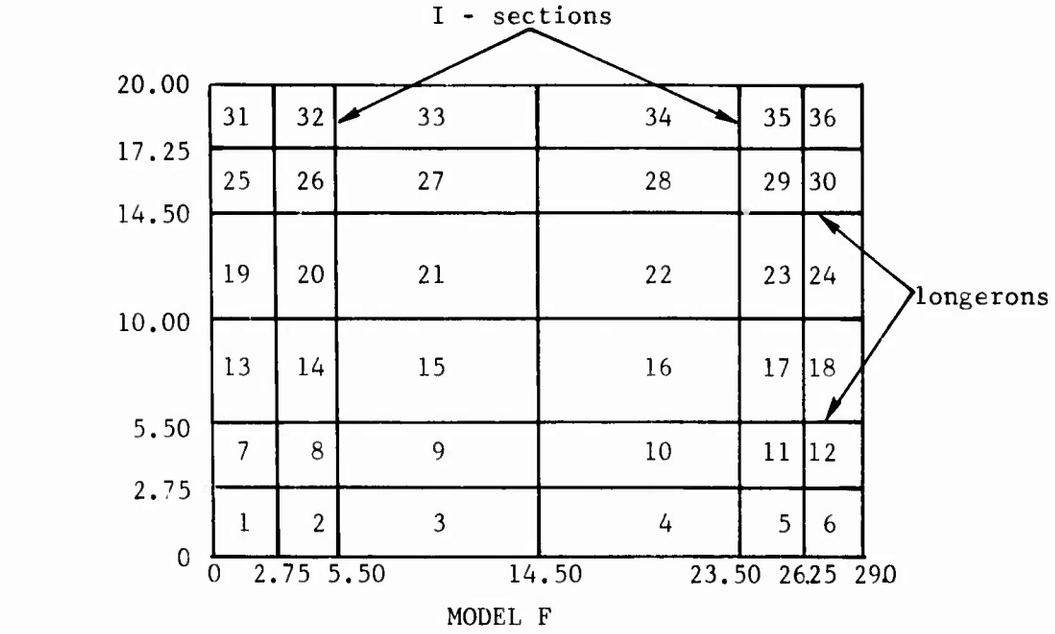

MODEL F

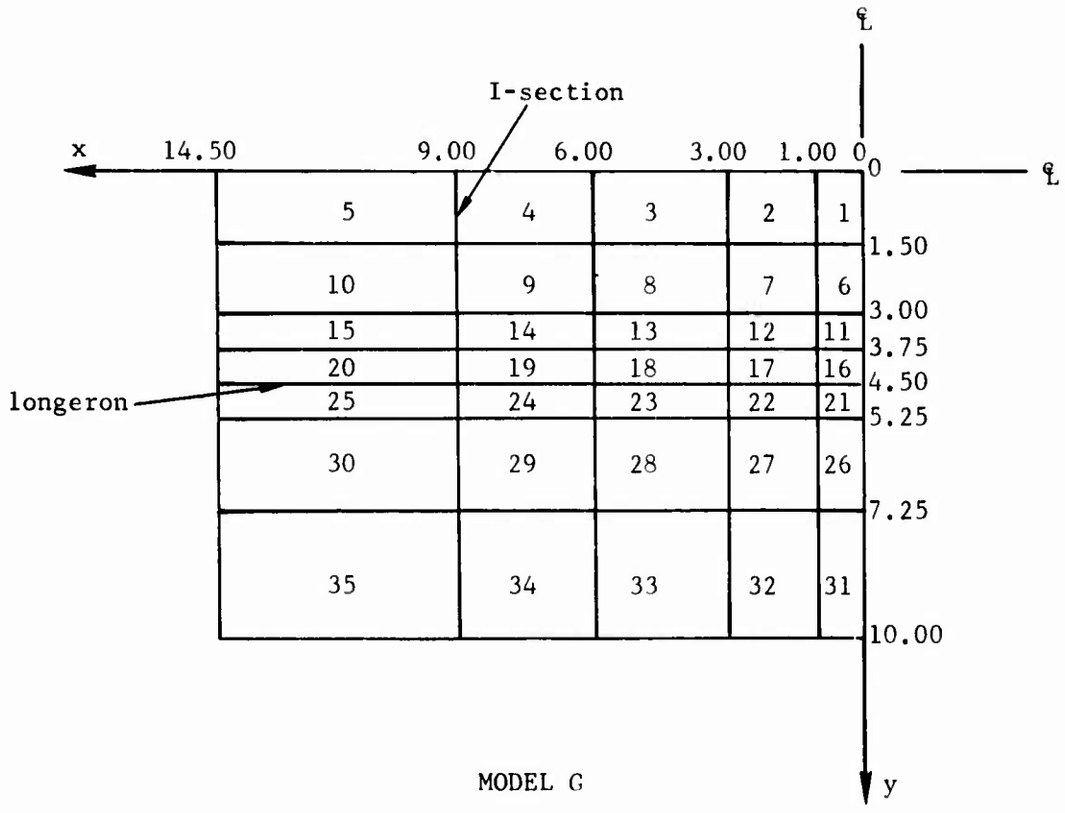

MODEL G

Figure B-2. Finite Element Models F and G

TABLE B-1. DESCRIPTION OF STRUCTURAL MODELS

STRUCTURAL MODEL	DESCRIPTION
A	This is a nine-bay rectangular panel modeled with one quadrant. There are scarfed substructure and equal spacing of finite element node points in the central bay.
B	This is a nine-bay rectangular panel modeled with one quadrant. Model B differs from Model A only by the addition of a picture frame doubler that is in Model B.
C	This is a nine-bay rectangular panel modeled with one quadrant. Model C differs from Model B only in that Model C possesses improved values of longeron moments of inertia for simulating the test panels.
D	This is a nine-bay rectangular panel modeled with one quadrant. Model D is the same as Model B except that Model D does not have scarfed substructure.
E	This is a nine-bay rectangular panel modeled with one quadrant. Model E differs from Model A only insofar as the spacing of the finite element grid lines.
F	This is a nine-bay rectangular panel modeled with all four quadrants. The substructure is the same as in Model A. Model F does not have a picture frame doubler.
G	This is a nine-bay rectangular panel modeled with one quadrant. Model G differs from Model C in that portions of the longeron flanges in Model G are modeled as part of the skin.

TABLE B-2. PARAMETERS THAT ARE COMMON TO MODELS A THROUGH G

Overall panel length (9-bays), in.	29
Overall panel width (9-bays), in.	20
Spacing of central I-sections, in.	18
Spacing of longerons, in.	9
Young's modulus of skins, psi	9.6×10^6
Shear modulus of skins, psi	3.61×10^6
Poisson's ratio of skins	0.33
Young's modulus of substructure, psi	10.3×10^6
Shear modulus of substructure, psi	3.87×10^6
Viscous damping factor for each mode	0.016
Weight density, lb/in^3	0.100

TABLE B-3. THICKNESS OF PLATE FINITE ELEMENTS

FINITE ELEMENT NUMBER	THICKNESS		
	MODELS A, E, F (inch)	MODELS B, C, D (inch)	MODEL G (inch)
1	0.05	0.05	0.05
2			
3			
4			0.05
5		0.05	0.08
6		0.10	0.05
7		0.05	
8			
9			0.05
10			0.08
11		0.05	0.05
12		0.10	
13		0.05	
14			0.05
15			0.08
16			
17		0.05	
18		0.10	
19		0.05	0.08
20			0.11
21			0.08
22			
23		0.05	
24		0.10	0.08
25		0.05	0.11
26			0.05
27			
28			
29		0.05	0.05
30		0.10	0.08
31			0.10
32			
33			
34			
35			0.10
36	0.05	0.10	none

TABLE B-4. SUBSTRUCTURE INERTIAS, AREAS, AND OFFSETS

PARAMETER	MODEL A, B, E, F	MODEL C	MODEL G	MODEI D
Area of I-sections, in^2	0.6048	0.6048	0.6048	0.640
Moment of inertia of I-sections about axis normal to plate, in^4	0.0409	0.0409	0.0409	0.05314
Moment of inertia of I-sections about the other principal axis, in^4	1.3619	1.3619	1.3619	1.5097
Torsional constant of I-section, in^4	0.00169	0.00169	0.00169	0.00191
Offset of centroid of I-section to plate midplane, in.	2.137	2.137	2.137	2.025
Area of longerons, in^2	0.1839	0.1839	0.1359	0.2025
Moment of inertia of longerons about axis normal to plate, in^4	0.01361	0.01545	0.00514	0.02232
Moment of inertia of longerons about the other principal axis, in^4	0.04538	0.04503	0.03038	0.04842
Torsional constant of longerons, in^4	0.00024	0.00024	0.00020	0.00031
Offset of centroid of longerons to plate midplane, in.	0.520	0.520	0.674	0.479

Inasmuch as it was assumed that the periphery of the 9-bays of the test panels were essentially fully clamped against all translation and rotation, fully clamped conditions in Models A through G were imposed on all six degrees of freedom at finite element nodes that represented points on the edges of the test panels. Finite element nodes that represented points on the center lines of the test panels were constrained in the one quadrant finite element models to deflect only in a direction normal to the plane of the structural model and with zero slope across the center line in order to ensure the symmetric response resulting from the spatially uniform loading.

Free vibration analyses with Model A were conducted (with REDYN) to obtain eight modal shapes that are briefly described in Table B-5. Also included in Table B-5 are natural frequencies for Models A through F. The bay numbers in Table B-5 are located in Figure B-3.

The modal shape corresponding to the lowest natural frequency for all seven structural models is best characterized as a 1-1 mode in the central bay (i.e., bay no. 5) of panel A-3-1. The lowest natural frequency ranged from 120 to 125 Hz for models A through F. Conclusions that are reached from examining Table B-5 are that the lowest three natural frequencies are not particularly sensitive to the effects of (1) the addition of a picture frame doubler around the periphery of the structural model, (2) the scarfing of the substructure, and (3) the differences in the grid spacing in the finite element models A through F. It should be noted that Model C simulates panel A-3-1 better than Models A, B, D, E, or F.

Model G was a superior structural model (insofar as obtaining better agreement with the fundamental frequency obtained in tests) for simulating panel A-3-1 than any of Models A through F, inasmuch as the substructure in models A through F is assumed to have line contact with the skin rather than area contact, which actually occurs. Area contact is simulated in Model G. From Table B-5, one observes that the lowest frequency is affected more percentagewise by considering the area contact, than are the next two higher frequencies.

Because of the assumed symmetry of response about the center lines in the one-quadrant models in Figure B-1, no antisymmetric modes may be obtained from the one-quadrant models. However, antisymmetric modal shapes and their corresponding natural frequencies were obtained from Model F, and they are tabulated in Table B-6.

An investigation to obtain the bending moments (as a function of the number of modes considered in the REDYN analysis) at the center of finite element Nos. 1, 4, and 19 (Figure B-1) in Model A was conducted, and the results are given in Table B-7. Spatially uniform white noise pressure loading with a power spectral density of 6.28×10^{3} psi^2/Hz was assumed. The conclusion was reached that the bending moments were not very sensitive to the modes above mode no. 3. Furthermore, because the bending moment in finite element

TABLE B-5. NATURAL FREQUENCIES AND BRIEF DESCRIPTION OF MODAL SHAPES

STRUCTURAL MODEL	FREQUENCIES							
	1-1 MODE BAY #5	3-1 MODE BAY #5	1-1 MODE BAY #2	1-1 MODE BAY #4	3-1 MODE BAY #2	5-1 MODE BAY #5	1-3 MODE OVERALL PANEL MODE	1-1 MODE BAY #1
	(Hz)	(Hz)	(Hz)	(Hz)	(Hz)	(Hz)	(Hz)	(Hz)
A	122	247	307	399	419	491	534	541
B	123	247	400					
C	124	247	403					
D	125	247	408					
E	120	245	293	397	391	540*	500	541
F	121	264*	293*	386	376*	472*	-	535
G	139	266	407					

*The modal shape is poorly defined.

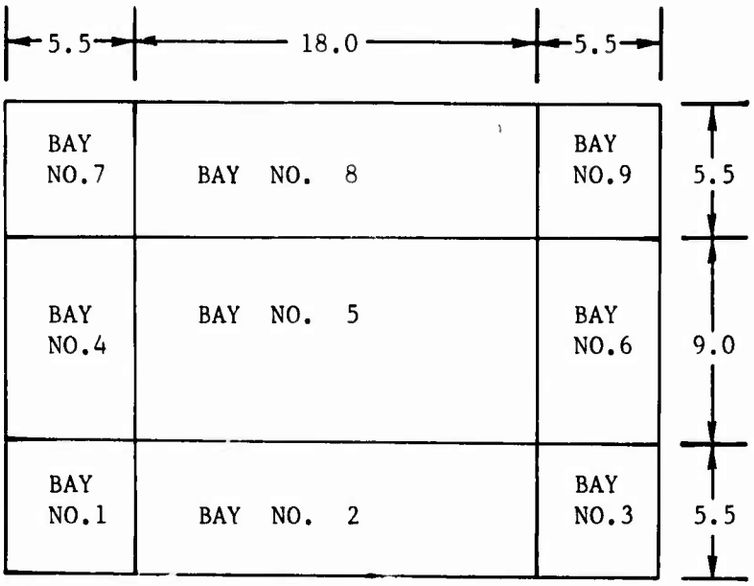

Figure B-3. Identification of Bays of Panels A-3-1, A-2-1, and A-1-1

TABLE B-6. PARTIAL MODAL STUDY WITH MODEL F

THE APPROXIMATE MODAL SHAPE	BAY NO.	NATURAL FREQUENCY (Hz)
1-1	5	121
2-1	5	146
2-1	2,8	184
(1)		

(1) Additional modal shapes and natural frequencies are included in Table B-5.

no. 19 was greater than the bending moment in finite element no. 4, it was (erroneously) concluded that in tests a sonic fatigue failure would occur in the skin or adhesive in the central bay near the center of the longeron (i.e., the J-section stiffener) prior to its occurrence in the skin or adhesive near the center of the I-section stiffener.

Because the principal sonic fatigue sensitive area along the periphery of the central bay (in Model A) was near the center of the longeron, only the longeron substructure was modeled by the area contact with the skin in Model G.

It was expected that the predominant response of the nine bay panels in the sonic fatigue test program will occur under 400 Hz, because the broadband excitation spectra would mainly be confined to frequencies under approximately 400 Hz. A comparison of bending moments that were obtained with Models C and G was obtained under the assumption that only the lowest three modes (with a maximum natural frequency of approximately 400 Hz) were responding in each case and the white noise loading was 6.28×10^{-5} psi^2/Hz and spatially uniform. The comparison is given in Table B-8 and it is to be noted that the bending moments are significantly less in Model G. An explanation for the lower bending moments in Model G is that the central bay length and width are effectively reduced when area contact between the substructure and skin is included in the finite element model and therefore the central bay is stiffer and responds less to the white noise acoustic excitation.

TABLE B-7. BENDING MOMENTS AS A FUNCTION OF NUMBER OF MODES (MODEL A)

PLATE FINITE ELEMENT NUMBER	BENDING MOMENTS					
	TYPE	1 MODE	2 MODES	3 MODES	5 MODES	8 MODES
		(in-lb/in)	(in-lb/in)	(in-lb/in)	(in-lb/in)	(in-lb/in)
19	M_x	2.11	2.14	2.31	2.31	2.33
4	M_y	0.83	0.88	0.88	0.88	0.88
1	M_x	2.38	2.40	2.44	2.44	2.52
1	M_y	1.29	1.42	1.43	1.43	1.45

TABLE B-8. COMPARISON OF BENDING MOMENTS IN MODEL C AND G

TYPE OF MOMENT	FINITE ELEMENT NO.	BENDING MOMENT IN MODEL C	FINITE ELEMENT NO.	BENDING MOMENT IN MODEL G	LOCATION OF THE FINITE ELEMENT
		(in-lb/in)		(in-lb/in)	
M_x	19	2.31	11	1.86	In the central bay near the center of the long side.
M_x	4	0.88	4	0.49	In the central bay near the center of the short side.
M_x	1	2.44	1	2.04	Near the center of Panel A-3-1.
M_x	1	1.43	1	1.05	Near the center of Panel A-3-1.

The bending moments were converted to bending stresses by the equation

$$s = \frac{6M}{h^2} \qquad \text{(B-1)}$$

The peak bending stress near the longeron predicted by REDYN with Model G was in element No. 11 (Table B-8) and was

$$s = \frac{6\ (1.86)}{(.050^2)} = 4{,}464 \text{ psi-rms}$$

REDYN analyses were also conducted to obtain the structural response to the spatially uniform white noise loading at 6.28×10^{-5} psi^2/Hz of panels A-1-1, A-2-1, A-4-1, and A-5-1. The principal variables in the test panel structural designs are summarized in Table B-9. Model G in Figure B-2 was used as the model for locating the finite element nodes of panels A-1-1, A-2-1, and A-3-1. Model H in Figure B-4 was used for the finite element nodes of panels A-4-1 and A-5-1. The material properties given in Table B-2 were used for all five test panel designs. The thickness of the plate finite elements is given in Table B-10 and the offset distances from the centroids of the longerons and I-sections to the plate midplanes are given in Table B-11.

With the moments of inertia, torsional constants, and areas of the Model G substructure that are listed in Table B-4, the natural frequencies and structural response were calculated with REDYN for the five different panel

TABLE B-9. TEST PANEL PARAMETERS

PANEL DESIG-NATION	OVERALL PANEL DIMENSIONS	NOMINAL DIMENSIONS OF CENTRAL BAY	SKIN THICKNESS
	(inch)	(inch)	(inch)
A-1-1	29 x 20	18 x 9	0.032
A-2-1	29 x 20	18 x 9	0.040
A-3-1	29 x 20	18 x 9	0.050
A-4-1	36 x 24	24 x 12	0.050
A-5-1	36 x 24	24 x 12	0.062

panel designs. The results are listed in Table B-12. The bending stresses obtained from Equation (B-1) and using the moments in Table B-12 are given in Table B-13. The bending stresses are at the centroid of the finite element and therefore may not be a highly accurate estimate of the maximum (RMS) bending stress when there is a stress concentration at the edge of an element resulting from a boundary condition or change in cross-section, and more importantly when there is a rapid change in curvature in and near the element. In any event, there was not good agreement between predicted (with REDYN) rms stresses and experimental rms stresses at gages No. 1 through 4 on the unstiffened side of the skins at the edges of the bonded joints.

A concluding remark is that the bending stresses obtained with any linear finite element program such as REDYN, STARDYNE, or NASTRAN will be in error in estimating the dynamic stress response of panels that are subjected to sufficiently high intensity noise that produces a nonlinear acoustic pressure versus strain response relation.

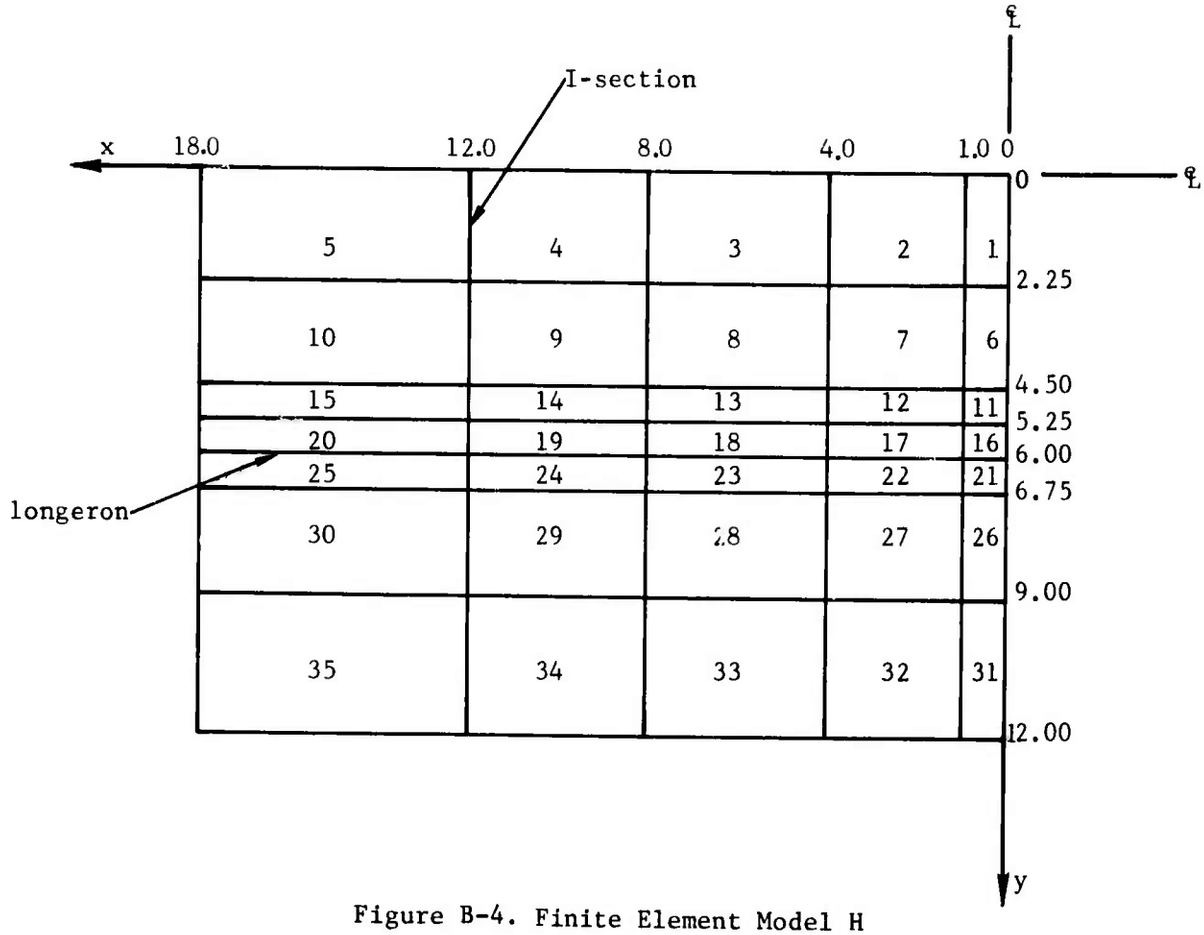

Figure B-4. Finite Element Model H

TABLE B-10. THICKNESSES FOR DIFFERENT STRUCTURAL MODELS

FINITE ELEMENT NUMBER	PANEL A-1-1	PANEL A-2-1	PANELS A-3-1 AND A-4-1	PANEL A-5-1
	(inch)	(inch)	(inch)	(inch)
1	0.032	0.040	0.05	0.062
2				
3				
4	0.032	0.040	0.05	0.062
5	0.051	0.064	0.08	0.099
6	0.032	0.040	0.05	0.062
7				
8				
9	0.032	0.040	0.05	0.062
10	0.051	0.064	0.08	0.099
11	0.032	0.040	0.05	0.062
12				
13				
14	0.032	0.040	0.05	0.062
15	0.051	0.064	0.08	0.099
16	0.062	0.07		0.092
17				
18				
19	0.062	0.07	0.08	0.092
20	0.081	0.094	0.11	0.129
21	0.062	0.070	0.08	0.092
22				
23				
24	0.062	0.070	0.08	0.092
25	0.081	0.094	0.11	0.129
26	0.032	0.040	0.05	0.062
27				
28				
29	0.032	0.040	0.05	0.062
30	0.051	0.064	0.08	0.099
31	0.064	0.080	0.10	0.124
32				
33				
34				
35	0.064	0.080	0.10	0.124

TABLE B-11. OFFSETS FOR TEST PANEL MODELS

ITEM	OFFSETS				
	PANEL A-1-1	PANEL A-2-1	PANEL A-3-1	PANEL A-4-1	PANEL A-5-1
	(inch)	(inch)	inch	(inch)	(inch)
Distance from the centroid of simulated longeron to plate midplane	0.665	0.669	0.674	0.674	0.678
Distance from the centroid of I-section to plate midplane	2.128	2.132	2.137	2.137	2.143

TABLE B-12. MODAL AND RESPONSE DATA FROM REDYN FOR THE FIVE ACOUSTIC TEST PANEL DESIGNS

PARAMETER (1)	PANEL A-1-1	PANEL A-2-1	PANEL A-3-1	PANEL A-4-1	PANEL A-5-1
Frequency, first mode, Hz.	103	120	139	75	88
Frequency, second mode, Hz.	176	217	266	145	177
Frequency, third mode, Hz.	294	343	407	283	340
Deflection at panelcenter(1), in-rms.	0.25	0.15	0.10	0.26	0.17
M_x in finite element No. 1, in.-lb./in. rms.	1.53	1.75	2.04	2.82	3.29
M_x in finite element No. 11, in.-lb./in. rms.	1.75	1.79	1.86	2.85	2.96
M_x in finite element No. 16, in.-lb./in. rms.	2.94	3.07	3.26	4.38	4.73
M_x in finite element No. 31, in.-lb./in. rms.	1.11	1.52	2.07	2.09	2.63

(1) Only modes that are symmetric about both center lines of the plate are considered. The acoustic loading is assumed to be spatially uniform white noise at 6.28×10^{-5} psi^2/Hz. The finite element locations are defined in Models G and H in Figures B-2 and B-4.

TABLE B-13. PREDICTED STRESSES IN THE TEST PANELS SUBJECTED TO WHITE NOISE (LINEAR THEORY)

FINITE ELEMENT NUMBER	BENDING STRESS(1)				
	PANEL A-1-1	PANEL A-2-1	PANEL A-3-1	PANEL A-4-1	PANEL A-5-1
	(ksi-rms)	(ksi-rms)	(ksi-rms)	(ksi-rms)	(ksi-rms)
1	9.0	6.6	4.9	6.8	5.1
11	10.2	6.7	4.5	6.9	4.6
16	4.6	3.8	3.1	4.1	3.4
31	1.6	1.4	1.2	1.3	1.0

(1) The acoustic loading is assumed to be spatially uniform white noise at 6.28×10^{-5} psi^2/Hz. The predicted stresses are at the centroids of the finite elements. The finite element models are shown in Figure B-2 (Model G) and Figure B-4.

B.3 Static Analysis to Obtain Adhesive Stresses

The two basic finite element models for NASTRAN analyses to obtain adhesive stresses are shown in Figures B-5 (Model S) and B-6 (Model R). Figure B-5 contains the simulation of the scarfed flange of the longeron substructure. The substructure in Figure B-6 differs from the substructure in Figure B-5 by the omission of the scarfing. The reason for preparing the structural model in Figure B-6 was to obtain the effect of not scarfing the flanges of the longerons.

The structural models were prepared to simulate a one-inch wide strip (of the acoustic test panels) that is perpendicular to the longerons and midway between the two I-section frames. Line AB in Figures B-5 and B-6 represents a section through the thickness of the skin that includes the centroid of finite element No. 11 of Models G and H in Figures B-2 and B-4. The bending moments and transverse shears at the Section AB for panels A-1-1, A-2-1, A-3-1, A-4-1, and A-5-1 are listed in Table B-14 and were obtained in REDYN computer runs.

Only one-half of the flange width of the longerons (i.e., 0.80 inch) is contained in the structural models in Figures B-5 and B-6. Furthermore, the boundary conditions in the NASTRAN computer runs were that all degrees of freedom were constrained at the cross section OD. The fixed boundary condition along OD is expected to closely simulate the situation when adjacent bays are in phase. When the adjacent bays are out-of-phase, the boundary condition at OD is not expected to cause a major error in the stress distribution in the vicinity of the edge of the bonded joint (i.e., the location where fatigue failures are expected to be initiated).

The bending stresses that produced the bending moments were assumed to be linearly distributed across the cross-section AB. The shearing forces that produced the transverse shear were assumed to be parabolically distributed across the cross-section AB. Under these assumptions, the forces T_1 through T_6 and V_2 through V_5 that are depicted in Figures B-5 and B-6 were calculated and they are listed in Table B-15.

The identification of the dimensional parameters a, b, and s in Figures B-5 and B-6 are in Table B-16. The parameter a is the adhesive thickness; the parameter s is one-fifth of the skin thickness; and the parameter b is one-sixth of the longeron flange thickness in the unscarfed zone.

The most highly stressed finite elements in the NASTRAN computer runs were the triangular finite element at the right edge (Figures B-5 and B-6) of the adhesive and the skin finite element that is in contact with the triangular adhesive element. The stresses of particular interest in the analyses with Model S are listed in Table B-17. The x, y coordinate systems are defined in Figures B-5 and B-6.

Of particular interest in this investigation were stress ratios that may be used to compare the relative importance of bending in the skin, peel in the adhesive, and shear in the adhesive. Stress ratios that were calculated are listed in Table B-18.

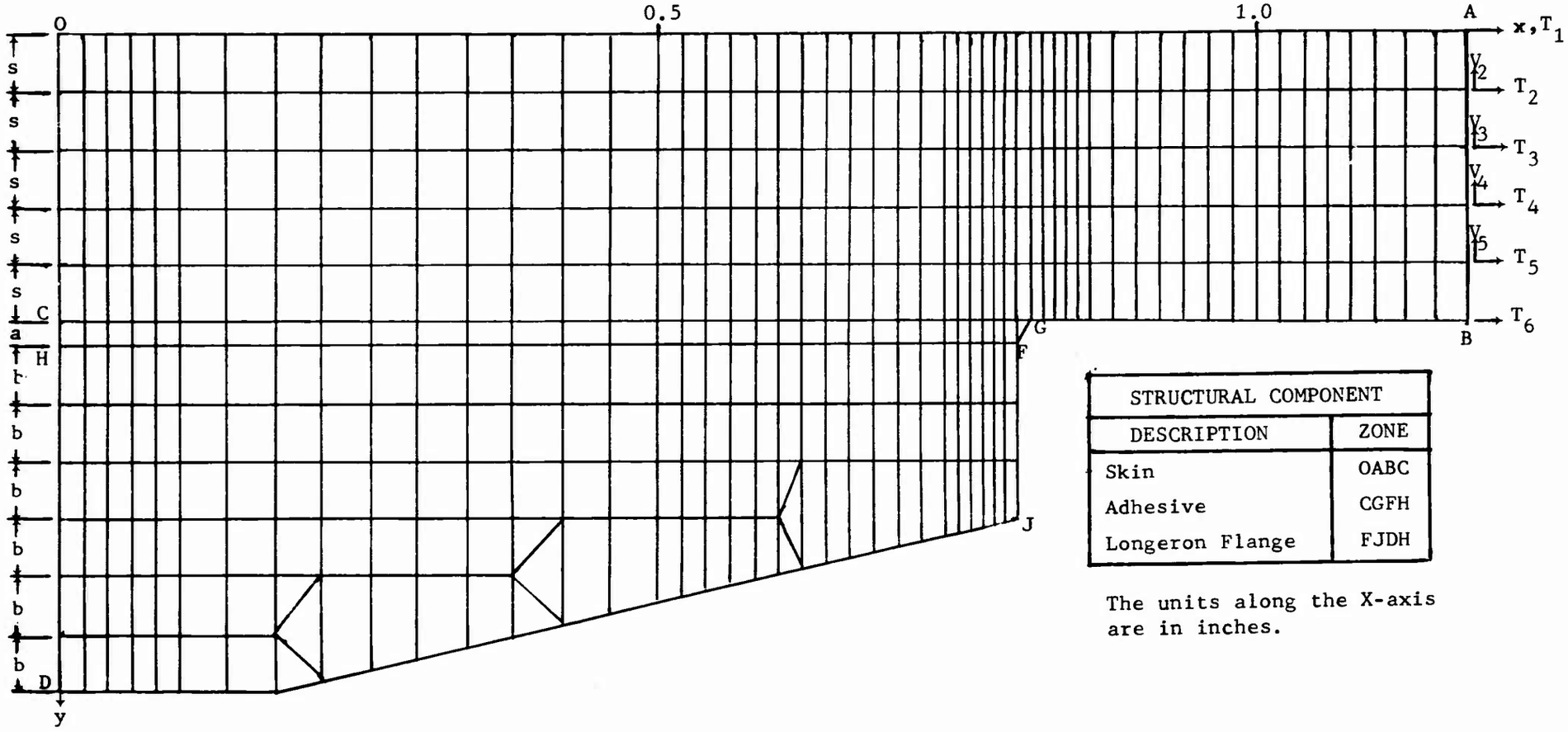

STRUCTURAL COMPONENT	
DESCRIPTION	ZONE
Skin	OABC
Adhesive	CGFH
Longeron Flange	FJDH

The units along the X-axis are in inches.

Figure B-5. NASTRAN Structural Model S

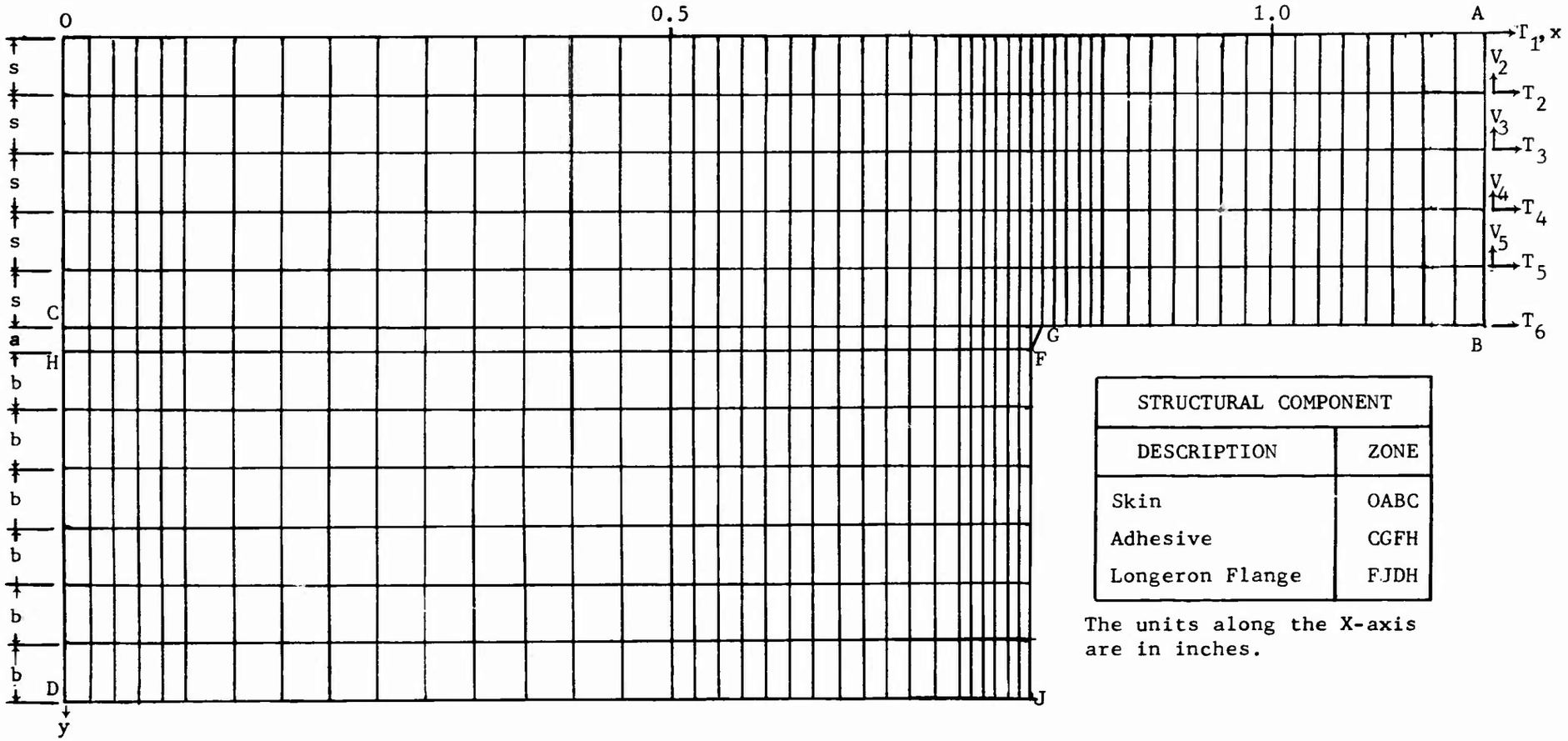

STRUCTURAL COMPONENT	
DESCRIPTION	ZONE
Skin	OABC
Adhesive	CGFH
Longeron Flange	FJDH

The units along the X-axis are in inches.

Figure B-6. NASTRAN Structural Model R

TABLE B-14. BENDING MOMENTS AND SHEARS

PARAMETERS	PANEL A-1-1	PANEL A-2-1	PANEL A-3-1	PANEL A-4-1	PANEL A-5-1
M_x, lb-in/in	1.745	1.792	1.856	2.845	2.957
Q_y, lb/in	1.728	1.876	2.067	2.162	2.568

TABLE B-15. EXTERNAL LOADS FOR NASTRAN COMPUTER RUNS

FORCE	PANEL A-1-1	PANEL A-2-1	PANEL A-3-1	PANEL A-4-1	PANEL A-5-1
T_1, lb	-38.951	-32.000	-26.514	-40.643	-34.069
T_2, lb	-23.371	-19.200	-15.908	-24.386	-20.441
T_3, lb	-4.674	-6.400	-5.303	-8.129	-6.814
T_4, lb	4.674	6.400	5.303	8.129	6.814
T_5, lb	23.371	19.200	15.908	24.386	20.441
T_6, lb	38.951	32.000	26.514	40.643	34.069
V_2, lb	0.173	0.188	0.207	0.216	0.257
V_3, lb	0.691	0.751	0.827	0.865	1.027
V_4, lb	0.691	0.751	0.827	0.865	1.027
V_5, lb	0.173	0.188	0.207	0.216	0.257

TABLE B-16. GEOMETRICAL PARAMETERS FOR NASTRAN STRUCTURAL MODELS

PARAMETERS	PANEL A-1-1	PANEL A-2-1	PANEL A-3-1	PANEL A-4-1	PANEL A-5-1
a, inch	0.004	0.004	0.004	0.004	0.004
s, inch	0.0064	0.008	0.010	0.010	0.0124
b, inch	0.010	0.010	0.010	0.010	0.010

TABLE B-17. KEY STRESSES OBTAINED IN THE NASTRAN RUNS WITH THE SCARFED LONGERON

	PANEL A-1-1	PANEL A-2-1	PANEL A-3-1	PANEL A-4-1	PANEL A-5-1
s_x in skin, psi	11,180	7,617	5,197	7,223	5,086
s_x in adhesive, psi	1,049	748	530	733	533
s_y in adhesive, psi	1,971	1,436	1,036	1,427	1,052
s_{xy} in adhesive, psi	1,445	1,122	864	1,191	933
σ, max. principal stress in adhesive, psi	3.027	2,266	1,684	2,320	1,762
τ, max. shear stress in adhesive, psi	1,517	1,174	901	1,240	969

TABLE B-18. STRESS RATIOS

STRESS RATIOS	PANEL A-1-1	PANEL A-2-1	PANEL A-3-1	PANEL A-4-1	PANEL A-5-1
$A = \frac{(s_y)_{adh}}{(s_x)_{skin}}$	0.18	0.19	0.20	0.20	0.21
$B = \frac{\sigma_{adh}}{(s_x)_{skin}}$	0.27	0.30	0.32	0.32	0.35
$C = \left(\frac{s_y}{s_{xy}}\right)_{adh}$	1.36	1.28	1.20	1.20	1.13
$D = \left(\frac{s_y}{s_x}\right)_{adh}$	1.88	1.92	1.95	1.95	1.97
$E = \left(\frac{\sigma}{\tau}\right)_{adh}$	2.00	1.93	1.87	1.87	1.82

The stress ratios A and B of Table B-18 imply that as the skin thickness increases, the peel stresses in the adhesive increase (as expected) relative to the bending stress in the skin. The stress ratios C imply that as the skin thickness increases, the peel stresses in the adhesive decrease relative to the shear stresses in the adhesive; and furthermore, the peel stress is, in each of the five cases, greater than the shear stress. The stress ratios D imply that the peel stress normal to the interface between the skin and adhesive exceeds the s_x extensional stress in the adhesive; and as the skin thickness increases, the s_y peel stress decreases relative to the s_x extensional stress. The stress ratios E imply that as the skin thickness increases, the maximum principal stress σ in the adhesive decreases relative to the maximum shear stress τ in the adhesive.

The stresses that are tabulated in Table B-17 and the stress ratios in Table B-18 were calculated for a shear modulus of 100,000 psi, a Poisson's ratio of 0.33 and Young's modulus of 266,000 psi on the basis of isotropy. In addition, calculations were performed with a shear modulus of 60,000 psi that has been reported for FM73 adhesive. Therefore, for panel A-3-1, NASTRAN computer runs were performed with Models R and S, with a shear modulus of 60,000 psi, a Poisson's ratio of 0.33 and a Young's modulus of 159,600 psi and results are in Table B-19.

A comparison of the results in Table B-19 shows the beneficial effect of scarfing insofar as reducing the peel stress is concerned. The structural loading for all cases in Table B-19 is given in the column for Panel A-3-1 in Table B-15.

TABLE B-19. KEY STRESSES IN PANEL A-3-1

STRESSES	SHEAR MODULUS = 100,000 psi		SHEAR MODULUS = 60,000 psi	
	SCARFED FLANGE	UNSCARFED FLANGE	SCARFED FLANGE	UNSCARFED FLANGE
s_x in skin, psi	5,197	5,173	5,170	5,147
s_x in adhesive, psi	530	605	389	458
s_y in adhesive, psi	1,036	1,271	839	1,054
s_{xy} in adhesive, psi	865	802	692	628
σ, maximum principal stress, psi	1,684	1,806	1,342	1,451
τ, maximum shear stress, psi	901	868	728	695

The results obtained with the static NASTRAN analyses are expected to provide a qualitative view of the stress response in the adhesive when multi-bay panels are subjected to acoustic excitation. The static analysis is presented in this report principally to provide information that may be useful in explaining the modes of fatigue failures and lifetime comparisons of the beam specimens and acoustic test panels. In that regard, the discussion of the stress ratio results in Table B-19 may be particularly useful.

Reference for Appendix B.

B-1. M. J. Jacobson, "Advanced Composite Joints; Design and Acoustic Fatigue Characteristics," Technical Report AFFDL-TR-71-126, April 1972.